Temperature variability within the upper water masses of the western tropical Atlantic during rapid climate transitions

By

Lea Toska Oppedal

MASTER THESIS IN GEOLOGY

Department of Earth Science

University of Bergen

December 2010

Table of Contents

Abstract

Rapid reorganization of the ocean circulation in the Atlantic Ocean has been linked to widespread varations in climate on both millennial and glacial-interglacial timescales. The response of the tropical Atlantic upper ocean to such circulation changes, has been investigated in both proxy studies and modelling experiments. It is believed that reduction of the thermohaline overturning leads to decreased cross-equatorial northward transport of warm surface waters. Consequently, heat accumulates in the upper water column of the tropical Atlantic.

In this thesis, temperature variability within the upper water masses of the western tropical Atlantic is investigated in six timeslices associated with different modes of overturning circulation. The timeslices represent the Last Glacial Maximum, Heinrich event 1, Bølling-Allerød, the Younger Dryas and the early and late Holocene. Changes in the thermal stratification of the upper water column are inferred from stable oxygen isotope- and Mg/Ca measurements on five species of planktonic foraminfera that live vertically dispersed in the upper water masses.

The proxy measurements provide evidence that more heat was stored in western tropical Atlantic waters during the Last Glacial Maximum when the thermohaline overturning was reduced. Heat was released in the present interglacial, which is associated with vigorous overturning. Concomitant to reductions in the overturning circulation, centred on the deglaciation, possible evidence is given that heat accumulated in the upper tropical water masses. However, on this scale, the results are not conclusive, and further investigation is needed.

Acknowledgements

First of all, I would like to show my graditude to my supervisor Trond M. Dokken for his excellent guidance and assistance over the last two years, and for giving me the opportunity to work on a very interesting topic. Through working on this thesis I have been able to participate in almost every step in the research process. I am very greatful for the opportunity to participate in the RETRO III cruise off the coast of North Brazil in October 2009 and to visit the Vrije Universiteit in Amsterdam in May 2009. A great thank you to Frank J. C. Peeters for his hospitality and for taking the time to teach me all about tropical planktonic foraminfera. I would also like to thank Vincent Scao for his assistance and advice in the ICP laboratory of the University of Bergen. Furthermore, Rune E. Søraas has been of great help at the GMS laboratory at the BCCR. I am also greatful to Amandine Tisserand for providing me with some very nice figures, and to Saskia Kars from the Vrije Universiteit Amsterdam who has been very kind to let me use her SEM images of the planktonic foraminferal species used in the study.

Thank you to my fellow students at the Department of Earth Science for support and friendship, and to my family and friends for showing interest in my work.

Finally, a great thank you to Erla, my greatest supporter.

Bergen, December 2010

Lea Toska Oppedal

List of Figures

List of Tables

List of Appendices

Appendix C Correlation of $\delta^{18}O_{IVC}$ and Mg/Ca

Figure C.1: *G. ruber* $\delta^{18}O_{IVC}$ versus Mg/Ca. Pearson's correlation coefficient, r =-0.69

Figure C.2: *G. truncatulinoides* (dex) $\delta^{18}O_{IVC}$ versus Mg/Ca. Pearson's correlation coefficient, r =-0.04.

List of Abbreviations

AABW Antarctic Bottom Water

AAIW Antarctic Intermediate Water

AC Angola Current

AMOC Atlantic Meridional Overturning Circulation

AMS Accelerator Mass Spectrometry

B/A Bølling-Allerød

BP Before Present

BC Brazil Current

CC Caribbean Current

CCD Carbonate Compensation Depth

cSEC central South Equatorial Current

dex dextral

D/O Dansgaard-Oeschger

EUC Equatorial Undercurrent

GC Guinnea Current

GS G. O. Sars

H1 Heinrich event 1

ICP Inductively Coupled Plasma

ICP-AES Inductively coupled plasma atomic emission spectrometry

ICP-OES Inductively coupled plasma optical emission spectrometry

ITCZ Intertropical Convergence Zone

LGM Last Glacial Maximum

MD Marion Dufresne

MOC Meridional Overturning Circulation

NADW North Atlantic Deep Water

NBC North Brazil Current

NBUC North Brazil Undercurrent

NBS National Bureau of Standards

NEC North Equatorial Current

NECC North Equatorial Countercurrent

nSEC northern South Equatorial Current

RETRO Respons of the Tropical Atlantic Surface and Intermediate Waters to changes in the AMOC.

SACW South Atlantic Central Waters

SECC South Equatorial Countercurrent

SEUC South Equatorial Undercurrent

SML Surface Mixed Layer

SMOW Standard Mean Ocean Water

sSEC southern South Equatorial Current

SSS Sea Surface Salinity

SST Sea Surface Temperature

Sv Sverdrup (0.001 km^3/s)

T Temperature (in °C)

TCD Thermocline Depth

THC Thermohaline Circulation

TSW Tropical Surface Water

uCDW upper Circumpolar Deep Water

PDB Peedee Belemnite (in ‰)

VPDB Vienna Peedee Belemnite (in ‰)

XRF X-ray Fluorescence

YD Younger Dryas

$\delta^{18}O$ Stable oxygen isotope composition (in ‰)

$\Delta\delta^{18}O$ Stable oxygen isotope gradient (in ‰)

$\delta^{18}O_c$ Stable oxygen isotope composition of foraminiferal calcite

$\delta^{18}O_{IVC}$ Ice volume corrected stable oxygen isotope composition (in ‰)

$\delta^{18}O_w$ Stable oxygen isotope composition of seawater

1 Introduction

The world ocean plays a fundamental role in the climate system. Due to it's heat capacity and circulation, substantial amounts of heat can be stored and redistributed before it is released to the atmosphere (Rahmstorf, 2002). The transfer of heat has great impacts on the global distribution of climate, and past changes in ocean circulation have been associated with major climatic shifts. In the Atlantic Ocean the Atlantic Meridional Overturning Circulation (AMOC) moves warm, saline tropical waters northward to the northern North Atlantic. This provides a net northward transport of heat from the South Atlantic Ocean (Delworth et al., 2008). North of Iceland the tropical waters give off heat to the atmosphere, become denser and contribute to the formation of cool North Atlantic Deep Water (NADW) which flows southward. This latitudinal exchange of water masses maintains the relatively mild climate of northwestern Europe, making the region habitable all year around (Rahmstorf, 2002).

For many years the AMOC has been a major research focus because of its climatic relevance. Several studies (McManus et al., 2004; Rahmstorf, 2002) have suggested that changes in the AMOC are connected to ocean-wide reorganizations in heat transport and climate distribution. Abrupt cooling events recorded in Greenland ice cores, have been linked to weak meridional overturning and reduced northward heat transport by upper water masses. These events have been related to abrupt changes in climate in many parts of the world. Hence, the meridional overturning circulation comprises a major uncertainty in the prediction of future climate (Rühlemann et al., 2004).

To be able to reliably assess the ocean's vulnerability to future changes and the climatic repercussions such changes could have, it is important to improve our understanding of why and how the world's general ocean circulation has changed in the past. The tropics have long been regarded as a zone of weak environmental variations, and consequently few paleoceanographic studies have taken place there. Hence, the role played by the tropics during changes in ocean circulation is not well understood, and, it is important to carry out more studies in this region. By reconstructing temperature variations in the upper ocean of the tropical Atlantic during key transitions of the AMOC, this thesis will contribute to improve

our understanding of changes in tropical ocean circulation and the connections between climate variability at high and low latitudes.

1.1 Project

The present study is part of a collaborative research project within the framework of the program EuroMARC, initiated by the European Science Foundation (ESF). The project is called "**Re**sponse of **tro**pical Atlantic surface and intermediate waters to changes in the Atlantic meridional overturning circulation" (RETRO). It is a co-operation between the University of Bergen, the Bjerknes Centre for Climate Research, the Vrije University of Amsterdam, the Universidade Federal Fluminense and the Universidade Federal do Rio de Janeiro. The thesis has been supervised by Dr. Trond M. Dokken from the Bjerknes Centre for Climate Research in Bergen.

The RETRO project aims to reconstruct variations in tropical Atlantic surface, thermocline, intermediate and deep waters through key transitions of the Atlantic Meridional Overturning Circulation. The project focuses on three work packages, which aims are:

3. To reconstruct tropical ocean responses during millennial scale changes associated with Dansgaard/Oeschger (D/O) events between 60,000 to 30,000 years before present (BP).
4. To investigate large changes in tropical ocean parameters during the transition from the last glacial maximum (19-21 kyrs BP) to the present interglacial (11,500 yrs BP).
5. To detect the amplitude of the typical tropical ocean variability for the recent interglacial period (Holocene) between 11,500 years BP and present.

1.2 Objective

This thesis contributes to the RETRO project as a preliminary study of the tropical Atlantic upper-ocean response to variations in the AMOC during the last 20,000 years. It investigates the link between variations in upper-ocean temperature in the tropical Atlantic and abrupt

changes in climate observed in Greenland ice cores. Several modelling studies (Dahl et al., 2005; Manabe and Stouffer, 1997; Vellinga and Wood, 2002) have shown that freshwater induced reductions in the AMOC result in cooling in the North Atlantic and warming in the tropics and South Atlantic. The reduction in the strength of the AMOC is believed to have lead to weaker northward transport by tropical ocean currents. Hence, less heat is exchanged across the equator, and heat is believed to accumulate in the southern hemisphere. Modelling studies, as well as proxy reconstructions, concerning variations in ocean temperature and ventilation, have related variations in the strength of the AMOC to changes in the thermal stratification of the upper tropical Atlantic Ocean.

Manabe and Stouffer (1997) investigated the response of a coupled ocean-atmosphere model to the discharge of freshwater into the northern North Atlantic over a period of 500 years. They observed a weakening in the overturning while the surface air temperatures over the northern North Atlantic and surrounding continental areas were reduced. As the input of freshwater ceased, the AMOC stepped up and regained its original intensity within a few hundred years. The climate of the northern North Atlantic and surrounding regions quickly resumed its original distribution (1997) .

As the overturning circulation slowed down, the model simulation showed a rise in temperature in the upper layers of the Atlantic in low to middle latitudes (Figure 1). The largest warming anomalies occurred in the Southern Hemisphere at low latitudes and were most pronounced at intermediate water depths between 200 and 1000 m. A maximum warming of 3-3.5°C is shown at depths of 300-700 m. The anomalies quickly weaken when the AMOC reintensifies (Manabe and Stouffer, 1997).

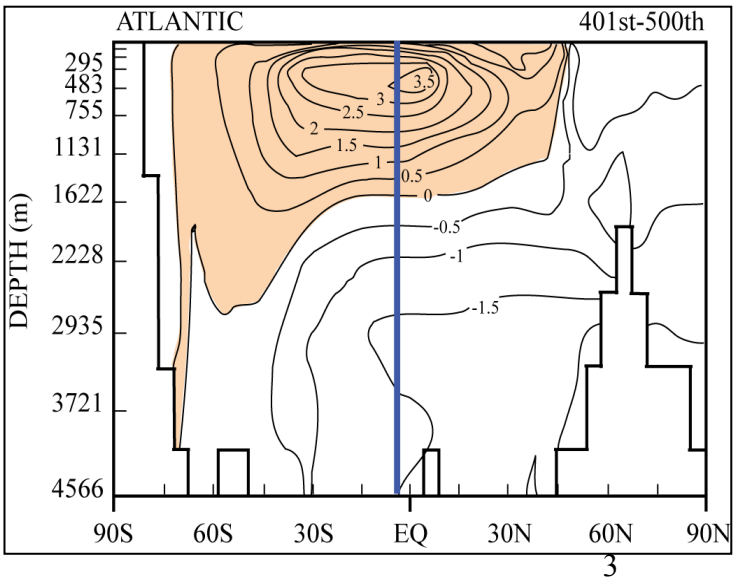

Figure 1: Zonal mean temperature anomaly (°C) in the Atlantic Ocean averaged over the last 401st to 500th year. (After Manabe and Stouffer, 1997). The temperature anomalies are largest in low to middle latitudes in the Southern Hemisphere. The blue line indicates the approximate latitude of the study area (after Tisserand, 2009).

This study aims to test the hypothesis that the modelling study by Manabe and Stouffer (1997) show a realistic picture of the tropical response to changes in overturning circulation. An attempt to reconstruct past thermal stratification of the upper water column is made for six time slices, thought to be associated with different modes of AMOC. The six time slices represent the Last Glacial Maximum (LGM), Heinrich event 1 (H1), Bølling-Allerød (B/A), the Younger Dryas (YD) and the early and late Holocene. In the periods where the AMOC is believed to be weak, decreased upper ocean stratification is exptected, as heat is assumed to accumulate in tropical waters. In contrast, increased stratification of the upper waters is expected for periods with strong AMOC, when heat was transported northwards in the cross-equatorial surface currents. A more detailed review of the hypothesis will be given in Chapter 6

1.3 Research approach

In order to test the hypothesis, oxygen isotope and Mg/Ca ratios are obtained from five species of planktonic foraminfera that live vertically dispersed in the tropical upper ocean. The oxygen isotope and Mg/Ca composition of the foraminifera are used as paleotemperature proxies to reconstruct variations in temperature at different depths in the upper water column. A stratification proxy based on the difference in oxygen isotope and Mg/Ca ratios between shallow and deep dwelling species, is used to investigate changes in thermocline depth.

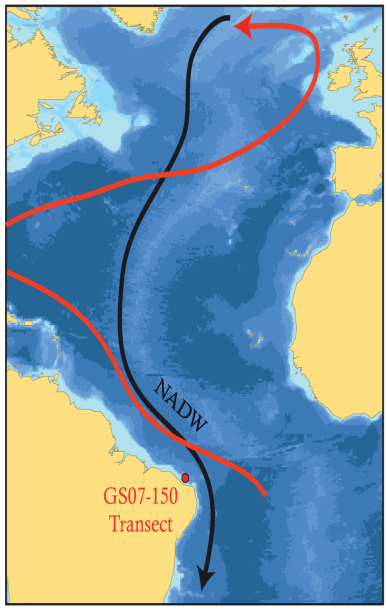

The foraminfera are sampled from the six mentioned time slices in three cores placed along a depth transect on the continental margin off North-east Brazil (Figure 2).

Figure 2: Chart of the Atlantic Ocean showing the location of the core transect and illustrating the cross-equatorial exchange of water masses. Northward-flowing surface and intermediate waters are shown by the red arrow, while southward-flowing NADW is depicted by the black arrow (after Tisserand (2009)).

This area is directly influenced by the North Brazil Current (NBC) (Arz et al., 1998), which is an integrated part of the AMOC. Hence, changes in the NBC might be

related to global changes in ocean circulation and climate (Arz et al., 1999b). This makes the core sites ideal for detecting thermocline variability in response to changes in the AMOC. The approach of using samples from three cores is chosen because the data obtained in this study will be used in combination with paleotemperature data from benthic species in the same timeslice samples. With the benthic data, variations in the deepest part of the thermocline can be assessed by measuring specimens that lived at different depths. Hence, when the data from both planktonic and benthic species are combined, temperature variations in large parts of the water column can be assessed.

1.4 Overview of the thesis

In the following sections of Chapter 1 a short «state-of-the-art» is given. The Atlantic Meridional Overturning Circulation is explained, as well as it's major climatic impacts. Climatic extremes, believed to be associated with AMOC variability during the last 20,000 years are then presented. Finally, previous studies of the tropical response to changes in the AMOC are examined. Chapter 2 presents the geological and oceanograpic setting of the study area. The vertical distribution of water masses, well as the surface circulation are described. Furthermore, a short account of the air-sea interaction in the area is given.

In Chapter 3 the foraminiferal species are described, and the proxy methods are discussed. Chapter 4 presents the age model used in the study and further explains how the cores were correlated using XRF element intensity records of the three cores. In Chapter 5 the oxygen isotope- and Mg/Ca measurements are presented, and the quality of the results is assessed. Chapter 6 provides a detailed account of the expectations of the study, as given by the hypothesis. Subsequently, the results are discussed and the hypothesis is evaluated. Finally, conclusions and a future perspective is given in the Chapter 7.

1.5 Background and previous work

1.5.1 The Atlantic Meridional Overturning Circulation (AMOC)

A simplified sketch of the global overturning circulation system is given in Figure 3. This circulation pattern is often referred to as the meridional overturning circulation (MOC), and the Atlantic branch of the system is called the Atlantic Meridional Overturning Circulation (AMOC) (Delworth et al., 2008). The AMOC is a system of vertical and horizontal currents with four key features: (1) deep water formation in a few localized areas at high latitudes where waters become dense and sink, (2) spreading of deep water away from the source regions toward lower latitudes, (3) upwelling processes that transport deep water masses to the ocean surface and (4) warm surface currents feeding the deep water formation areas with relatively light water, closing the circulation loop (Kuhlbrodt et al., 2007; Rahmstorf, 2006).

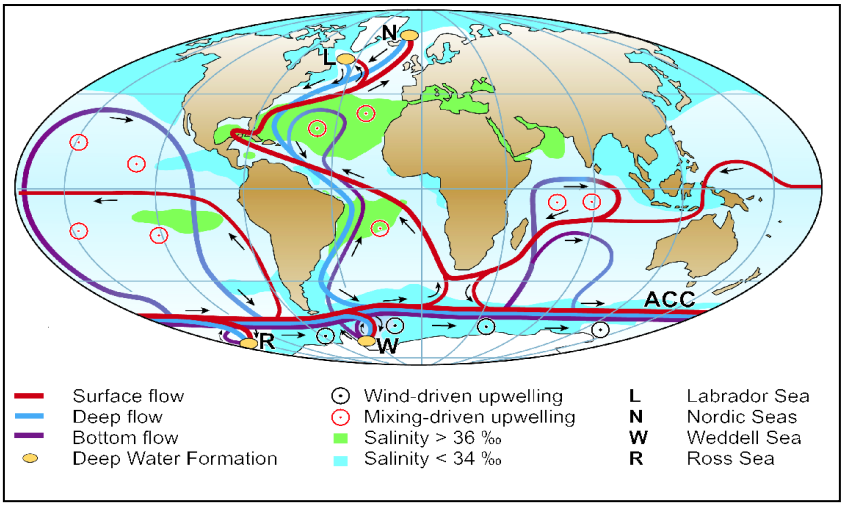

Figure 3: Simplified representation of the global overturning circulation system. Surface currents are shown in red, deep waters in light blue, bottom waters in dark blue and deep water formation sites in orange. (after Kuhlbrodt et al., 2007).

The thermohaline circulation (THC) is a concept related to the MOC, and the two terms are often mistaken to be synonymous with each other. The MOC is simply a geographical term used to describe the ocean circulation in the meridional-vertical plane, while the term THC refers to a driving mechanism behind the flow and is thus not an observational but a physical concept (Kuhlbrodt et al., 2007; Rahmstorf, 2006). Rahmstorf (2006) defines the THC as «that part of the ocean circulation which is driven by fluxes of heat and freshwater across the sea surface and subsequent interior mixing of heat and salt» and stresses the distinction between the bouyance-driven thermohaline circulation and wind-driven circulation. The term

MOC, however, includes clearly wind-driven parts and does not refer to any particular forcing mechanism (Rahmstorf, 2006). The term MOC (or AMOC) will be used consistently in this thesis, in order to avoid misunderstandings.

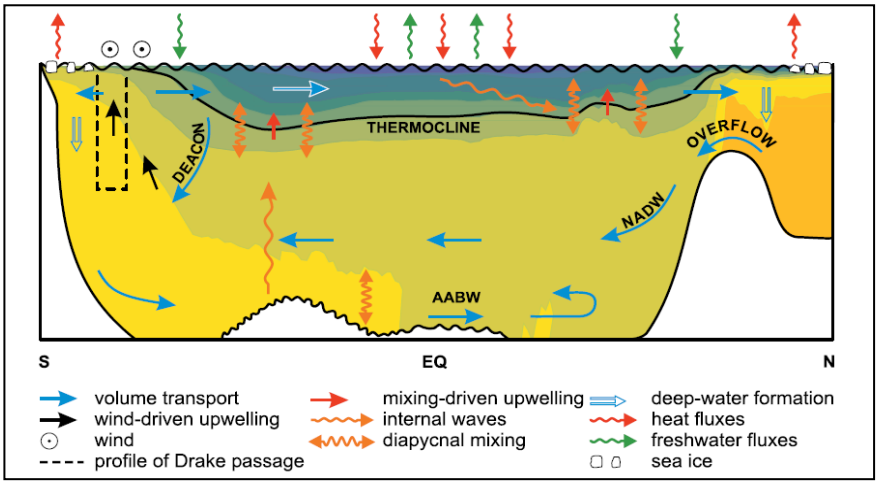

Figure 4: Side view of the circulation in the Atlantic Basin. The blue arrows represent the AMOC, while the colour shading illustrates density differences. The waters with the highest density are coloured in yellow, while the lowest density waters are blue. The thermocline, the region where the temperature gradient is high, is indicated by a black line (after Kuhlbrodt et al., 2007).

The AMOC consists of two main overturning cells (Figure 4). In the «upper» cell warm, saline surface waters flow northward in the upper 1000 m supplying the formation of North Atlantic Deep Water (NADW) in the Nordic and Labrador Seas. This deep water then flows southward across the equator at depths of approximately 1500-4500 m. In the «deep» cell Antarctic Bottom Water (AABW) flow northward below 4500 m and ascends gradually into the NADW. The upper cell is the most important transporter of heat in the Atlantic due to the large difference in temperature (~15° C) between the northward-flowing surface waters and the southward-flowing NADW (Delworth et al., 2008). The overturning circulation thus results in a northward flux of heat from the Tropics and Southern Hemisphere toward the North-Atlantic, where heat is transferred to the atmosphere (Delworth et al., 2008; Richardson, 2008). In the North-Atlantic the maximum northward heat transport is reported to be about 1 PW (10^5 W) (Kuhlbrodt et al., 2007; Rahmstorf, 2006).

1.5.2 Climatic impacts of the AMOC and changes in its mode of circulation

Due to its ability to store and redistribute heat, the Atlantic Meridional Overturning Circulation has a profound impact on the distribution of climate. Substantial amounts of heat are transported from the South Atlantic and tropical North Atlantic to the subpolar and polar North Atlantic (Delworth et al., 2008). Large surface air temperature deviations from the zonal mean are found over the main regions of deep water formation, where surface water

sinks after releasing heat to the atmosphere (Rahmstorf, 2002). Over the northern North Atlantic the magnitude of that temperature anomaly is up to 10°C, while the effect of the oceanic heat transport decreases in land over the continents (Rahmstorf, 2002). The climatic impact is clearly evident in North-western Europe, where winters are relatively mild compared to other regions at similar latitudes.

Because of the AMOC's role as a heat distributor in the climate system, variations in its strength or pattern have the potential to make significant and rapid changes in climate. Extensive evidence for abrupt climate change on various time scales during the last glacial period is found in marine and terrestrial climate records in many parts of the world. The variations are considered to reflect rapid reorganization of the atmosphere-ocean system. According to Broecker et al. (1985) the abrupt changes ensued from rapid shifts in the AMOC from one mode of circulation to another. The most widely accepted trigger behind these shifts is the release of glacial melt water from either ice-dammed lakes or ice surges. Rapid discharge of low-density freshwater into the North Atlantic capped the ocean surface water and prevented the formation of deep water The overturning circulation weakened rapidly, and the flow of warm water from the subtropical North Atlantic to the subpolar Atlantic was greatly reduced. As a consequence the North Atlantic region cooled and climate repercussions were widespread (Broecker et al., 1985; Seager and Battisti, 2006).

Paleoceanographic data (e.g. Sarnthein et al., 1994) have shown that three distinct circulation modes have prevailed in the Atlantic Ocean (Figure 5): the interstadial mode, the stadial mode and the Heinrich mode, or the warm, cold and off mode, respectively. Switches between the modes have been rapid, and the climate changes associated with them have been abrupt. In the interstadial mode vigorous formation of NADW took place in the Nordic Seas as heat was released to the atmosphere, warming Greenland and northern Europe. In the stadial mode NADW formed in the subpolar open North-Atlantic (south of Iceland). The deep water's penetration depth was shallower and gave room for Antarctic Bottom Water to flow further north. As a result, less heat was provided to heat Greenland and northern Europe during stadial times. During Heinrich modes the formation of deep water in the North-Atlantic was greatly reduced or even shut down, and Antarctic Bottom Water filled the deep Atlantic basin. These periods were associated with especially cold climate in the North Atlantic. (Alley and Clark, 1999; Rahmstorf, 2002).

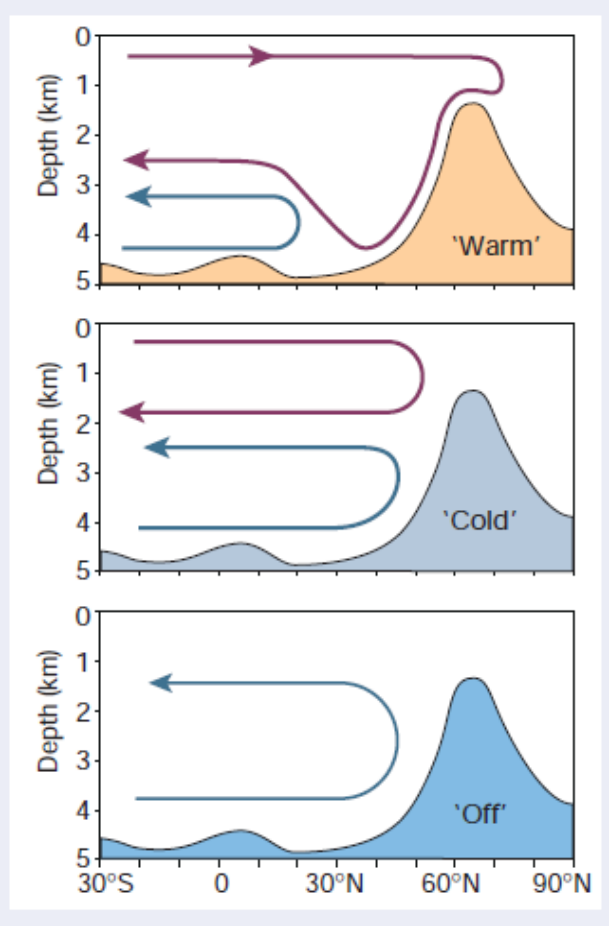

Figure 5: Sketch of the three modes of ocean circulation that have prevailed during different times of the last glacial period. The red line is representing North Atlantic overturning, and Antarctic Bottom Water is shown by the blue line (after Rahmstorf, 2002).

During the Last Glacial Maximum (LGM) (~23-19 kyr B.P) the AMOC was in a stadial mode, and although climate was a lot cooler than today, the period was characterized by relatively low climate variability. By contrast, the deglaciation that followed (11,5-19 ka B.P.) included several large and abrupt climate changes that have been attributed to changes in the AMOC. The two most pronounced types of climate variability during this period were Dansgaard-Oeschger (D/O) events and Heinrich (H) events (Figure 6). D/O events are recorded in Greenland ice-cores as rapid warmings by 5-10°C within a few decades followed by several centuries of slow cooling and then a more rapid drop back to cold stadial conditions. The events have an approximate spacing of 1500 years (Figure 6) (Alley and Clark, 1999; Rahmstorf, 2002).

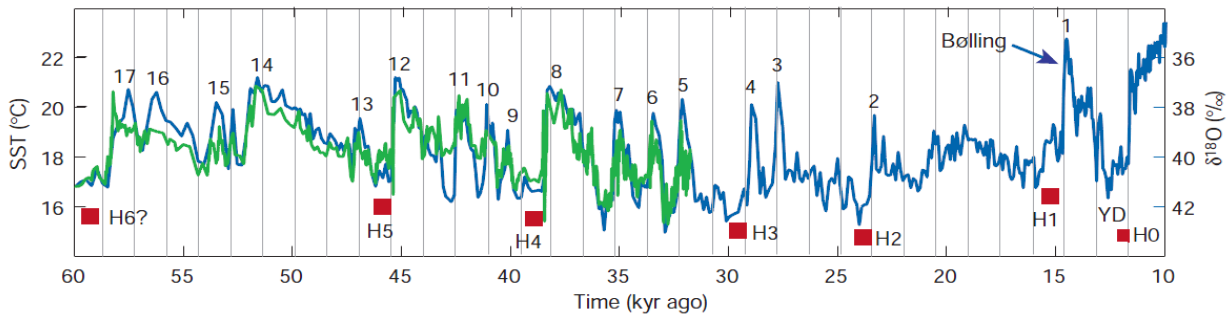

Figure 6: Temperature reconstructions from ocean sediments and $\delta^{18}O$ from Greenland ice. The D/O events are numbered and the timing of Heinrich events is marked in red. Grey lines at intervals of 1470 years illustrate the tendency of D/O events to occur with this spacing, or multiples thereof (after Rahmstorf, 2002).

Heinrich events occurred mostly in the latter half of the last glacial. They are recognized in the North Atlantic sediment record as distinct layers of coarse material (Heinrich, 1988). These sediments must have been transported to the ocean by icebergs, and are therefore referred to as ice-rafted debris. The Heinrich layers are spaced at intervals of the order of 10,000 years. The thickness of the layers decrease from several meters in the Labrador Sea to a few centimetres in the eastern Atlantic. This suggests that Heinrich events are massive episodic iceberg discharges from the Laurentide ice sheet through the Hudson Strait. Sediment data relate Heinrich events to the «off» mode of Atlantic Meridional Overturning Circulation, by showing that NADW formation ceased or was at least strongly reduced during these periods (Rahmstorf, 2002).

The deglaciation started approximately 19 kyr ago as a result of increased northern summer insolation (Alley et al., 2002). A subsequent rise in atmospheric CO_2 provided a global warming feedback, and the ice sheets started to melt. The melt water induced a reduction in NADW formation, and at about 17.5 ka BP the AMOC switched to the «off» mode of Heinrich event 1 (H1) (Figure 1.4). During this event NADW was significantly reduced or even shut down (Boyle and Keigwin, 1987; Keigwin and Lehman, 1994; McManus et al., 2004; Sarnthein et al., 1994). A northward shift in ocean circulation marked the onset of Bølling-Allerød at 14.6 ka BP, which represents D/O event 1 (Figure 1.4). During this period Greenland warmed abruptly, as the AMOC switched to the interstadial mode (Rahmstorf, 2002).

At about 12.9 ka BP this mode of circulation was disrupted as the Younger Dryas period began. This period has been associated to the first major retreat of the Laurentide ice sheet, during which the route of the melt water discharge switched from the Gulf of Mexico through the St. Lawrence spillway to the North Atlantic (Arz et al., 1999b; Rahmstorf, 2002). Hence, the melt water was released closer to the formation areas of NADW and could more effectively reduce the deep water production (Broecker et al., 1988; Teller, 1990). The YD has been called H0, but differ from other H-events because other forcing mechanisms than a change in ocean circulation might have been involved. Nevertheless, because of the high melt water influx NADW formation was greatly reduced, almost as during H-events (Rahmstorf, 2002). The YD ended with an abrupt warming that is sometimes called D/O 0. This warming marks the end of the last glacial period and the beginning of the Holocene (11,5-0 ka B.P.), which is the interglacial period we are currently in. The Holocene has been characterized by relative climate stability compared to glacial climate and vigorous NADW formation

(Delworth et al., 2008; Rahmstorf, 2002). The only major northern cooling observed in the Holocene occurred 8,200 years BP. This event was also a result of a melt water-induced reduction in the AMOC (Kleiven et al., 2008).

1.5.3 Response of the tropical Atlantic Ocean to AMOC variability

Model results imply that the tropical and extratropical Atlantic are closely connected on decadal to glacial-interglacial timescales {Gu, 1997 #200;Bush, 1998 #201}. Variations in tropical Atlantic SST and trade winds appear to be tightly linked to ocean-atmospheric variability in higher latitudes associated with the AMOC. Paleoceanographic evidence seem to confirm this relationship. According to sediment records from the Cariaco Basin off Venezuela, changes in the tropical Atlantic Ocean and atmosphere correlate with variations in Greenland ice core records since the last glacial period (Hughen et al., 1996; Lea et al., 2003; Peterson et al., 2000). The records reveal that southward shifts of the Intertropical Convergence Zone (ITCZ) and associated changes in north-easterly trade winds are linked to cooling episodes recorded in Greenland ice cores. Model results suggest that the two regions may be connected through an atmospheric bridge, as changes in the extent of high latitude sea ice can affect meridional displacements of the ITCZ (Chiang et al., 2003).

Today's seasonal migration of the ITCZ, which is a zone of low pressure, has large climatic impacts in tropical Atlantic regions. During boreal winter the Cariaco Basin cool and dry as the north-easterly trade winds lie directly overhead. In the summer, however, the ITCZ migrates north and is responsible for the annual rainfall maximum in the region. For the north-eastern Brazil, the effect is opposite as the ITCZ overlies the region during winter (Lea et al., 2003). Hence, winter is the time of maximum precipitation, while summer is associated with dry climate as the ITCZ has moved northward. Paleoceanographic proxies suggest that the modern system is an analogue for past long-term variability. During North Atlantic cooling the Cariaco Basin experienced dry climate (Peterson et al., 2000) , while north-eastern Brazil was wet (Wang et al., 2004). The variations in rainfall is also reflected in the Ti and Fe content of marine sediments off the northern South American coast. High input of Fe and Ti is interpreted to reflect high input of fine terrigenous components as a result of increased runoff from the continent. In the Cariaco Basins the highest Fe and Ti

concentrations are found in sediments deposited during periods of northern warming (Lea et al., 2003). In contrast, increased runoff from north-eastern Brazil occurred during northern cooling (Arz et al., 1999a).

The migration of the ITCZ is related to SST, and the SST in the Cariaco Basin and the north-east Brazilian shelf area thus also differ from each other. In the Cariaco Basin SST variations demonstrate an in-phase relationship with variations in the northern North Atlantic. A little further east, however, the relationship is opposite. During Heinrich event H1 and the Younger Dryas, which were periods of intense cooling in the Northern Hemisphere, significant warming is detected in the western tropical Atlantic. The opposite variations in climate experienced by the two tropical locations, suggest that the atmospheric bridge is not the only pathway that has influenced tropical ocean changes in the past. The anti-phase response agrees more with what would be expected due to changes in the AMOC. Reduced North Atlantic deep water formation would result in a northern cooling, while the tropical thermocline and much of the southern hemisphere would experience concomitant warming (Crowley, 1992). This anti-phase relationship between the hemispheres has been documented by proxies for both SST and ocean ventilation (e.g. Arz et al., 1999b; McManus et al., 2004; Rühlemann et al., 1999) .

Furthermore, it has been proposed that intermediate water formed in high southern latitudes can influence the tropical thermocline (Liu and Curry, 1999). Hence, an oceanic tunnel also connects high and low latitudes. The meridional transport of heat by intermediate water masses is similar to that of the deep water masses {Talley, 1999 #202}, and changes in the flux or properties of intermediate waters feeding the thermocline, could influence the temperature conditions in the tropical upper ocean both at intermediate depths and at the surface. The most important of the intermediate water masses is the Antarctic Intermediate Water.

2 Study area

The study area is located around 4°S 37°W on the continental margin off North-eastern Brazil and is directly influenced by the North Brazil Current (NBC) (Arz et al., 1998). The sediments used in the geochemical analyses are sampled from three gravity cores taken along a transect at depths of 700 m, 898 m and 1000 m. Core locations and major water currents are indicated in Figure 7.

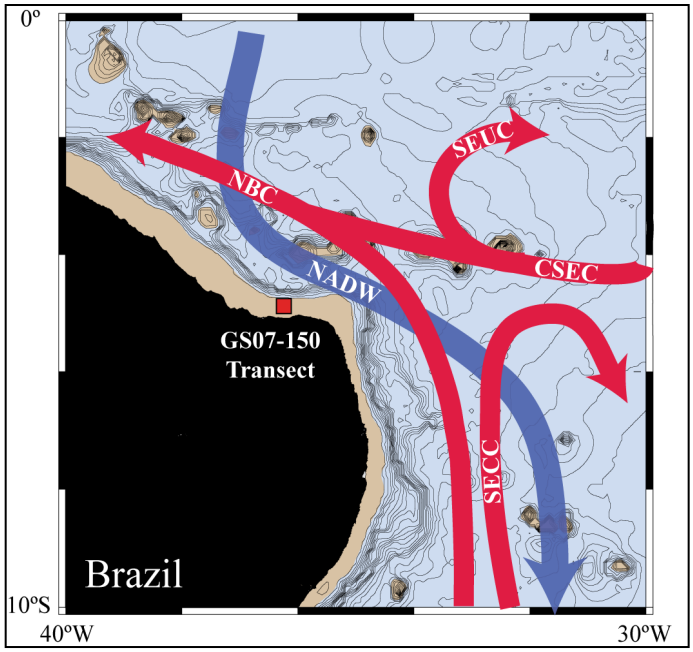

Figure 7: Chart of the western tropical Atlantic Ocean showing the surface circulation patterns and the location of the core transect (after Tisserand, 2009). Abbreviated terms are CSEC = Central South Equatorial Current, SEUC = South Equatorial Undercurrent, SECC = South Equatorial Countercurrent, NBC = North Brazil Current and NADW = North Atlantic Deep Water

2.1 Geological setting

The Northeast Brazilian coast consists of a 50 to 100 km wide belt of plains that borders a coastal mountain chain as high as 1500 m (Arz et al., 1999a). The climate is semi-arid (Knoppers et al., 1999), and only small rivers drain the area, with the exception of the Rio Jaguaribe which has a relatively wide drainage basin (Arz et al., 1999a). The continental shelf along the coast is narrow (30 km wide on average) and shallow (50-80 m) (Arz et al., 1998, 1999a; Knoppers et al., 1999) with large erosional channels cutting into it. Due to little freshwater runoff, the shelf is mainly covered by biogenic carbonate sediments (Knoppers et al., 1999) with terrigenous sediments only occurring on the inner shelf area (Arz et al., 1998). The supply of terrigenous sediments to the shelf has, however, varied in the past depending

on changes in the continental climate. A study by Arz et al. (1999a) linked the Fe/Ca and Ti/Ca ratios in sediment cores to increased runoff from the Northeast Brazilian continent due to humid climate conditions during the repeated slowdown of the THC in the last deglacial period.

The low gradient upper continental slope is characterized by smooth settling area incised by large canyons and channels. These morphological features were probably formed during periods of low sea level (Arz et al., 1998). At about 1000 m depth an escarpment marks the transition from the low gradient upper continental slope to a much steeper lower slope with a gradient of up to 11°. The depth of the base of the slope is 1600±3600 m. From here, the ocean basin stretches out, characterized by a chain of seamounts of which several pierce the surface (Knoppers et al., 1999) (Figure 7). A three-dimensional image of the core transect area is given in Figure 8. The image show the main coring transect of the third RETRO cruise (MD09-173). The core sites in this study are positioned along the same straight line. They are «twin cores» of the CASQ cores marked in pink. GS07-150-20/2-GC, GS07-150-18/2-GC GS07-150-17/1-GC are positioned on the transect, at 700 m, 898 m and 1000 m, respectively. As indicated by the 3D image, extensive site surveying was necessary in order to be able to place good coring sites, avoiding the many canyons or channels that split the sea floor.

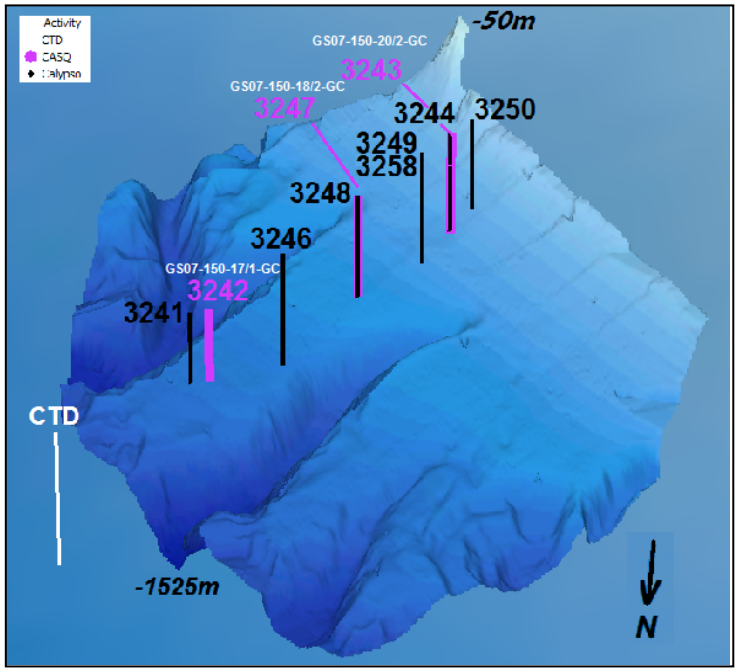

Figure 8: Three-dimensional image of the main coring transect of the MD09-173 RETRO III coring expedition. In the figure, the shallowest core MD09-3250 (04°16.22'S; 37°09.03'W) is from 600 m, while the deepest core MD09-3241 (04°12.98'S; 37°04.48'W) is from 1000 m. As indicated in the figure, the cores used in this figure are «twin cores» of the CASQ cores marked in pink. GS07-150-20/2-GC, GS07-150-18/2-GC GS07-150-17/1-GC are positioned on the transect, at 700 m, 898 m and 1000 m, respectively.

2.2 *Oceanographic setting*

The surface- and deepwater hydrography of the region off northeastern Brazil is an important part of the circulation of the tropical Atlantic Ocean. Considering that a large part of the Atlantic Meridional Overtuning Circulation (AMOC) passes through this region, changes in heat and volume transport by the water masses in this area would have a significant effect on North Atlantic climate.

2.2.1 Vertical distribution of the water masses

Figure 9 displays a schematic profile of the water column of the study area, showing the major water masses that are carried along the North East Brazilian shelf. Moving northwards in the upper 1200 meters are the Tropical Surface Water (TSW), South Atlantic Central

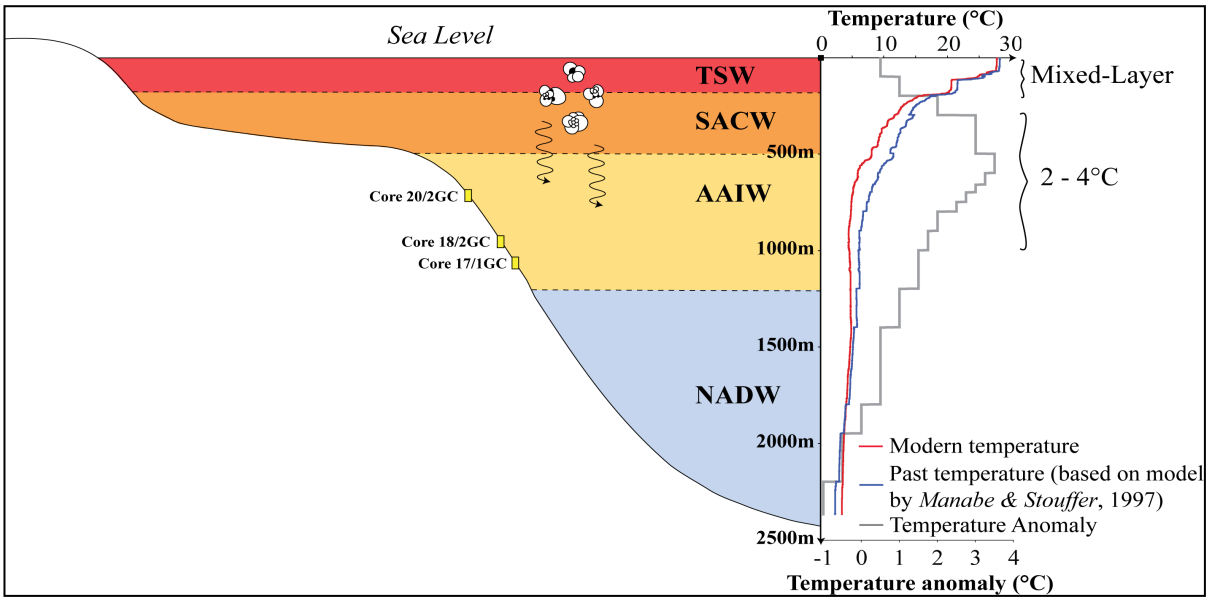

Figure 9: Vertical distribution of water masses in the study area (after Tisserand, 2009). Abbreviated terms are: TSW = Tropical Surface Water, SACW = South Atlantic Central Water, AAIW = Antarctic Intermediate Water and NADW = North Atlantic Deep Water. Planktonic foraminifera are observed to live in the TSW and SACW. The core locations are indicated by yellow rectangles. A modern temperature profile is drawn in red (Bainbridge, 2004), while past temperature, based on the model by Manabe and Stouffer (1997) is depicted in blue. The temperature anomalies are shown in grey.

Water (SACW), Antarctic Intermediate Water (AAIW) and upper Circumpolar Deep Water (uCDW). North Atlantic Deep Water (NADW) moves southward between 1200 and 4000 m (Stramma and Schott, 1999). North of the study area, between 0°40N and 1°40S Antarctic Bottom Water (AABW) is carried into the northern hemisphere at a depth of 4500m (Schott et al., 2003). A modern temperature profile based on measurements from a site close to the study area (Bainbridge, 2004) is shown to the right. A temperature profile associated with

weak AMOC is depicted in blue. This curve is based on the model by Manabe and Stouffer (1997). The temperature anomalies are shown in grey, highlighting the warming at intermediate depths.

The TSW with temperatures of about 27°C is the surface mixed layer of the tropical Atlantic Ocean. Due to mixing this layer is characterized by uniform hydrographic properties. It constitutes an essential element of heat and freshwater transfer between the atmosphere and ocean. Below the mixed layer is a zone of rapid transition, called the seasonal thermocline, where temperature drops from 25°C to 15°C in approximately 50 m. The lower boundary of the TSW is considered to be the 20°C isotherm. Two types of SACW are found spreading northward underneath the TSW. The lighter type has its source in the southwestern subtropical South Atlantic and circulates in the subtropical gyre, while the denser type is from the southern South Atlantic and the South Indian Ocean and flows northward with the Benguela Current (Stramma and Schott, 1999). According to Sprintall and Tomczak (1993) and Tomczak and Godfrey (1994) most of the SACW found in the tropics originate from the

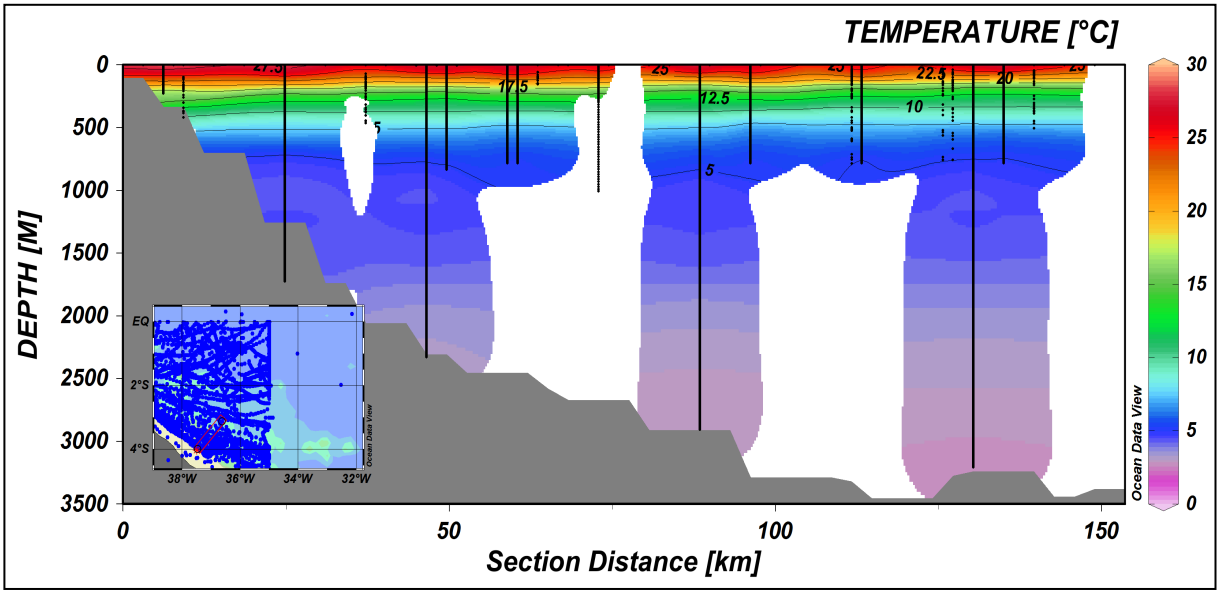

Figure 10: Observed autumn temperature (°C) in the water column along a southwest-northeast transect off north-east Brazil, close to the study area. The data are provided by World Ocean Circulation Experiment (WOCE, 2002).

Indian Ocean. The isopycnal, σ=27.1, at about 500 m indicate the transition between the SACW and the AAIW. The AAIW originates from a surface region of the Antarctic Circumpolar Current. Beneath the AAIW is the uCDW. Both these water masses flow from the South Atlantic towards the North Atlantic, and because of its small vertical extent near the equator the uCDW is included in the AAIW layer in Figure 9 (Stramma and Schott, 1999).

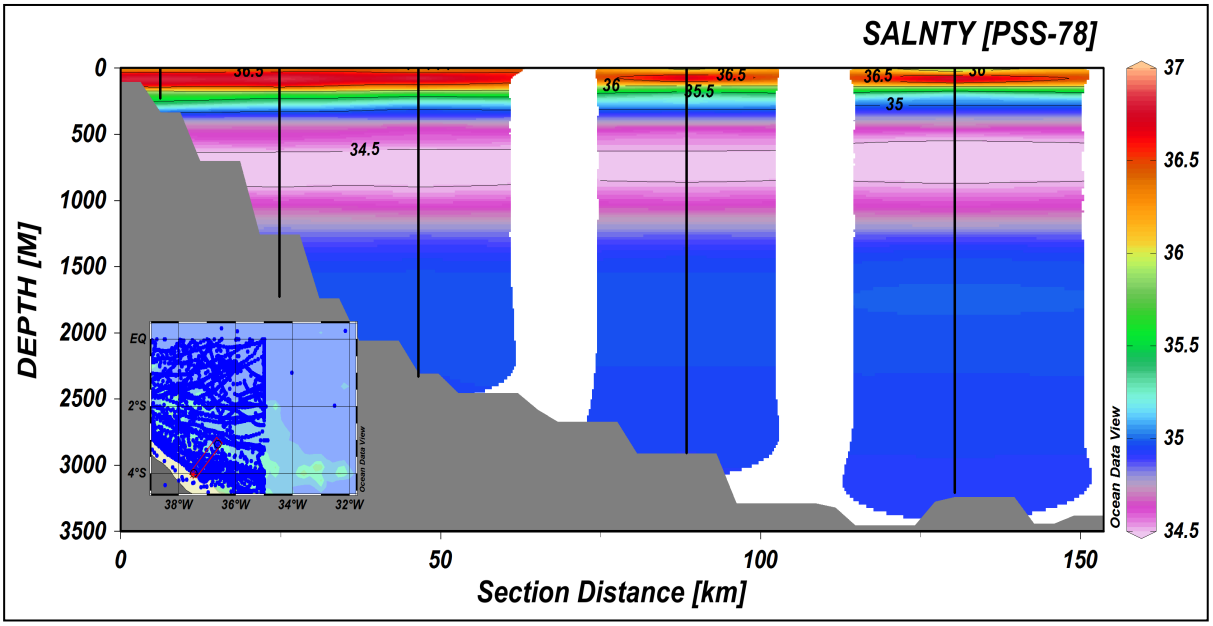

Figure 11: Observed autumn salinity in the water column along a southwest-northeast transect off north-east Brazil, close to the study area. The data are provided by World Ocean Circulation Experiment (WOCE, 2002).

The subpolar gyre in the Greenland Sea is believed to be the main source region of the NADW, while AABW has two source areas; the continental shelf around Antarctica and deep levels in the Antarctic Circumpolar Current (Brown et al., 2001).

Figure 10 and Figure 11 display profiles over the observed temperature and salinity in the water column along a depth transect off the northeastern Brazilian coast, close to the study area. The transect is shown in the lower left corners of each figure, and all the measurements are indicated by black dots and lines. The profiles are made by gridding the measurement data, and due the scarcity of measurements, parts of the profiles are left blank. It is still evident from both parameters that the upper waters are highly stratified. The AAIW and NADW can be recognized in both the temperature and the salinity profile. All three cores used in the study, are bathed in AAIW, and the mixed layer can be distinguished by the largest temperature gradient that seems to be around 200 m.

2.2.2 Surface hydrography

The subtropical gyre of the South Atlantic lies beneath the subtropical high-pressure zone between 10°S and 40°S (Brown et al., 2001) and reaches depths of 500-1000 m (Peterson and Stramma, 1991). The gyral current system is related to the overlying anticyclonic wind system that blows around the subtropical high-pressure region and creates a geostrophic current in the anticlockwise direction. The centres of oceanic gyres tend to be displaced towards the western side of the oceans. Consequently, western boundary currents, which flow along the western sides of oceans, are fast, deep and narrow, while eastern boundary currents are slow, wide and shallow. The South Atlantic has the Brazil Current as its western boundary current and the Benguela Current as its eastern boundary current (Brown et al., 2001). The Benguela Current carries TSW and SACW in a north-westward direction across the basin (Garzoli et al., 2004). It sets out as a northward flow off the Cape of Good Hope before it bends towards the northwest and separates from the African coast at around 30°S while widening quickly (Peterson, 1990). The current feeds into the South Equatorial Current (SEC) that flows westward towards the north-eastern coast of South America (Peterson and Stramma, 1991). The large-scale upper-level surface currents in the South Atlantic Ocean is illustrated in Figure 12.

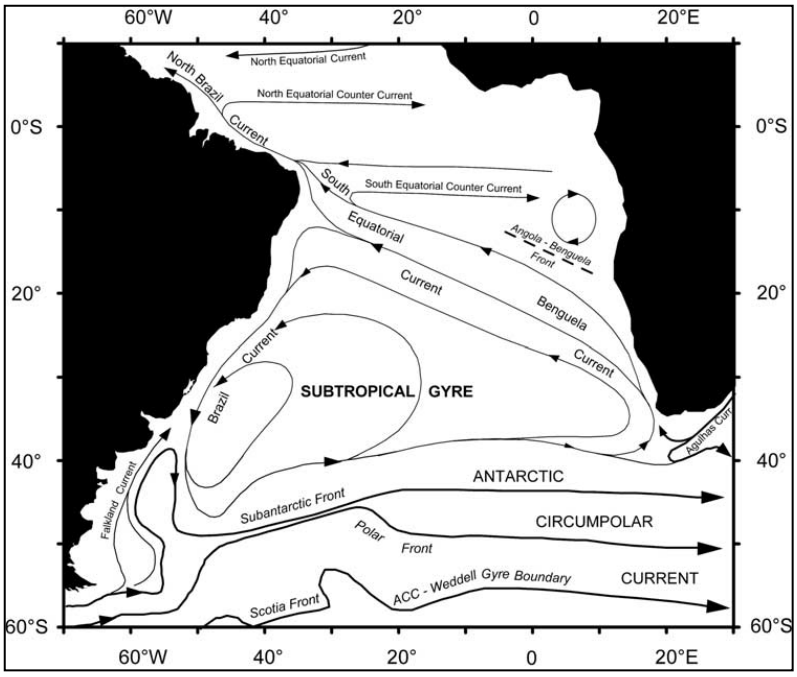

Figure 12: Schematic representation of the large-scale, upper-level surface currents and fronts in the South Atlantic Ocean (after Peterson and Stramma, 1991).

Near 10°S the southernmost of three branches of the SEC, the Southern South Equatorial Current (SSEC), splits into the northward-flowing North Brazil Current (NBC) and the southward-flowing Brazil Current (BC) (Stramma and Schott, 1999). The NBC is the stronger of the two. It continues its flow into the northern hemisphere and partly accounts for the net northward transport of warm surface water from the South Atlantic to the north (Peterson and Stramma, 1991). South of 5°S the NBC is a weak surface current transporting only 3-5 Sv in the surface layer. Most of

the transport occurs in the thermocline, in an undercurrent component called the North-Brazil Undercurrent (NBUC). The NBUC follows the coast carrying around 23 Sv above 1000 m depth with a velocity maximum near 100-200 m (Arz et al., 1998; Johns et al., 1998). Near 5°S the northward transport is approximately 15-20 Sv (Peterson and Stramma, 1991; Stramma et al., 1995). At this latitude water from the Central South Equatorial Current enters the NBC system from the east at about 35°W, intensifying the transport. The NBUC rises to the surface and transforms the NBC into a more surface-intensified current as it moves towards the equator (Arz et al., 1999a; Johns et al., 1998). At about 44°W, the NBC has become about 300 km wide and transports approximately 32 Sv equatorward in the upper 600 m (Schott et al., 1993). A schematic overview of the upper ocean circulation in the tropical Atlantic is shown in Figure 13.

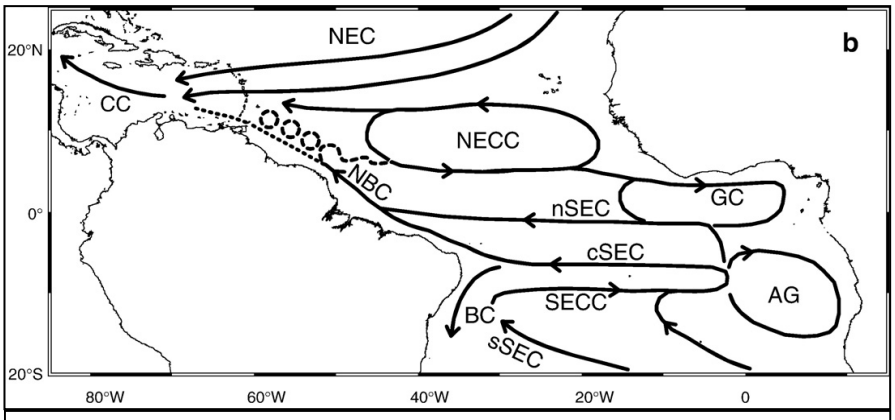

Figure 13: Modern oceanographic setting of the tropical Atlantic and Caribbean, showing major surface currents. Abbreviated terms are CC = Caribbean Current, NEC = North Equatorial Current, NECC = North Equatorial Countercurrent, NBC = North Brazil Current, BC = Brazil Current, GC = Guinnea Current, n(s;c) SEC = northern (southern; central) South Equatorial Current; SECC; South Equatorial Countercurrent and AC = Angola Current (after Steph et al., 2009).

North of the equator the NBC looses water to a number of eastward flowing counter currents: the North Equatorial Counter current (NECC), the Equatorial Undercurrent (EUC) and the North Equatorial Undercurrent (Johns et al., 1998). The surface layer of the NBC retroflects seasonally into the NECC at 6-7°N from June to January. During the rest of the year, however, NBC surface water is assumed to continue northward along the coast and join the westward flow of the North Equatorial Current as it enters the Caribbean. In the thermocline layer a portion of the NBC retroflects around the equator to feed the EUC. Another portion separates from the flow at 3-4°N and seasonally feeds into the NEUC. Parts of this retroflected thermocline water may be recirculated back into the NBC (Johns et al., 1998). At

retroflection rings are shed from the NBC (Figure 13). The shedding of rings represents a significant transfer of mass and heat. According to (Garzoli et al., 2004) it has been suggested that the rings might account for one third (ca. 3 Sv) of the total upper transport in the AMOC. Together with estimates of direct flow of NBC water to the Caribbean, the combined volume transport is in the order of 8 Sv/yr. This is about half of the volume needed to complete the upper interhemispheric loop of the MOC (Garzoli et al., 2004).

2.2.3 Intermediate and deep hydrography

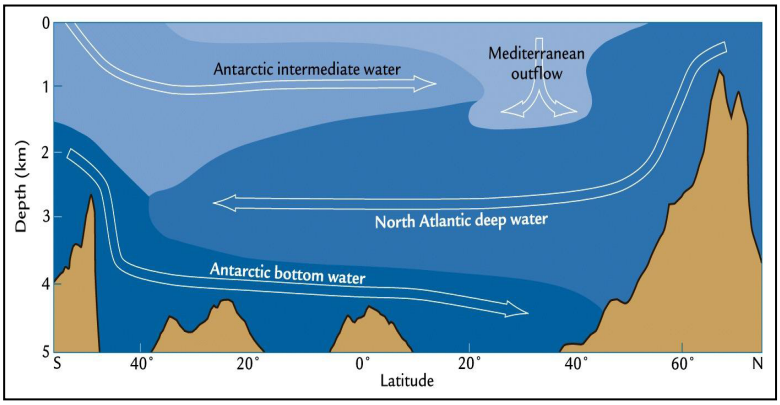

Figure 14: Side view of the circulation in the Atlantic. AAIW flows from the south toward northern high latitudes. It supplies the deep water formation areas in the northern North Atlantic with relatively warm and saline waters. NADW is formed at high northern latitudes, and flows south at depth, eventually joining the waters circling eastwards around Antarctica. Here, dense AABW is formed before it flows northward over the ocean floor (after Ruddiman, 2001).

A schematic figure of the main subsurface water masses in the Atlantic Ocean is presented in Figure 14. Only short descriptions of the AAIW, NADW and AABW are given, as focus in this research will be on the upper-ocean water masses.

Antarctic Intermediate Water is the most widespread intermediate water in the oceans. The water mass forms in the Antarctic Polar Frontal Zone which is located between 50°S and 60°S. It is characterized by low salinity and a temperatures of 2 to 4°C. After sinking at convergences in the Frontal Zone, the water mass spreads northwards throughout the Southern Hemisphere and can be traced to at least 20°N in the Atlantic Ocean. Due to vertical mixing at intermediate depths in the Southern Ocean, the salinity slowly rises as it moves northward. Moreover, the thickness of the water mass decreases from about 1000 m in its formation area to a few hundred meters at the equator (Brown et al., 2001).

North Atlantic Deep Water is primarily formed in the subpolar gyre in the Greenland Sea.

Cold, polar water and ice enter the region through the Fram Strait, while the Norwegian Current brings warm, saline surface water that has been transported from the Southern Hemisphere through the Gulf Stream and North Atlantic Current. In winter, the water becomes dense enough to sink and begins to flow south. The water mass can be followed around the southern tip of Greenland, before it flows along the coast of North-America at a depth of 2000-4000 meters. It continues southeastward, past the eastern tip of Brazil and across the South Atlantic before it ends up in the Southern Ocean where it mixes with Antarctic Circumpolar Deepwater (Brown et al., 2001).

Antarctic Bottom Water is the densest and most widespread water mass in the open ocean. The densest variety of this water forms at various locations over the continental shelf around Antarctica, where water becomes sufficiently dense to sink as a consequence of winter ice formation and cooling, especially in coastal polynyas. The water circulates for some time over the shelf and mixes with toungues of water from the Antarctic Circumpolar Current. The mixtures then flow westward down the continental slope into the deep ocean. Some of these water masses flow north into the subtropics via the Atlantic western boundary current along the continental slope of eastern South America (Brown et al., 2001).

2.2.4 Air-sea interaction

Seasonal changes in the strength of the southeast trade winds lead to variations in the depth of the sharp thermocline that separates TSW from SACW. The trade winds drives a westward flow of water across the basin that results in upwelling of cold water in the east and a pile-up of warm surface water in the west. The equatorial mixed-layer thickness therefore displays an east-west asymmetry as the thermocline dips from the eastern part of the basin towards the western side (Figure 15) (Steph et al., 2009; Wolff et al., 1999).

Trade wind strength is primarily forced by the atmospheric pressure gradient between tropical and subtropical latitudes. The pressure gradient is determined by the temperature contrast between the two regions, and changes in trade wind velocity is thus related to changes in the position of the Intertropical Convergence Zone (ITCZ) (Wolff et al., 1999). The ITCZ is a low pressure zone along which the northeast trades and southeast trades converge. It is generally related to the zone of highest surface temperature, and its position therefore varies seasonally (Brown et al., 2001). Following the march of the sun, the trade wind system moves

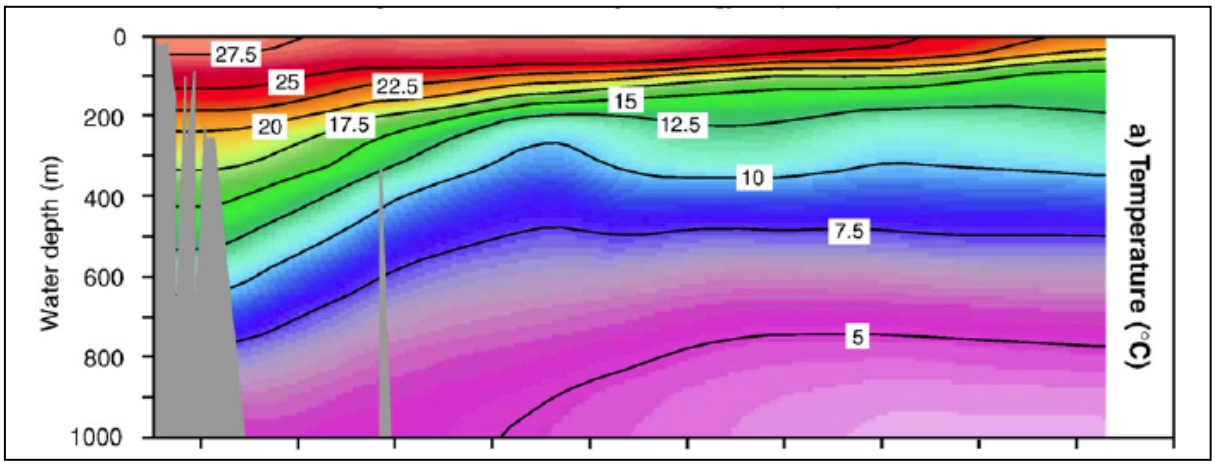

Figure 15: Annual temperature (°C) for the upper 1000 m of the tropical Atlantic and Caribbean water column along an east-west hydrographic section across the tropical Atlantic/Caribbean (13°E, 15°S – 83°W, 21°N). The westward-dipping thermocline is marked by yellow/orange colours (after Steph et al., 2009).

northward over land in the boreal summer and southward over land in the boreal winter (Figure 16).

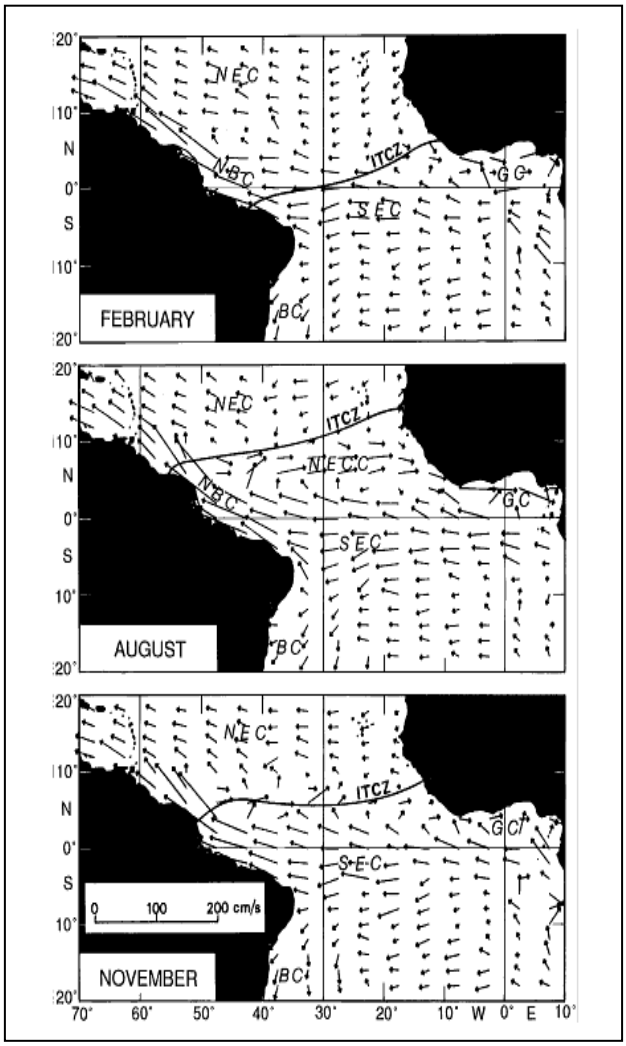

Figure 16: Ship drift velocity vectors for February, August and November, illustrating the variation of surface currents in the tropical Atlantic Ocean throughout the year. The position of the ITCZ is marked by a solid line. Abbreviated terms are NEC = North Equatorial Current, SEC = South Equatorial Current, NECC = North Equatorial Countercurrent, NBC = North Brazil Current, BC = Brazil Current and GC = Guniea Current (after Stramma and Schott, 1999).

Northward migration of the ITCZ in boreal summer leads to a larger temperature constrast between the subtropical and tropical latitudes and an increase in the strength of the southeast trade winds. The SEC is accelerated resulting in a significant increase in mixed-layer thickness in the western tropical Atlantic (Wolff et al., 1999). Consistent with this, Stramma et al.

(1995) observed larger transport by the NBUC and NBC during boreal autumn. In boreal winter the east-west pressure gradient is smaller resulting in weaker trade winds and a smaller thermocline asymmetry across the basin (Wolff et al., 1999). Stramma et al. (1995) observed reduced transport by the NBC and NBUC in boreal spring. Hasenrath and Merle (1987) reported a deepening mixed layer from 60 m in the boreal winter to 100 m in summer. The western Atlantic/Caribbean thus constitutes a major seasonal heat reservoar with large seasonal variations in heat storage. The modern seasonal cycle of the trade winds in the tropical Atlantic has been suggested as an analog for changes in the late Quaternary trade wind system (McIntyre et al., 1989). Studies (e.g. McIntyre and Molfino, 1996) have proposed an eastern shallowing and a western deepening of the thermocline during glacials as a response to enhanced trade wind velocity. With such a long term change in the trade wind system the heat reservoir in the western Atlantic/Caribbean would have a great impact on the Atlantic Ocean heat distribution.

3 Materials and methods

3.1 Marine sediments

The marine sediments used in this study are sampled from three gravity cores taken during the first RETRO cruise, GS07-150, from 7 to 20 December 2007. The cruise took place in the western Atlantic Ocean off North Brazil on the Norwegian research vessel G. O. Sars., which is owned by the Institute of Marine Research (IMR) and the University of Bergen (UoB). During the course of this site survey expedition, TOPAS and Multibeam survey lines as well as gravity cores and multicores were collected. The gravity cores used in this study are presented in Table 1, and the core sites are indicated in Figure 7 and 9. More information about the RETRO expeditions can be found on the RETRO website[1].

3.1.1 Cores GS07-150-20/2 GC, GS07-150-18/2 GC and GS07-150-17/1 GC

Core GS07-150-20/2 GC was taken at 04°15.66S, 37°08.24W at a water depth of 700 m. 264 cm of sediments were recovered, and the core was split in two sections. Section A (bottom) is 150 cm and section B (top) is 114 cm. In the cruise report[2] the top part of the core is described as carbonate clay that is very rich in foraminifera, while the bottom part is made of dark-grey clay.

Core GS07-150-18/2 GC was taken at 04°13.80S, 37°05.95W at 898 m water depth. The core is 276 cm long, and was split in a section A, which is 150 cm and a section B which is 126 cm. This core consists of brown/beige foraminifer rich clay in the top part and dark clay sediments with foraminifera in the bottom part.

The deepest core, GS07-150-17/1 GC, was taken from a water depth of 1000 m at 04°12.98S, 37°04.52W. 282 cm of sediments were retrieved, and the core was split in a 150 cm long A

[1] www.esf-retro.org
[2] http://www.esf-retro.org/page4/files/CR_RETRO_I_20080525.pdf

section and a 132 cm long B section. According to the cruise report, the top part of this core is made up of foraminferal ooze, and the bottom consists of foraminferal and pteropod rich medium grey clay. All the core sites are well above the present lysocline, defined as «the depth at which undersaturation of the carbonate ion occurs» (Takahashi et al., 1980). Hence, preservation of the carbonate material is good.

Gravity core	Latitude	Longitude	Water depth (m)	Core length (cm)
GS07-150-20/2	04°15.655S	37°08.243W	700	264
GS07-150-18/2	04°13.801S	37°05.945W	898	276
GS07-150-17/1	04°12.980S	37°04.515W	1000	282

3.2 Sampling

3.2.1 Sample preparation

All three cores were split lengthwise in an archive half and a working half. The archive halves were scanned using the ITRAX XRF core scanner of the core scanner laboratory at the Department of Earth Science, UoB. Sedimentological preparations of the cores were done at the sediment lab. From the working halves sediment slides were sampled at intervals of 1 cm downcore. Teaspoon samples were taken from each slide to preserve some original material if needed later on. Wet and dry weights of the remains of the samples were registered, before the samples were soaked in distilled water and shaken for about 24 hours to disperse the material. Each sample was wet sieved in tap water in the fractions 63-150 μm and >150 μm. They were then put in a drying cabinet (ca. 55°C) until the water had evaporated, and finally weighed and put in sample glasses.

3.2.2 Selection of timeslice samples

In order to select the sampling depths representing the climatic events of interest in each core, the XRF intensity records of Fe, Ti and Ca were used. The connection of Fe/Ca and Ti/Ca to climate (Section 4.3.1) enabled determination of sampling depths before the age model for the cores was in place. The depths were chosen based on the recognition of prominent variations in Fe/Ca and Ti/Ca assumed to be connected to large climatic changes (Arz et al.,

1999a). Samples were taken from core depths expected to be linked to the Last Glacial Maximum, Heinrich event H1, Bølling-Allerød, the Younger Dryas, the Early Holocene and the Late Holocene. The sample depths are given in Table 2.

Table 1: Timeslices in cores GS07-150 20/2 GC, GS07-150 18/2 GC and GS07-150 17/1 GC

	Core intervals (cm)		
Timeslices	GS07-150 20/2 GC	GS07-150 18/2 GC	GS07-150 17/1 GC
Late Holocene	2 – 3	2 – 3	2 – 3
Early Holocene	42 – 43	55 – 56	70 – 71
Younger Dryas	90 – 91	75 – 76	96 – 97
Bølling-Allerød	116 – 117	98 – 99	116 – 117
Heinrich H1	150 – 151	120 – 121	140 – 141
Last Glacial Maximum	185 – 186	150 – 151	165 – 166

3.3 *Foraminifera and proxy methods*

3.3.1 Foraminifera

The paleoceanographic reconstructions in this study are based on geochemical measurements of the carbonate shells of various species of foraminfera. Foraminifera are single-celled marine protozoans that have been present in the geologic record from the early Cambrian to the present. They can be planktonic or benthic and inhabit all marine environments; from the intertidal zone to the deep ocean floor. Their geographical distribution ranges from the poles to the tropics (Culver, 1993), but the largest variety of species are found at subtropical and tropical latitudes (Bé and Tolderlund, 1971a). 4000 species of foraminfers are estimated to live in the oceans today, out of which 40 live in the planktonic realm (Culver, 1993). In this research only planktonic species are used.

A foraminifer consist of a skeleton (or test) built of one or more chambers that surround the cytoplasm of the organism. The chambers are connected by holes called foramens from which the order Foraminiferida got its name. The walls of the chambers most commonly consist of

secreted calcium carbonate or silica, or secreted organic matter, but they can also be made up of agglutinated particles. Through perforations in the test, some species extend thin organic filaments called rhizopodia. Rhizopodia are used in locomotion, anchoring and feeding, depending on the various species. Their diet consists of diatoms, algae, bacteria and dissolved organic material, and some species host symbiotic algea that provide them with steady nourishment (Culver, 1993).

Planktonic foraminiferal species live in the upper parts of the ocean. However, observations have revealed that different species live and calcify at different depths in the water column. Three depth habitats are recognized: shallow (0-50 m), intermediate (50-100 m) and deep (>100 m). Typically thin-walled, symbiont-bearing, spherical forms inhabite near-surface waters, while thicker-walled, keeled, symbiont-free forms are more plentiful deeper in the water column (Culver, 1993). The species-specific preferential depth habitat is considered to be a function of environmental and/or hydrographical conditions.

Foraminifera make up a very important marine fossil group in geological studies. During sedimentation, the protoplasm of the foraminifera is dissolved, while their hard tests are preserved in the geologic record. The fossil tests have proven very useful in paleoclimatological studies. Past oceanic environments can be reconstructed based on the geographical distribution and geochemical properties of the foraminiferal tests. Oxygen and carbon isotopes, as well as trace elements like Mg and Sr, are incorporated into their carbonate shells and can be used to reconstruct past temperatures and ocean hydrography (Culver, 1993). In this study two geochemical temperature proxies are used: the Mg/Ca ratio and the oxygen isotopic composition of foraminiferal calcium carbonate tests. The study makes use of the observed depth stratification of various planktonic species in an attempt to reconstruct variations in temperature stratification in the upper water column.

3.3.2 Presentation of the planktonic foraminferal species

The selection of planktonic foraminiferal species was based on their respective preferred habitat depths in the water column and on which species were actually present in the samples. Emphasis was also put on choosing species that had previously been used in similar studies, so that comparison to the results in this study could be made. Two shallow dwellers, two

intermediate dwellers and one deep dweller were chosen: *Globigerinoides ruber* (white variety), *Globigerinoides trilobus*, *Globigerinita glutinata, Globigerinella siphonifera* and *Globorotalia truncatulinoides* (dextral). The species are presented below. The descriptions are based on an identification scheme by Bé (1967) which mostly agrees with the classification of Parker (1962). Scanning Electron Microscope (SEM) photographs of the different species (Figures 17, 18, 19, 20 and 21) are provided by Saskia Kars from the Vrije Universiteit in Amsterdam. The specimens photographed are from Multicore 24/3 MC-A, retrieved during the the first RETRO cruise (GS07-150).

Globigerinoides ruber (d'Obrigny, 1839)

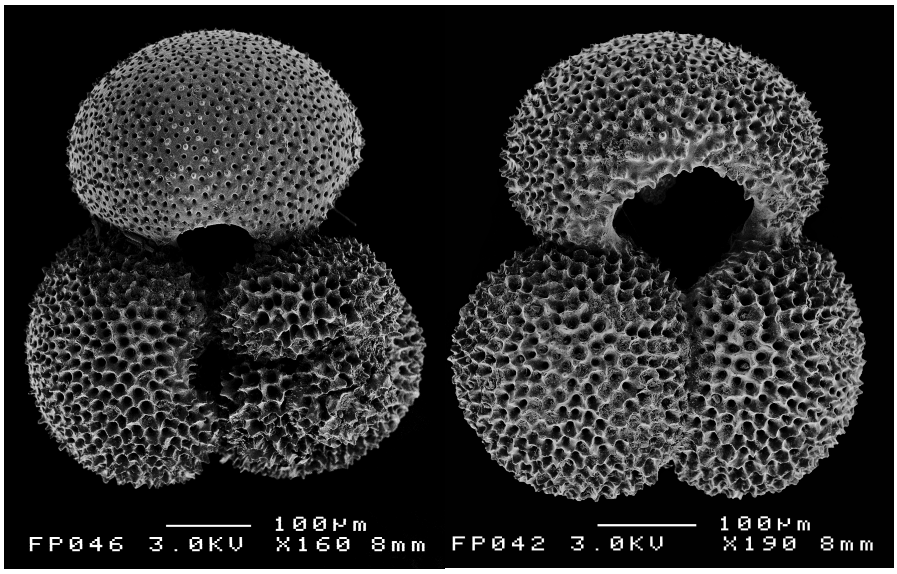

Figure 17: G. ruber (white). Spiral and umbilical view. The white line below each specimen represents a scale of 100 µm to indicate the size of the species.

G. ruber is found in subtropical and tropical surface waters, and is the second most abundant species of planktonic foraminfera in the tropical Atlantic Ocean. The species is trochospiral and spinose. It adds five chambers per whorl as a juvenile and three chambers per whorle as an adult (Bé, 1967). *G. ruber* is found over a surface temperature range of 13.3°C to 29.5°C, with the highest abundance occurring above 21.3°C. The optimum salinity range of the species is 34.5 to 36 psu (Bé and Tolderlund, 1971b).

Plankton-tow studies have indicated that *G. ruber* is a good indicator of tropical surface water conditions (Anand et al., 2003; Field, 2004; Ravelo and Fairbanks, 1992). The species show little variation in depth habitat and is confined to the mixed layer. Since it has a nearly uniform annual occurrence (Tedesco and Thunell, 2003), *G. ruber* is a useful species for reconstructing annual conditions (Lin et al., 1997). Some specimens of *G. ruber* have a pink

to red coloration. The pink colour has been attributed to a pigment within the shells lamellae (Bé and Hamlin, 1967), which might be related to the presence of zooxanthellae. Studies have shown that the abundance maximum of the pink variety of *G. ruber* is related to warmer waters than that of the abundance maximum of the white specimens (e.g. Bé and Tolderlund, 1971b). In agreement with this, Steph et al. (2009) observed lower $\delta^{18}O$ values for *G. ruber* (pink) than for *G. ruber* (white) in the tropical Atlantic. In order to lower the variability in the proxy measurements for *G. ruber*, only white specimens are picked.

Globigerinoides trilobus (Reuss, 1850) = *Globigerinoides sacculifer* (Brady, 1877)

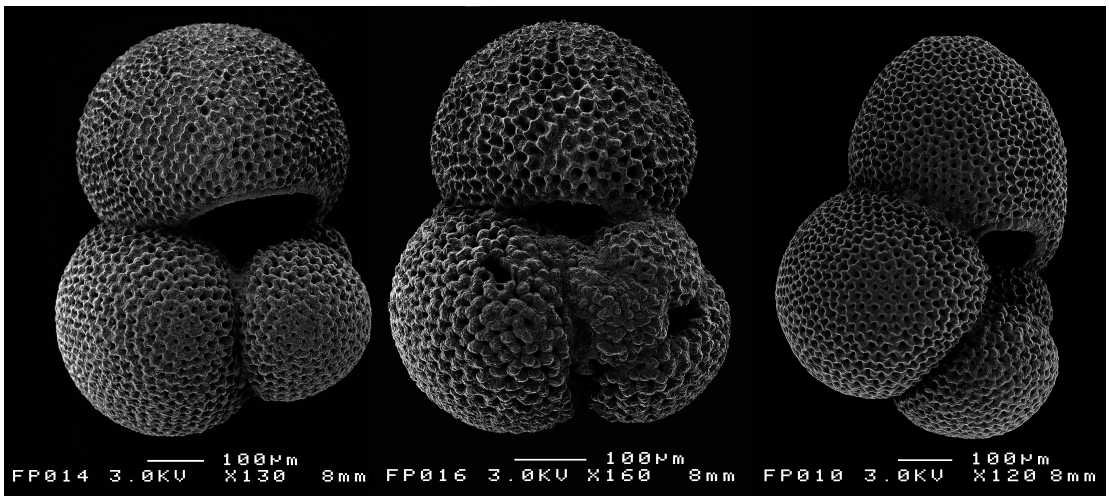

Figure 18: G. trilobus. Umbilical and spiral view. The white line below each specimen represents a scale of 100 µm to indicate the size of the species. The specimen to the right is a G. sacculifer with a sac-like final chamber.

G. trilobus is the dominant foraminiferal species in tropical surface waters, and is also commmon in the subtropics. The species is trochospiral and ovate with a spinose and honeycomb texture. Juveniles add six to seven chambers per whorl, while adult specimens add four (Bé, 1967). *G. trilobus* has a temperture range of 13 to 30°C (Boltovskoy and Wright, 1976) and a salinity range of 34.5 to 36 psu (Boltovskoy, 1981). Greatest abundances occur above a temperature of 22.1°C and above a salinity of 36.4 psu (Bé and Tolderlund, 1971b). Like *G. ruber*, *G. trilobus* calcifies in near surface conditions (Anand et al., 2003), and any differences in measured $\delta^{18}O$ between the species have been attributed to vital-effects. The species is essentially considered to be an indicator of summer and autumn conditions in the upper part of the mixed-layer (Bé and Tolderlund, 1971b). *G. trilobus* is the equivalent to the species *G. sacculifer* without it's final sac-like chamber. Specimens of *G.*

sacculifer with the sac-like chamber are considered to have gone through gametogenesis and added a crust of gametogenic secondary calcite which severely affects the over-all geochemical composition of the test.

Globigerinita glutinata (Egger, 1893)

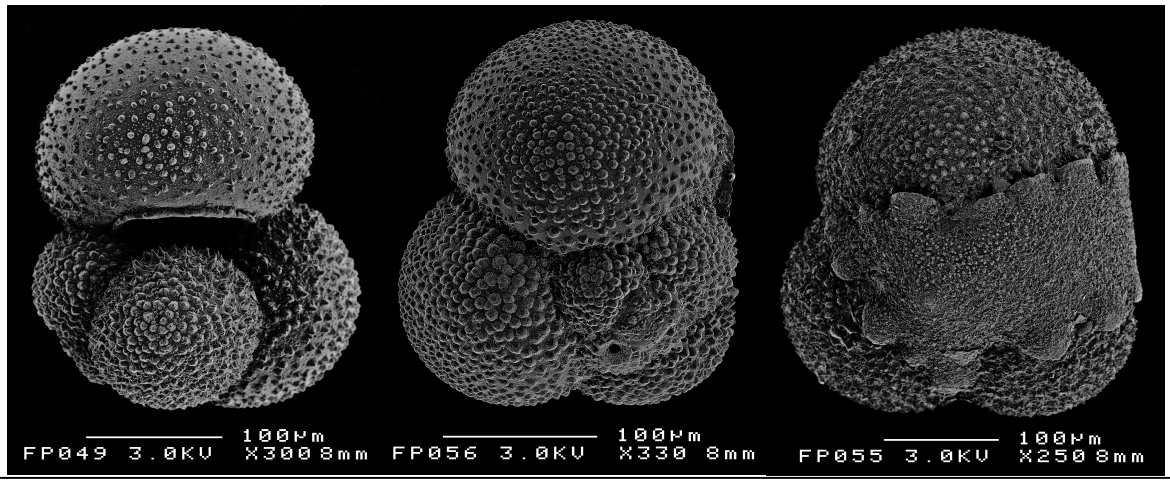

Figure 19: G. glutinata. Umbilical and spiral view. The white line below each specimen represents a scale of 100 µm to indicate the size of the species. In the specimen to the right a bulla covers the final aperture.

The distribution of *G. glutinata* extends from the subpolar regions to the tropics. The species is spherical and trochospiral with a smooth to finely hispid texture. It adds five chambers per whorl in juvenile stages of it's life-cycle and four chambers as an adult. Commonly a bulla covers the final aperture (Bé, 1967). *G. glutinata* lives in a temperature range of 0.3 to 30°C (Boltovskoy and Wright, 1976) with maximum abundance at 24 to 27°C (Bé and Tolderlund, 1971a). The species encompasses nearly the entire range of average surface salinity, occurring from 34.5 to 36.6 psu. Increased population densities are noted between 35.9 and 36.6 psu (Bé and Tolderlund, 1971b). *G. glutinata* is commonly confined to intermediate depths of about 50 to 100 m (Boltovskoy, 1981). It is rare throughout the year, with a possible peak in spring (Bé, 1960).

Globigerinella siphonifera (d´Orbigny, 1839) = *Globigerinella aequilateralis* (Brady, 1879)

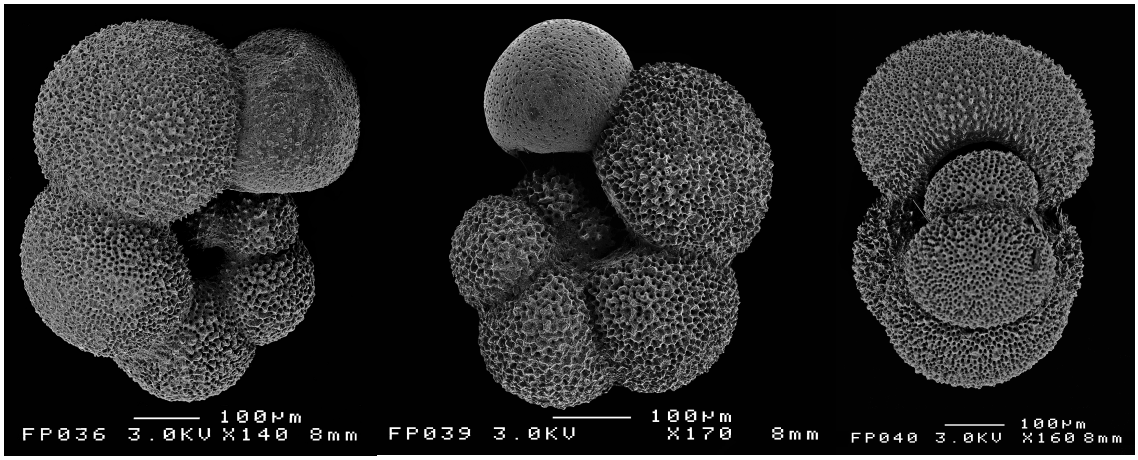

Figure 20: G. siphonifera. The white line below each specimen represents a scale of 100 µm to indicate the size of the species. The specimen to the right demonstrates the near-planispiral outline of the species.

G. siphonifera, which also goes by the name *G. aequilateralis*, is found in the tropics and subtropics. It has a nearly planispiral test with a spinose and hispid texture. The species adds five chambers per whorl as a juvenile and five to six chambers per whorle as an adult (Bé, 1967). *G. siphonifera* has a temperature range of 12-30°C (Boltovskoy and Wright, 1976) and a salinity range between 35.8 and 36.6 psu. Maximum abundance is observed in the temperature range of 17.4 to 25.3°C and the salinity range of 36.5 to 36.6 psu (Bé and Tolderlund, 1971b). *G. siphonifera* also lives at intermediate depths of about 50 to 100 m (Boltovskoy, 1981). It is common throughout the year, but observations from the Sargasso Sea revealed peak summer and fall occurrences (Bé, 1960).

Globorotalia truncatulinoides (d'Obrigny, 1839)

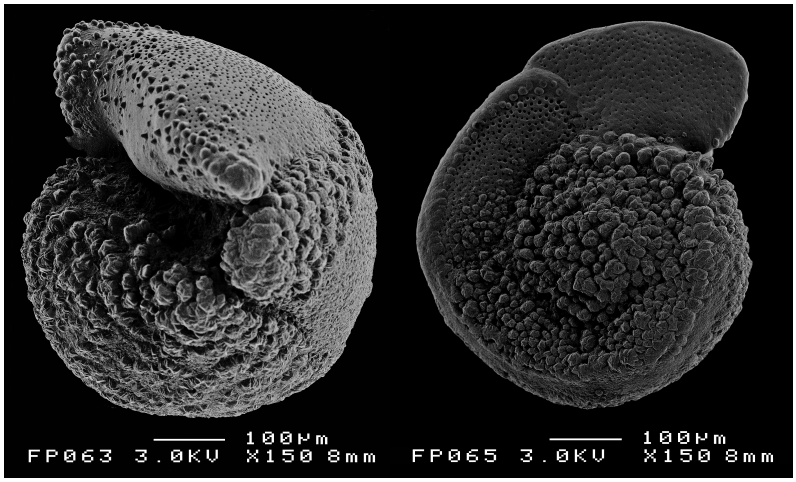

Figure 21: G. truncatulinoides (dextral). Umbilical and spiral view. The white line below each specimen represents a scale of 100 µm to indicate the size of the species.

G. truncatulinoides is most abundant in the subtropics, but is also found in tropical regions. The species has a trochospiral, conical test with a smooth to hispid texture and a well developed keel (Bé, 1967). *G. truncatulinoides* occurs over a broad range of temperatures and salinities. Boltovskoy and Wright (1976) reported a temperature range of 2.9 to 27.0°C, while optimum concentrations are registered between 15.4 and 22.0°C. It's tolerance of salinity ranges from 35.8 to 36.6 psu, but the speices is most abundant between 35.9 and 36.6 psu (Bé and Tolderlund, 1971b).

G. truncatulinoides has a sharply limited seasonal distribution which makes the species a good indicator for winter conditions (Bé and Tolderlund, 1971b). It is known to live at great depths, but migrates to shallower depths during spring for reproduction. The species shows a pronounced relationship with the vertical temperature or density gradients (Hilbrecht, 1996), and according to Mulitza et al. (1997) it lives beneath the thermocline in the western tropical Atlantic. Initial calcification occurs around 200 m, while secondary calcification happens at about 400 m depth. Hence, *G. truncatulinoides* can be assumed to record conditions in the central water masses, which in the tropical Atlantic is the SACW. Left and right coiling *G. truncatulinoides* constitute two different genetic species (de Vargas et al., 2001), which have different behavior with respect to trace element incorporation (Cléroux et al., 2008). Only right (dextral) coiling specimens were picked for this analysis.

3.3.3 Picking of planktonic foraminfers

The foraminifers were all picked from the >150 μm fraction using a brush to avoid crushing the shells. Prior to picking, the samples were split once, leaving one subset of complete samples and one subset to be picked from. Splitting was done with the use of a splitter that ensures random and equal division of samples. To minimize variability in isotopic values due to the ontogenetic fractionation effect (Section 3.4.2) (Ravelo and Fairbanks, 1995), the samples were dry sieved into narrower size fractions (150-250 μm, 250-400 μm and > 400 μm). The size range for each species was selected in an effort to minimize the growth effect and at the same time ensure that the species was abundant enough to get the material needed for the geochemical analyses. All species and fractions are shown in Table 3. Whole, visually clean specimens of similar sizes within each fraction were preferred.

Table 2: Species, approximate depth habitat and size fractions of planktonic foraminifera used in this study with references used to determine size fraction for each species.

Name of species	Depth habitat	Minimum size (μm)	Maximum size (μm)
G. ruber (w)	Shallow	250	400
G. trilobus	Shallow	250	400
G. sacculifer (w/sac-like chamber)	Shallow	250	400
G. glutinata	Intermediate	150	250
G. siphonifera	Intermediate	250	400
G. truncatulinoides (dex)	Deep	250	400

To aquire a rough $\delta^{18}O$ stratigraphy of each core, specimens of *G. sacculifer* (with the saclike chamber) were picked each 10 cm down core. Amandine Tisserand had previously done this for core 17/1, and the same was done in cores 18/2 and 20/2. For the upper-ocean stratification reconstruction, all five species described above, were picked for oxygen isotope measurements, and two species were picked for Mg/Ca measurements. In the samples the shallow-dwelling G. *trilobus, G. sacculifer* (w/ sac-like chamber) and *G. ruber* (w) generally occur in moderate to high amounts (5-10% to 10-20 %), while the intermediate dwellers, *G. siphonifera*, and *G. glutinata*, occur in moderate amounts. *G. truncatulinoides* was the only deep dweller abundant enough to pick. It's abundance was low throughout the cores, and no specimens were found in the youngest timeslice samples of cores 18/2 and 17/1. In order to ensure some indication of the Holocene oxygen isotope development at depth, specimens of *G. truncatulinoides* were picked at deeper levels in these cores.

For the Mg/Ca ratio analysis, one shallow dweller and one deep dweller were picked. *G. ruber* (w), which is regarded as the best recorder of tropical sea surface conditions (Ravelo and Fairbanks, 1992), was chosen along with *G. truncatulinoides* (dex). Between 28 and 38 individuals of *G. ruber* (w) and between five and 43 individuals of *G. truncatulinoides* (dex) were picked from the 250-400 μm fraction of each sample. Visually clean specimens of approximately the same size were preferred. The occurrence of G. truncatulinoides was very low in some samples, limiting the number of good specimens to pick. In the youngest samples, no individuals of this species were found. Due to the scarcity of this species, the individuals picked varied a lot in size within the 250-400 μm fraction.

3.3.4 The use of proxy measurements in paleoceanographic reconstructions

Most paleoceanographic reconstructions rely on the use of proxy measurements. «Proxy» is short for proxy variable and is commonly used to describe a stand-in. In paleoceanography a proxy is a measurable chemical, physical or biological parameter which «stands in» for an unobservable target parameter such as temperature or salinity. The target parameter is thus only measured indirectly, and «calibration» of the measured parameter to the desired parameter is needed (Wefer et al., 1999). The calibration is done by expressing the target parameter as a function of its proxy:

$$T_{arg} = f(Prox) \qquad \text{(Equation 1)}$$

The quality of the proxy is given by the confidence with which Equation 3.1 predicts the target. This is usually tested in calibration studies, for instance by using samples from core tops or sediment-traps to reconstruct observed present-day conditions in the water column (Wefer et al., 1999).

The correlation between the target parameter and the proxy variable is never perfect. Commonly, a number of parameters influence the same proxy variable, and hence one proxy can have different targets. The oxygen isotopic composition of foraminiferal calcite (expressed as $\delta^{18}O_c$) is a good example (Wefer et al., 1999). This proxy is influenced by both temperature and changes in the seawater chemistry (Emiliani, 1955), so that the temperature estimate has to be corrected for seawater composition. The incorporation of the different oxygen isotopes is also influenced by a number of other factors, which further complicates the interpretation of the measurements.

Moreover, since most proxy carriers are biological, natural variability should also be taken into account. Therefore, it is good practise to estimate the target parameter by using more than one proxy. Such a multiproxy approach gives a greater confidence in the reconstruction (Wefer et al., 1999). The combination of Mg/Ca and oxygen isotope composition has the advantage that temperature estimates can be acquired from the same foraminferal carbonate,

and calculation of the salinity influence on the oxygen isotope composition is sometimes possible (Barker et al., 2005). In Sections 3.4 and 3.5 the concepts of oxygen isotopes and Mg/Ca ratios are discussed, as well as their application in paleoceanographic studies in general and in this study in particular.

3.4 Oxygen isotopes

3.4.1 Stable isotopic fractionation

Isotopes are atoms with the same number of protons, but differing numbers of neutrons within their nuclei. Both stable and unstable (radioactive) isotopes exist. The three isotopes of oxygen are stable, consisting of: ^{16}O, ^{17}O and ^{18}O. Their relative natural abundances are 99.7 %, 0.04 % and 0.20 %, respectively. As the abundances of ^{16}O and ^{18}O are the highest, and the mass difference between them the greatest, research on oxygen isotopes normally concerns $^{18}O/^{16}O$ ratios (Cooke and Rohling, 1999).

Isotopes contain the same number and arrangement of electrons and thus display similar chemical behaviour. However, certain differences in physicochemical properties exist due to the mass difference between them. Consider the water molecules $H_2{}^{18}O$ and $H_2{}^{16}O$: The first molecule contains an oxygen atom with two extra neutrons in its nucleus making it slightly heavier than the latter. Molecules vibrate with a fundamental frequency, which depend on their mass. Hence, molecules of the same chemical formula that have different isotopic species, will have different fundamental frequencies. As a result, the molecules have different dissociation energies, so that the bonds formed by the light isotope are weaker than those formed by the heavy isotope. Consequently, $H_2{}^{16}O$ molecules will generally react slightly more readily than $H_2{}^{18}O$ molecules (Hoefs, 2004). An example of this is given by the evaporation of water at the sea-air interface:

$$H_2{}^{16}O_{liquid} + H_2{}^{18}O_{vapor} \leftrightarrow H_2{}^{18}O_{liquid} + H_2{}^{16}O_{vapor} \qquad \text{(Equation 2)}$$

As molecules made up of lighter isotopes have higher vapour pressures, they will evaporate more easily. Thus the lighter molecular species are preferentially enriched in the vapour phase. Continuing evaporation causes the vapour to be enriched in ^{16}O and depleted in ^{18}O,

while the water becomes enriched in ^{18}O and depleted in ^{16}O. This effect is called isotopic fractionation (Cooke and Rohling, 1999).

Isotopic fractionation refers to the process in which partitioning of isotopes between two substances or two phases of the same substance with different isotope ratios, occurs (Hoefs, 2004). There are three types of fractionation: isotope exchange reactions, kinetic fractionation, and molecular diffusion fractionation (Sharp, 2007). Isotope exchange reactions constitute the most important type of fractionation in paleoceanographic studies. The term is used for situations where there is no net reaction, but where the distribution of isotopes changes between different chemical substances or different phases that are in equilibrium {Hoefs, 2004 #38;}. The exchange is therefore also called «isotopic equilibrium fractionation». Isotopic equilibrium fractionation is basically temperature dependent; a fact that is applied in paleotemperature reconstructions. At very high temperatures fractionation tends to become zero, and at low temperature it is much higher (Allègre, 2008). Kinetic fractionation is associated with incomplete, unidirectional processes like evaporation, biologically mediated reactions and diffusion (Hoefs, 2004). This type of fractionation causes deviation from equilibrium and happens due to different chemical reaction rates of the various isotopic species (Cooke and Rohling, 1999). The deviations complicate the interpretation of oxygen isotope ratios in paleoceanographic studies.

Fractionation is expressed by the fractionation factor, α: $\alpha_{A\text{-}B} = R_A/R_B$, where R_A and R_B are the ratios of the light and heavy isotopes in two chemical compounds, A and B, that exchange isotopes (Hoefs, 2004). However, in practice it is common to express isotopic composition in terms of delta (δ) values rather than the absolute value of the fractionation factor. For oxygen isotopes the per mil difference (δ) is measured between the $^{18}O/^{16}O$ ratio in the sample and in a fixed standard by measuring the sample and the standard in an alternating fashion through a mass spectrometer (Emiliani, 1955). It is expressed as:

$$\delta^{18}O = (((^{18}O/^{16}O)_{sample} - (^{18}O/^{16}O)_{standard})/ (^{18}O/^{16}O)_{standard}) \times 1000 \qquad \text{(Equation 3)}$$

(Emiliani, 1955)

3.4.2 Paleoclimatological applications of oxygen isotopes

Most foraminiferal species precipitate calcium carbonate from the surrounding water and, thus, incorporate oxygen isotopes into their tests. The reaction involved in the precipitation is:

$$Ca^{2+} + 2HCO_3 \Leftrightarrow CaCO_3 + CO_2 + H_2O \qquad \text{(Equation 3.4)}$$

(Cooke and Rohling, 1999)

The oxygen isotope ratio that is incorporated into the test of an individual, mainly depends on the temperature and oxygen isotope composition of the ambient seawater and the so-called «vital effects» of the different species. These three parameters are discussed below.

During precipitation of calcium carbonate, equilibrium fractionation between $CaCO_3$ and water occurs. The fractionation is, as mentioned, a function of temperature which was first shown by Urey in 1947. In 1948 he introduced the idea of oxygen isotope paleothermometry. He suggested that variations in the temperature of precipitation of $CaCO_3$ from water should lead to measurable variations in the $^{18}O/^{16}O$ ratio of the calcium carbonate. Hence, if the $\delta^{18}O$ of the calcite is well preserved, it should be possible to determine the temperature of ancient oceans by measuring the $\delta^{18}O$ of carbonate fossils (Urey, 1947, 1948). The first empirical relationship between temperatures and $\delta^{18}O$ was presented by Mc Crea (1950). Epstein (1953) revised the relationship, which became the classic paleotemperature equation:

$$T(°C) = 16.5\text{-}4.3(Ox_c\text{-}Ox_w)+0.14(Ox_c\text{-}Ox_w)^2 \qquad \text{(Equation 4)}$$

where T is temperature, Ox_c is the $\delta^{18}O$ of the calcite and Ox_w is the $\delta^{18}O$ of the water which the carbonate precipitated from.

The equation reveals that in order to obtain the temperature estimate, the $\delta^{18}O$ of the water must be known. This value has fluctuated through geological time, depending largely on the amount of ice on the continents (Shackleton and Opdyke, 1973). Build-up of ice provides storage of water highly enriched in ^{16}O due to fractionation during repeated evaporation and condensation as the vapour is transported from the tropics to higher latitudes. As a consequence the ocean water is enriched in ^{18}O during ice-build up, and the $\delta^{18}O$ of

foraminiferal calcite varies on glacial-interglacial timescales. Therefore, using the $\delta^{18}O$ of foraminferal shells as a temperature proxy requires an estimation of ice volume (Lea, 2003).

After a correction for ice-volume has been made, the residual $\delta^{18}O$ signal, $\delta^{18}O_{\text{Ica Volume Corrected}}$ (hereinafter $\delta^{18}O_{IVC}$), is related to variations in temperature and salinity of the ambient water, and to so-called «vital effects» of the different foraminiferal species. Salinity is controlled by continental runoff and regional and temporal differences in the precipitation-evaporation balance that influence the $\delta^{18}O$ signature of the ocean water. Increased salinity is reflected in the carbonate as an increase in $\delta^{18}O$, which could lead to a misinterpretation of the data as cooling of the water masses. Separating the salinity signal from the temperature signal is complicated, but in combination with Mg/Ca temperature estimates it is sometimes possible.

The various vital-effects on $\delta^{18}O$ are responsible for out-of-equilibrium fractionation during calcification of the foraminferal tests. Vital-effects are species-specific, and can be divided into four main sources of deviation from equilibrium: the ontogenic effect; the symbiont photosynthesis effect; the gametogenic effect; and the effect of changes in $[CO_3^{2-}]$ (Cooke and Rohling, 1999). The various effects are presented below. They may operate in opposite ways, masking one another. Correcting for vital-effects in this study is not very important as the reconstruction of the past ocean temperature stratification is based on differences in $\delta^{18}O$ between different species. Hence, if the assumption is made that the vital-effects have exerted the same influence on the oxygen isotope incorporation by the respective species through time, the effects can largely be ignored. Still, some thoughts about the effects are given.

<u>The ontogenic effect</u>

Laboratory experiments have shown that the relationship between temperature and foraminiferal $\delta^{18}O$ changes as the foraminifer grows. For each chamber the organism forms, $\delta^{18}O$ increases, so that the juvenile chambers are much more depleted in ^{18}O than the final chamber. The trend is also observed in data from fossils, although the difference is a lot smaller (Cooke and Rohling, 1999). To minimize this size dependent ontogenic effect, smaller grain size fractions were avoided when picking foraminifers for oxygen isotope measurements, and specimens of similar sizes within narrow fractions were preferred. This is done to ensure that only adult specimens are measured (Ravelo and Fairbanks, 1995). Still, for *G. truncatulinoides* (dex), the ontogenic effect might constitute a bias. In some samples, the occurrence of this species was scarce, and the specimens used for the oxygen isotope

analysis varied quite a lot in size within it's sieved sized fraction. This could result in increased intraspecific variability in the measurements.

The symbiont photosynthesis and respiration effect

Some planktonic foraminifera bear photosynthetic symbionts. In a laboratory experiment Spero and Lea (1993) observed an average $\delta^{18}O$ decrease for increasing irradiance levels. This could reflect a relationship between light intensity, photosynthetic activity of the symbiont algae and $\delta^{18}O_{calcite}$. Swart (1983) concluded that it is the respiration of the symbionts that causes the depletion in $\delta^{18}O$. Respiration makes the $\delta^{18}O$ values of the water decrease, and if the foraminifera use these respiration products during calcification, they would incorporate less ^{18}O (Cooke and Rohling, 1999). Of the species used in this study, the effect of symbiont photosynthesis could be a problem for the surface dwellers and maybe also for the intermediate dwellers. *G. ruber* and *G. trilobus* are known to bear symbionts, while *G. glutinata* and *G. siphonifera* are facultative symbiont-bearers. Deep dwellers like *G. truncatulinoides* do not carry any symbionts (Mulitza et al., 2003). As photosynthetic symbionts are associated with a decrease in $\delta^{18}O$, the $\delta^{18}O$ difference between shallow and deep dwellers (Section 5.3) is probably exaggerated. However, since this study does not attempt to quantitatively estimate changes in temperature, the symbiont effect is not important for the interpretation of the results.

Vertical migration/ the gametogenic effect

Many species migrate vertically during their life-cycles and add a secondary crust of calcite in deep waters right before reproduction (gametogenesis). This veneer of calcite is more enriched in ^{18}O (Bemis et al., 1998). The calcite make up quite a large share of the shell's mass, and is thus decisive for its over-all isotopic composition (Cooke and Rohling, 1999). Of the species used in the study, secondary crustification is mainly a problem for *G. truncatulinoides*. As observed in the tropical Atlantic, this species is believed to form it's initial calcite crust at a depth of about 200 m, and then secondary calcite is added at about 400 m (Mulitza et al., 1997). The large depth range of the calcification makes it difficult to assign a particular depth to the temperature signal given by the $\delta^{18}O$ of this species, and large intraspecific variability in $\delta^{18}O$ can be expected.

The effect of changes in $[CO_3^{2-}]$

The effect of carbonate ion concentrations has also been studied through laboratory

experiments. Spero et al. (1997) concluded that $\delta^{18}O$ in foraminiferal carbonate decreases with increasing [CO_3^{2-}] and that the magnitude is strongly species-specific. Carbonate ion concentration in the study area today is low as reported by Bainbridge (2004). Assuming little change since the LGM, this effect can be ignored.

3.4.3 Mass spectrometry

All stable isotope measurements were carried out in the Finnegan MAT 253 mass spectrometer of the Geological Mass Spectrometry (GMS) laboratory at the BCCR. This is a Nier type dual inlet gas source Isotope Ratio Mass Spectrometer (IRMS) that provides an effective method for measuring isotope abundances. The measurements are reported against the VDPD standard. The MAT 253 can measure 46 glass vials in one run, usually with 38 samples and eight standards. In this study, 311 samples of whole foraminiferal tests were measured in total. Any cleaning procedures were skipped as they may cause removal of foraminiferal calcite as well as contaminants, and this may affect the isotopic values. The machine has shown good reproducibility if allowed to expand (Ulysses Ninnemann, personal communication, 2010). Hence, in order to achieve expansion, samples weighing more than 50 µg were used. All the samples were weighed prior to the measurements to ensure that they were large enough.

To reach the required weight, two shells of *G. sacculifer*, two shells of *G. trilobus*, four shells of *G. ruber* (w), three shells of *G. siphonifera*, 11-23 shells of *G. glutinata* and two shells of *G. truncatulinoides* (dextral) were, in general, used for the respective samples. All the foraminiferal species were measured in duplicates for every timeslice in each core.

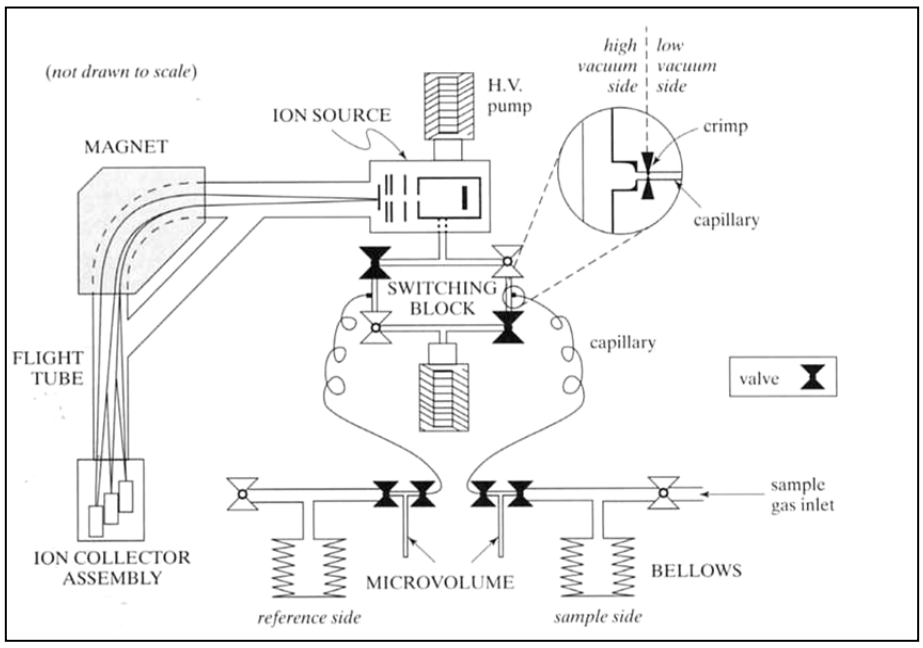

Figure 22: Schematic diagram of a modern spectrometer (after Sharp, 2007)

Duplicate measurements are used as a check on the results, based on the idea that if the two measurements are in reasonable agreement they can be accepted, and the average of the two readings is taken as the reported value (Tietjen and Beckman, 1974). For all *G.truncatulinoides*, (except those of Late Holocene age), an extra set of duplicate measurements were made. This species proved important for the interpretation in the upper-ocean stratification analysis, and it was desireable to make the isotopic signal more robust.

Figure 22 displays a schematic diagram of a mass spectrometer. The instrument consists of four essential parts: the inlet system, the ion source, the mass analyzer, and the ion detector. Before the samples can be introduced in the system, the carbonate has to be converted to CO_2-gas. The Finnegan MAT 253 is equipped with a Kiel carbonate preparation device, which provides automatic generation of CO_2 gas from the carbonate shells, and direct pumping of CO_2 into the inlet system. By reacting 100 % phosphoric acid (H_3PO_4) with the carbonate at 70°C, as demonstrated by McCrea (1950), CO_2 is generated:

$$CaCO3 + H3PO4 \; CaHPO4 + CO2 + H2O \qquad \text{(Equation 5)}$$

A dual inlet system provides one inlet for the reference (standard) gas and one for the sample gas. The pressures of both gases are set to the same value by adjusting the volume of two bellows connected to the system. After the pressures are adjusted, the gases pass through a capillary with a crimp that helps reduce the flow rate and assure viscous flow. Viscous flow, in preference to molecular flow, ensures that isotopic fractionation in the capillary does not happen, and bias in the isotopic signal is avoided. The gases enter the switching block where rapid switching between the reference and sample gas allows for seqential measurements of the isotopic ratios of both gases under almost identical conditions. Hence, noise caused by electronic instability and other factors is eliminated (Hoefs, 2004; Sharp, 2007).

Entering the ion source, sample molecules are ionized by bombardment with electrons. Outer electrons are stripped off, and the resulting positive ions are accelerated and focused into a narrow beam by a series of electric lenses. The ion beam enters the mass analyzer, which is a magnetic field generated by an electromagnet. Here, the ions are deflected into circular paths whose radii are proportional to their mass/charge ratios. Light ions are deflected more strongly than heavier ions of the same charge. In this way, ions are separated into beams according to their ratio of mass to charge. After passing through the magnetic field, the

separated ions are collected simultaneously by multiple Faraday cups, and the inputs are converted into electrical impulses and recorded. The intensities of the recorded voltages are proportional to the amount of gas being collected. The difference between the recorded voltage ratio of the sample and that of the standard is recorded as per mil deviation from the isotopic composition of the standard gas, given as the delta value, δ (Hoefs, 2004; Sharp, 2007).

3.4.4 Standards

The isotopic composition of a sample is measured relative to a working standard. However, the values measured are reported relative to an international standard. Calibration to such international reference standards makes it possible to compare isotopic data from different laboratories. These standards are only available in small quantities, but they can be used to establish larger supplies of working standards. The first international calcite standard was the PeeDee Belemnite (PDB), a powdered specimen of *Belemnita americana* from the Upper Cretaceous Peedee formation in South Carolina. The original supply of PDB is now exhausted, but new standards, such as the Vienna PeeDee Belemnite (VPDB) have been carefully calibrated against the isotopic composistion of the PDB (Sharp, 2007). The International Atomic Energy Agency (IAEA) and the National Institute of Standards and Technology (NIST), formerly known as the National Bureau of Standards (NBS), provides international standards for use in mass spectrometry.

At the BCCR the GMS laboratory calibrates its own internal Carrera Marble working standard (CM03), which is used in the mass spectrometer. External reference standards NBS 19 and NBS 18 are used to convert the measured values to the VPDB reference scale. The long term reproducability of CM03 and NBS 19 is better than 0.1 for $\delta^{18}O$ for all samples running between 6 and 90 µg. In order to compare the $\delta^{18}O$ values of carbonate foraminfera reported relative to VPDB with the oxygen isotopic composition of ocean water which is reported relative to VSMOW, conversions have to be made (Equations 3.7 and 3.8) (Coplen et al., 1983).

$$\delta^{18}O_{VSMOW} = 1.03091 \cdot \delta^{18}O_{VPDB} + 30.91 \qquad \text{(Equation 6)}$$

$$\delta^{18}O_{VPDB} = 0.97002 \cdot \delta^{18}O_{VSMOW} - 29.98 \qquad \text{(Equation 7)}$$

3.5 Mg/Ca

3.5.1 Mg/Ca paleothermometry

Mg/Ca paleothermometry is a relatively new method for reconstructing past ocean temperatures. In 1954, Chave reported that the Mg content in marine microfossils decreased towards higher latitudes. He drew the conlusion that the Mg/Ca ratio in biogenic calcium carbonate is sensitive to temperature, and thus supported early observations of this relationship from the 1920s (Clarke and Wheeler, 1922). Cronblad and Malmgren (1981) suggested the potential application of foraminiferal Mg content in paleoclimatic studies, and in recent years planktonic foraminiferal Mg/Ca thermometry has come about as a powerful proxy to reconstruct past changes in ocean temperature (Barker et al., 2005; Dekens et al., 2002; Elderfield and Ganssen, 2000; Lea et al., 2000; Martin and Lea, 2002; Mashiotta et al., 1999; Nürnberg, 1995; Nürnberg et al., 1996; Skinner and Elderfield, 2005).

The basis for Mg/Ca thermometry is that the substitution of Mg^{2+} into calcite is endothermic and consequently favoured at higher temperatures (Erez, 2003). As a result Mg/Ca ratios in foraminiferal calcite is influenced by the temperature of the surrouding seawater during growth, and will increase with increasing temperature. In calibration studies an exponential relationship has been observed between the calcification temperature and Mg/Ca ratio of foraminfera (Barker et al., 2005). Exponential functions have been fitted to empirical data from core-top (Cléroux et al., 2008; Dekens et al., 2002), sediment trap (Anand et al., 2003; McConnell and Thunell, 2005) and culturing studies (Lea et al., 1999; Nürnberg et al., 1996), expressing the calibrations in the following form:

$$Mg/Ca = B \exp(A \times T) \qquad \text{(Equation 8)}$$

Here T is the calcification temperature in °C, and *A* and *B* are constants dependent on the species in question. Almost all foraminiferal species seem to share a similar Mg/Ca temperature sensitivity. *A* is normally found to be around 0.09-0.1, reflecting a temperature sensitivity of ca. 10 % per °C (Barker et al., 2005; Elderfield and Ganssen, 2000; Lea et al., 1999). Still, differences in uptake of Mg between species do exist, and species-specific calibrations are statistically preferable giving more accurate tempererature estimates (Barker

et al., 2005).

3.5.2 Secondary effects

Other parameters than temperature also affect the Mg/Ca ratio in foraminiferal shells. This complicates the interpretation of Mg/Ca results and calls for corrections of the measurements before any temperature signal can be extracted. Dissolution, salinity, gametogenesis and changes in seawater Mg/Ca are the major secondary effects. A short overview of the influence they can excert on Mg/Ca is given below, and the parameters that might have affected the measurments in this study are discussed in Chapter 5.

Dissolution

Dissolution of calcite can occur within the water column, at the water-sediment interface and within the sediments (Dekens et al., 2002). It systematically reduces the Mg/Ca ratios of the foraminiferal tests due to the preferential dissolution of calcite with high Mg/Ca ratios, which is calcite formed in relatively warm waters (e.g. surface waters) (Rosenthal et al., 2000). This causes a bias towards colder temperature estimates (Barker et al., 2005). Typically, the dissolution effect is ignored unless the core locations are situated below the lysocline. However, dissolution can affect Mg/Ca at shallower depths if the water is undersaturated with respect to carbonate ions, CO_3^{2-}. Foraminferal tests are built from a mixture of HCO_3^- and CO_3^{2-}. In cases where the carbonate ion concentration at the site, $[CO_3^{2-}]_{in\text{-}situ}$, is less than the saturation concentration of carbonate ion, $[CO_3^{2-}]_{satureation}$, seawater will dissolve calcite in an effort to reach a saturated state. The effect of the carbonate ion concentration on the Mg/Ca ratio in specific samples can be evaluated by comparing the observed carbonate ion concentration at the site with the saturation concentration of carbonate ion:

$$\Delta CO_3^{2-} = [CO_3^{2-}]_{in\text{-}situ} - [CO_3^{2-}]_{satureation} \qquad \text{(Equation 9)}$$

If the ΔCO_3^{2-} is a negative value, the water at the site is underaturated with respect to carbonate ions, and a dissolution effect on the foraminiferal Mg/Ca can be assumed.

Salinity

Large salinity changes also appear to influence the Mg/Ca ratios of biogenic calcite.

Especially in cases where Mg/Ca-derived temperatures are used to extract the salinity signal from oxygen isotope measurements, it is important to assess the salinity affect on Mg/Ca. A culturing experiment by Nürnberg et al. (1996) showed that a salinity increase of 10 % gave an increase of 110 % in Mg/Ca. Variations smaller than 3 % showed no systematic impact, however. Hence, salinity is thought to mostly effect Mg/Ca uptake by foraminifera in closed basins where large salinity variations occur (Nürnberg et al., 1996). In an open ocean, like the Atlantic, it can be assumed that the foraminiferal Mg/Ca ratios are not affected by salinity.

Changes in the seawater Mg/Ca

Changes in the Mg/Ca ratio concentration in the ocean could potentially affect the uptake of Mg by foraminifera. However, since both Ca and Mg have relatively long oceanic residence times (10^6 and 10^7 years, respectively), the Mg/Ca ratio of seawater can be considered constant over glacial-interglacial timescales (Rosenthal et al., 2000). Hence, variations in foraminiferal Mg/Ca are mainly due to physical fractionation factors like temperature.

Vertical migration/gametogenesis

As mentioned, many planktonic foraminfera migrate vertically in the water column during their life-cycle. As they mature, they commonly descend to deeper waters often forming calcite over a large depth- and temperature range (Barker et al., 2005). Moreover, many species add a secondary crust of calcite in deep waters right before reproduction (gametogenesis). Due to biophysiological controls, this gametogenic calcite may have a Mg/Ca ratio which is distinct from the primary calcite even when formed under similar temperature conditions (Nürnberg et al., 1996). The Mg/Ca ratio of the test of an individual thus reflect the average ratio incorporated througout the life-cycle of the organism at different times, depths and temperatures (Barker et al., 2005).

3.5.3 Cleaning methods

It is important that the carbonate samples are clean in order to avoid bias in the measurements caused by clays or other contaminants that can influence the Mg/Ca ratios. Following the cleaning procedures described by Barker et al. (2003), contaminants were removed from the foraminiferal calcite before any measurements were made. The cleaning process involves five steps and is carried out in a clean-lab. A short overview of the steps are given below:

1. Crushing of foraminfera

In order to open all the chambers and allow chamber fill to escape, the foraminferal tests are carefully crushed between two glass plates and transferred to a clean sample vial. It is important to avoid over-crushing, because powdered carbonate will stay in suspension and be removed during cleaning instead of settling at the bottom of the vial.

2. Removal of clay materials

Test fill is brought into suspension by adding ultrapure water (UHQ) to the samples. After the carbonate has settled, most of the overlying solution is removed. The samples are placed in an ultrasonic bath in order to encourage the separation of clay which is still bound to the test surfaces. UHQ is again added to the sample to bring loose clays into suspension. The sample is briefly allowed to settle and the overlying solution is removed. These water cleaning steps are repeated a minimum of four times, before ethanol is used instead of water for further clay removal. Ethanol has lower viscosity than water and can better separate clays still attached to the tests. The ethanol cleaning steps are repeated once.

3. Removal of organic matter

Alkali buffered 1% H_2O_2 solution is added to each vial. The tubes are secured in a rack with a lid to prevent them from opening while under pressure. The rack is placed in boiling water in ten minutes to dissolve organic material. At 2.5 and 7.5 minutes it is taken out of the bath, and shaken to release any gas bubbles, and at 5 minutes the rack is placed in ultrasonic bath for the same reason. These steps are performed to maintain contact between reagent and sample. The vials are then centrifuged and the overlying solution removed, before all the steps are repeated. Any remaining oxidizing reagent is removed by water cleaning.

4. Weak acid leach

The dilute acid, 0.001 M HNO_3, is then added to remove any adsorbed contaminants from the test fragments. The samples are ultrasonicated and the acid is replaced with UHQ. Brief settling is allowed before the overlying water is removed. The water cleaning step is repeated, and any remaining solution is removed from each sample.

5. Dissolution

Finally, the samples are dissolved in 350 µl 0.1 M HNO_3. To aid dissolution, the vials are

placed in ultrasonic bath, and a vortex is used to remove CO_2 gas bubbles. The samples are then centrifuged to allow settling of any remaining silicate particles, and 300 µl of the solution is transferred to a clean sample sube, leaving any particles to be discarded in the residual 50 µl.

3.5.4 Element analysis

The Mg/Ca ratios of the samples are determined through element analysis using an ICP-AES device. Inductively coupled plasma atomic emission spectrometry is a method used to identify elements in a sample and quantify their concentration. The method provides accurate and precise measurements of the Mg/Ca content in carbonates, and is an effective tool for the production of high-resolution paleoceanographic data (deVilliers et al., 2002). The procedure basically concerns three steps: atom formation, excitation and emission. Before going into the plasma, the dissolved sample is converted to an areosol consisting of tiny droplets by using a nebulizer with a nebulizing gas. Water is driven off, and the remaining sample is converted into gaseous form. The plasma has a temperature of 6000 to 10 000°C, and as the sample enters, gas phase bonds are broken and only atoms remain present. The atoms gain energy from collisions, and excitation of electrons to a higher energy level takes place. When an electron returns from its excited state, light with a distinctive wavelength for that particular element is emitted. By measuring the wavelengths of the emitted light on specific «lines», the elements present in the sample can be identified. The quantity of each element is given by the light intensitiy (Manning and Grow, 1997).

Mg/Ca measurements in this study were performed with the use of the ICP-OES Thermo IRIS Radial View of the ICP-lab at the Department of Earth Science (UoB). The concentration of Mg is measured on line 279 nm, and the Ca concentration is measured on the line 315 nm. Two runs of each sample are required. For the first run, 280 µl of 0.1 M HNO_3 are added to 70 µl of sample solution and vortexed. The diluted samples are run in the ICP-OES to determine their Ca concentrations. Using these concentrations, a second set of samples is made from the remaining sample solutions. The sample solutions are diluted to gain an optimum Ca concentration of 40 ppm for the intensity calibration of Mg/Ca {deVilliers, 2002 #120;}.

During the analysis a standard solution with the same Ca concentration as the sample solutions are run for every ten sample. The elemental concentrations in the standard solutions are known, and can therefore be used to evaluate the precision of the measurements. The reproducability of the measurements given by the drift of these «quality checks» is better than 0.01. Finally, an intensity ratio calibration of the analysed samples is performed. The measured Mg/Ca intensity ratios of the known standards are regressed against the Mg/Ca concentration ratios of the known standard solutions. As a result, linear calibration curves are obtained enabling simple conversion from intensity ratios to concentration ratios. The concentrations are given in millimol per mol (mmol/mol) (deVilliers et al., 2002).

3.5.5 Mg/Ca temperature equations

A number of species-specific Mg/Ca:temperature calibration studies have been carried out over the last decade. Since G. ruber is frequently used for reconstructing sea surface temperatures, many temperature equations have been made for this species. To select which temperature equation to use for G. ruber, several equations were considered (Cléroux et al., 2008; Dekens et al., 2002; McConnell and Thunell, 2005; Regenberg et al., 2009). The calibrations of Dekens et al. are based on core-top sediments from the Rio Grande Plateau in the western South Atlantic. McConnell and Thunell base their calibrations on sediment-trap material from the Bay of California in the eastern Pacific Ocean, Regenberg et al. use tropical Atlantic and Caribbean sediment-surface samples, while the calibrations by Cléroux et al. is based on core-top sediments from all over the North Atlantic Ocean.

Each equation was used to estimate modern ocean temperature based on the measured Mg/Ca ratios in the youngest sample in each core (2-3 cm). The estimates are expected to represent the temperature at 25 m; the assumed fixed habitat depth of *G. ruber*. These temperatures were compared to observed modern temperatures at this depth given by temperature data from a station located near the core sites, at 37.33°W, 03.87°S (WOCE, 2002). Hence, an indication of which equation is best suited for estimating modern sea surface temperatures at the three core-sites is provided. Ideally Mg/Ca ratios of core-top samples from a multicore should have been used for this comparison, as they would better represent modern conditions. However, the samples used are from the Late Holocene so the estimates should roughly correspond with modern temperatures. Fewer calibrations studies have concerned the deep-

dwelling *G. truncatulinoides*, which has a complicated life-cycle with vertical migration of up to several hundred meters (Mulitza et al., 1997). Temperature equations do exist for this species as well (Cléroux et al., 2008; Regenberg et al., 2009), but with fewer equations to compare, the selection was more random.

3.6 Reconstruction of upper-ocean temperature stratification

The difference in $\delta^{18}O$ between planktonic foraminiferal species with different habitat depths can be used as a proxy for the temperature stratification in the upper ocean. Mulitza et al. (1997) demonstrated the usefulness of this method by successfully reconstructing the latitudinal change in upper-ocean stratification in the Atlantic ocean from 60°S to 10°N. They compared the measured $\delta^{18}O$ of two mixed-layer species with the $\delta^{18}O$ values of the deep-dwelling *G. truncatulinoides* (dex). Their results showed a clear increase in $\Delta\delta^{18}O$ towards the tropics, interpreted to reflect the increased surface-to-deep temperature gradient in the upper part of the water column. Capable of reflecting various modern conditions, the method can be applied to reconstructions of changes in upper-ocean stratification in the past. Increased $\Delta\delta^{18}O$ between shallow- and deep-living species is taken as an indication of increased stratification of the upper ocean with shallower mixing and a decrease in thermocline depth. In contrast, decreasing $\Delta\delta^{18}O$ suggests low-stratified surface waters with deeper mixing and a smaller vertical temperature gradient. In other words, thermocline depth increases as $\Delta\delta^{18}O$ drops. In this study, the method of Mulitza et al. is used in an attempt is to reconstruct upper-ocean stratification in the western tropical Atlantic associated with specific climatic extremes in the North Atlantic. The differences in both $\delta^{18}O$ and Mg/Ca between the shallow dwellers, *G. ruber* and *G. trilobus* and the deep dweller, *G. truncatulinoides* are calculated for each timeslice. The results are used to investigate the link between variations in the Atlantic thermohaline circulation and changes in the tropical thermocline depth.

4 Chronology

In order to compare the three cores with each other, a chronology is developed allowing time to be the common axis for all the cores. The chronology is based on Accelerator Mass Spectrometry (AMS) ^{14}C datings of monospecific foraminiferal samples from core GS07-150-17/1 GC. Amandine Tisserand picked the foraminifers, and the AMS ^{14}C measurments were performed at Poznan Radiocarbon Laboratory in Poland. An age model for the dated core is constructed with the use of linear interpolation between the ^{14}C dates. Using down-core variations in X-ray Fluorescence (XRF) intensities of iron (Fe), titanium (Ti) and calcium (Ca), core 18/2 and 20/2 are correlated with core 17/1, and a common chronology is established.

4.1. Radiocarbon (^{14}C) dating

Radiocarbon is produced in the upper atmosphere by neutron bombardment of cosmic nitrogen atoms:

$$^{14}_{7}N + ^{1}_{0}n \rightarrow ^{14}_{6}C + ^{1}_{1}H \qquad \text{(Equation 10)}$$

The ^{14}C atoms quickly combine with oxygen to form $^{14}CO_2$. Along with the rest of the carbon dioxide they are mixed throughout the atmosphere and absorbed by oceans and by living organisms through photosynthesis and respiration. Living organisms use carbon to build new tissues that are more or less in equilibrium with atmospheric CO_2, and the ^{14}C that decays to ^{14}N is continuously replaced by new ^{14}C atoms. Upon death, however, the decay of ^{14}C within the organism continues without replacement of new ^{14}C. Hence, if the rate at which the radiocarbon decays is known, the time passed since the organism died can be calculated (Lowe and Walker, 1997; Walker, 2005).

AMS ^{14}C dating can be used to measure the age of very small samples. To obtain the radiocarbon age of a sample, the $^{14}C/^{12}C$ ratio is measured in an accelerator mass spectrometer and compared to a standard ratio of modern material. Because of temporal

variations in ^{14}C production in the atmosphere, however, ^{14}C ages deviate from calendar ages. Reduced production of ^{14}C in the atmosphere leads to plateaux of constant ^{14}C age and an underestimation of the true age of samples. To obtain the «true» age, calibration from radiocarbon ages to calendar ages is necessary (Lowe and Walker, 1997). Such calibrations are done using calibration curves based on absolutely dated tree-ring chronologies and other archives (Reimer et al., 2009; Stuiver et al., 1998).

Before calibration, the ^{14}C ages of marine samples also have to be corrected for the marine reservoir effect. The radiocarbon content of a given sample depends on the organism's source of carbon, and due to differences between atmospheric and oceanic radiocarbon content, the ages of marine samples are overestimated. Mixing of old deep water into upper-ocean water affects the radiocarbon content of the surface water, as deep water is depleted in ^{14}C due to its isolation from the atmosphere. Hence, organisms living in these waters are seemingly older than they really are and a reservoir age has to be substracted from the radiocarbon age (Walker, 2005).

From core GS07-150-17/1 GC, seven AMS ^{14}C dates were obtained (Table 4). They were all measured from tests of *G. sacculifer* in the size range of 250-400 μm. The weight of each sample was approximately 8 – 10 mg. The dates were corrected for a marine reservoir age of 400 years (Arz et al., 1999b; Bard, 1988; Hughen et al., 1998), and conversion to calendar years was performed using the calibration program Calib 6.0 with the Marine09 calibration data set (Reimer et al., 2009). The ages are given in years before 1950 (BP 1950).

Table 4: AMS ^{14}C datings from core GS07-150-17/1. All ages were measured from tests of G.sacculifer. Depth and Laboratory reference number are given in the two leftmost columns. A marine reservoir age of 400 years was subtracted from the AMS ^{14}C dates before calibration. The calibrated ages are given in calendar years before year 1950 (BP 1950)

Depth (cm)	Lab.no.	Dated material	C-14 yrs (BP 1950)	Error ±	Cal. yrs (BP 1950)	Age range ± 1σ	Sed. rate (cm/1000 yrs)
0	Poz-34998	G.sacculifer	1255	30	796	746 – 846	
10	Poz-34999	G.sacculifer	3060	30	2816	2772 – 2859	4,95
50	Poz-35000	G.sacculifer	8570	50	9210	9127 – 9293	6,26
100	Poz-35002	G.sacculifer	11680	80	13183	13106 – 13260	12,58
150	Poz-35003	G.sacculifer	15450	80	18194	18065 – 18322	9,98
200	Poz-35004	G.sacculifer	21840	120	25669	25420 – 25918	6,69
250	Poz-35005	G.sacculifer	27110	180	31180	31081 – 31278	9,07

4.2 Age model

An age model for core GS07-150-17/1 GC (Figure 23) has been constructed using linear interpolation between the calibrated dates from Table 4. The age model is based on the assumption that the sedimentation rate has been constant between two dated levels. The sedimentation rate between two datings is given by the difference quotient of the linearly interpolated line between the dates. The sedimentation rates for each interval are given in Table 4, and the mean sedimentation rate is ~8.23 cm/1000 years. The sedimentation rates are used together with the radiocarbon dates to calculate a «running age» for the core, giving an approximate age to every cm downcore.

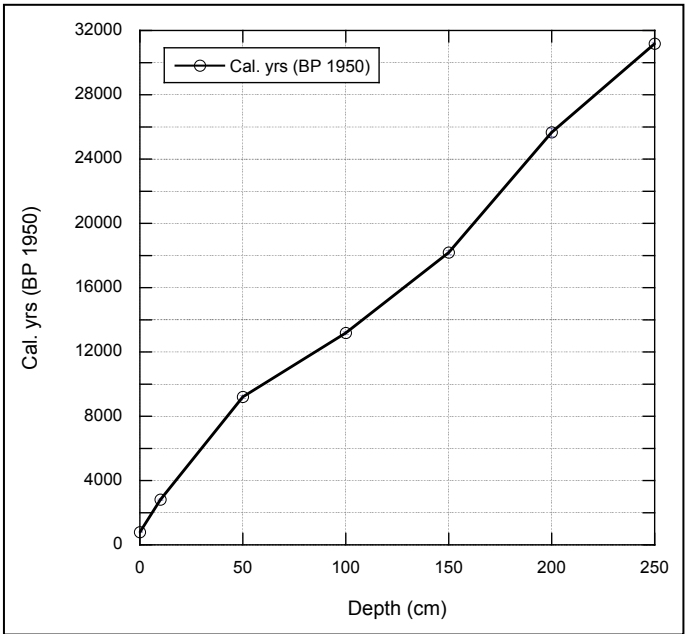

Figure 23: Age model for core GS07-150 17/1 GC based on linear interpolation of the calibrated ages in Table 4.

4.3 Correlation

Core GS07-150-18/2 GC and core GS07-150-20/2 GC are stratigraphically linked to the ^{14}C AMS dated core by correlation of X-ray Fluorescence (XRF) derived intensities of calcium (Ca), titanium (Ti) and iron (Fe). The three cores were scanned at the Department of Earth Science (UoB) with the use of the ITRAX Core scanner developed by Cox Analytical Systems (Croudace et al., 2006). Correlation between the cores was carried out in the computer program AnalySeries 2.0 (Paillard et al., 1996).

4.3.1 XRF analysis

X-ray Fluorescence is an analytical method used to determine the chemical composition of materials (Brouwer, 2003). The application of XRF analysis to paleoclimate research provides a very efficient way of establishing lateral elemental variations in sediment cores. Variations in element content along core profiles can be used to infer changes in the sedimentary environment and to provide a basis for correlation between cores (Croudace et al., 2006). In XRF spectrometry, X-rays produced by a source irradiate a sample, and the elements present in the sample emit energy in the form of fluorescent light. Each element releases radiation with a distinctive wavelength. By measuring the wavelengths of the emitted radiation, it is possible to find out which elements are present in the sample. The amount of each element is given by the intensity of their radiation (Brouwer, 2003).

The ITRAX Core scanner used in this study, produces high-resolution XRF elemental profiles at a maximum resolution of 200 μm. The scanning is carried out without disturbing the sediments, leaving the cores intact for further analysis (Croudace et al., 2006). A molybdenum X-ray tube was used as the source to irradiate the cores. This tube gives good results for both transition and heavy elements. The alternative was the chromium tube which is best suitable for analysing lighter elements only (Croudace et al., 2006), and would not have given optimal results for the intensity of titanium and iron which are used for the correlations. The resolution was set to 500 μm which is high, but less than maximum. It was chosen to lower the measuring time. The exposure time of each measuring point was set to 10

seconds and the Mo X-ray source was set to set to 30 kV and 55 mA.

The elemental intensities of Ti and Fe in marine sediments provide a chemical proxy for the input of terrigenous material from continental areas by fluvial and eolian transport. The carbonate content in the sediments, represented by the Ca intensity, is mainly related to marine biogenic production. Thus, the Ti/Ca and Fe/Ca ratios can be used to quantify the dilution of marine carbonate by terrigenous sediments (Arz et al., 1999a; Haug et al., 2001; Peterson et al., 2000). The supply of terrigenous material to the ocean is mainly controlled by river discharge, which is linked to the continental climate. Hence, variations in the ratios of Ti/Ca and Fe/Ca give indications of changes in the climate of the continental source areas (Arz et al., 1998). The precipitation regime of the North East Brazilian coast is of major importance to the river discharge and sediment supply to the continental margin where the cores in this study are from. Hence, increased humidity over the continent may have increased the river runoff and sediment supply to the continental slope.

Several studies from the western tropical Atlantic relate periods of increased terrigenous input to the continental margin, reflected by higher Ti/Ca and Fe/Ca ratios, to more humid conditions in the adjacent coastal areas (Arz et al., 1998, 1999a; Haug et al., 2001; Peterson et al., 2000). Arz et al. (1998) demonstrate that warming of the surface water off NE Brazil concurred with pulses of land-derived sediments which suggest humid conditions on the north-eastern Brazilian continent. XRF measurements from their cores show high ratios of Fe/Ca during the YD and especially during H1. Low ratios of Fe/Ca occurred during the Bølling-Allerød and the Holocene with very low ratios during the late Holocene. A similar pattern was also demonstrated by Arz et al. (1999a) for Fe/Ca and Ti/Ca ratios. Hence, according to Ti/Ca and Fe/Ca NE Brazil was warm and humid during stadial times, and less so during the Bølling-Allerød interstadial and the Holocene. The results of the XRF analysis of the cores in this study show similar development in Fe/Ca and Ti/Ca to those presented by Arz et al. (1999a) and Arz et al. (1998). The results are, however, not used for climatic interpretation. They are mainly used as a tool for the correlation of the three cores.

4.3.2 Correlation of the cores

The correlated down-core Ca, Ti/Ca and Fe/Ca variations in the three cores from this study are shown in Figure 24. Climate periods are marked with grey and white bars, while the black dotted lines indicate the mean age of the respective timeslice samples. The yellow dotted line represents the late Holocene timeslice in core 20/2. This particular timeslice sample deviated a lot in age from the corresponding timeslices in the two other cores. The purple dotted lines marks the age of two samples from which *G. truncatulinoides* was picked, as this species could not be found in the youngest timeslice in core 18/2 and 17/1. The Fe/Ca and Ti/Ca records show several large peaks in ratio values, and a rough pattern is recognized in all three cores. The pattern resembles that of the Fe/Ca and Ti/Ca ratios from the cores of Arz et al. (1999a). Fe variations

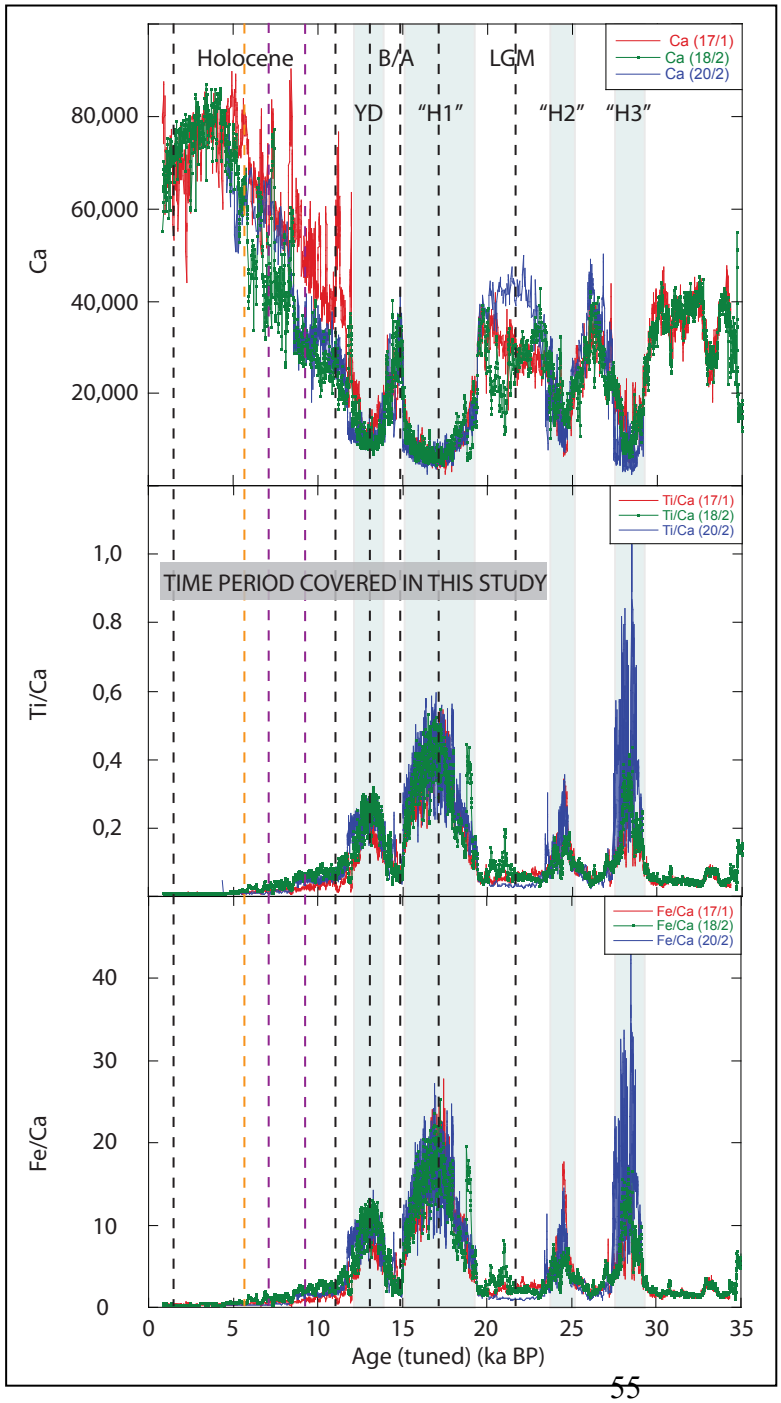

Figure 24: Correlated Ca, Ti/Ca and Fe/Ca variations in gravity cores GS07-150-20/2, GS07-150-18/2 and GS07-150-17/1. Climate periods are marked with grey and white bars, while the black dotted lines indicate the mean age of the respective timeslice samples. The yellow dotted line represents the late Holocene timeslice in core 20/2. The purple dotted lines marks the age of two samples from which G. truncatulinoides was picked.

alone could be attributed to redox changes in the sediment, while Ti is insensitive to environmental redox variations (Haug et al., 2001; Yarincik et al., 2000). Since Fe and Ti seems to vary with similar patterns, Fe is considered as not diagenetically controlled, and both Fe and Ti are interpreted to reflect changes terrigenous input to the study area.

The inter-core similarity between the elemental and ratio records provides a rational for making correlations based on the curves. The records of core 20/2 and 18/2 are therefore «tied» to the records of 17/1 using AnalySeries 2.0 (Paillard et al., 1996). Tie points are chosen manually based on matching prominent features in the records. They are placed where relatively large shifts in elemental intensities occur, assuming that these transitions represent regional changes in the sedimentary environment and are thus time parallel. The fitting of tie points allows stretching and squeezing of the records so that time can be the common axis for all the cores. A simple quality control for the correlation is the computer program's automatic display of downcore changes in sedimentation rates. Tie points are chosen as to avoid sudden changes to very high or very low sedimentation rates within brief time intervals. As a result of the correlation, the three cores receive the same «running age» with an approximate age for each cm. Hence, the age of each sample is estimated (Table 5).

Table 5: Timeslices in cores GS07-150 20/2 GC, GS07-150 18/2 GC and GS07-150 17/1 GC. Depth and age

	GS07-150 20/2 GC		**GS07-150 18/2 GC**		**GS07-150 17/1 GC**	
Timeslices	*Depth (cm)*	*Age (ka BP)*	*Depth (cm)*	*Age (ka BP)*	*Depth (cm)*	*Age (ka BP)*
Late Holocene	2 – 3	5,57	2 – 3	1,29	2 – 3	1,16
Early Holocene	42 – 43	11,19	55 – 56	11,13	70 – 71	10,80
Younger Dryas	90 – 91	13,34	75 – 76	13,26	96 – 97	12,86
Bølling-Allerød	116 – 117	14,93	98 – 99	14,93	116 – 117	14,79
Heinrich H1	150 – 151	17,24	120 – 121	16,89	140 – 141	17,19
LGM	185 – 186	21,77	150 – 151	22,87	165 – 166	20,43

5 Results

In this chapter the results of the oxygen isotope and Mg/Ca measurements are presented, as well as the steps taken to reconstruct the paleo upper-ocean thermal stratification at the core-sites. Several factors complicate the use of foraminferal $\delta^{18}O$ and Mg/Ca as temperature proxies, and it is important to evaluate how these potential sources of error might have affected the geochemical composition of the shells. Therefore, the quality of the measurements is assessed, and any corrections made are described.

5.1 Age control

When estimating climate variability and correlating records, age control is of key importance. This is particularly critical in timeslice studies as they only concern short intervals of the climate record. If the selected samples do not actually represent the time periods of the climatic events, the study fails to detect the proxy targets at the times of interest. Hence, in order to assess the quality of the timeslice study, an evaluation of the age control on the samples is necessary. The age model of core 17/1 is based on linear interpolation between seven radiocarbon ages. The sedimentation rate seems to have been quite steady throughout the whole period of deposition, and the age model is considered to be acceptable. The age models for core 18/2 and 20/2 are based on correlations of the high-resolution XRF intensity records with the dated core. The records of Fe, Ti and Ca all reveal the same major variations. Hence, the deglacial climatic extremes were easily recognized i all cores, but the tuning proved problematic for the Holocene. In this epoch climatic variability has occurred on a smaller scale, and specific climatic events are more difficult to distinguish. Since no fine tuning was done, the Holocene ages may include large errors.

In order to save time, the sample depths in each core were chosen before the radiocarbon ages were estimated and the age models were made. Instead, the XRF intensity records of Fe, Ti and Ca were used. The selection was based on the recognition of prominent variations in Fe/Ca and Ti/Ca ratios assumed to be connected to the Last Glacial Maximum, Heinrich event H1, Bølling-Allerød, the Younger Dryas, the Early Holocene and the Late Holocene. Figure 24 show the tuned element records of the three cores with the time span of the samples from each timeslice marked with bars. The samples seem to cover the targeted climatic events

well, though problems might be expected in the short-lasting Bølling-Allerød timeslice, which is bound by abrupt excursions on both sides. Hence, a sample that deviates slightly from the age of the timeslice could yield proxy measurements with values very different from those representative for Bølling-Allerød.

Although the samples seem to cover the timeslices well, basing the sample selection on Fe/Ca and Ti/Ca records instead of an age model might be problematic. Even though Fe/Ca and Ti/Ca respond to the same climatic forcing as Mg/Ca and $\delta^{18}O$, the signal might be delayed differently in different proxies. Therefore, there is a risk that the selected samples are not quite representative for the timeslices of interest, and the measurements might not actually represent the climatic extremes as well as intended. Furthermore, even if the samples do represent the timeslices well, many of the timeslices are from periods of large changes in climate. Hence, a one cm thick sediment slice could include foraminiferal specimens, which calcified under very different climatic conditions. It is therefore difficult to assess if the average measurements from i.e. the B/A timeslice is indicative of the Bølling period, the OD or the Allerød period. A futher evaluation of the timeslices is made in the Chapter 6.

5.2 Oxygen isotope measurements

5.2.1 General $\delta^{18}O$ stratigraphy

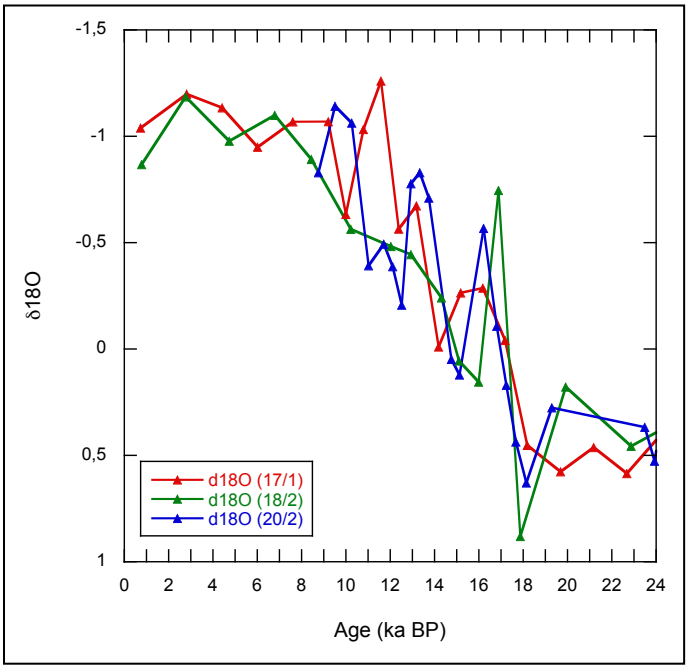

To obtain preliminary indications of the oxygen isotope development in the three cores, the $\delta^{18}O$ of the planktonic foraminifer, *G. sacculifer* (with the final sac-like chamber), was measured every 10 cm downcore. The resulting $\delta^{18}O$ stratigraphies are plotted in Figure 25. As *G. sacculifer* is a surface-dweller, the records are believed to represent mixed-

Figure 25: General $\delta^{18}O$ stratigraphies of cores GS07-150 20/2, 18/2 and 17/1 plotted against age.

layer conditions. All three cores display several large shifts in $\delta^{18}O$ superimposed on a negative glacial-interglacial trend that is evident also when the ice-volume effect is taken into account (Appendix A, Figure A.1).

Most of the major shifts are recognized in all the cores, but deviations in timing and amplitude are observed. Core 17/1, which has the best age control, shows the following development: A negative shift of about 0.7 ‰ occurs in the isotopic residuals between 18 and 16 ka BP. From about 15 ka BP an increase of about 0.4 ‰ is followed by a decrease of almost 1 ‰ starting around 14 ka BP and reaching its minimum around 12 ka BP. Between 12 and 10 ka BP the $\delta^{18}O$ residuals increase by about 0.9 ‰, and through the Holocene several shifts of up to 0.3 ‰ occur.

5.2.2 $\delta^{18}O$ raw data for the timeslice study

Figures 26, 27, 28, 29 and 30 show the respective $\delta^{18}O$ values of planktonic foraminifers *G. trilobus*, *G. ruber* (w), *G. glutinata*, *G. siphonifera* and *G. truncatulinoides* (dex) plotted against age. The measurements from core 17/1, 18/2 and 20/2 are given in red, green and blue, respectively. Yellow curves are drawn between the average $\delta^{18}O$ values for each timeslice. In the following section the integrity of the raw data is evaluated.

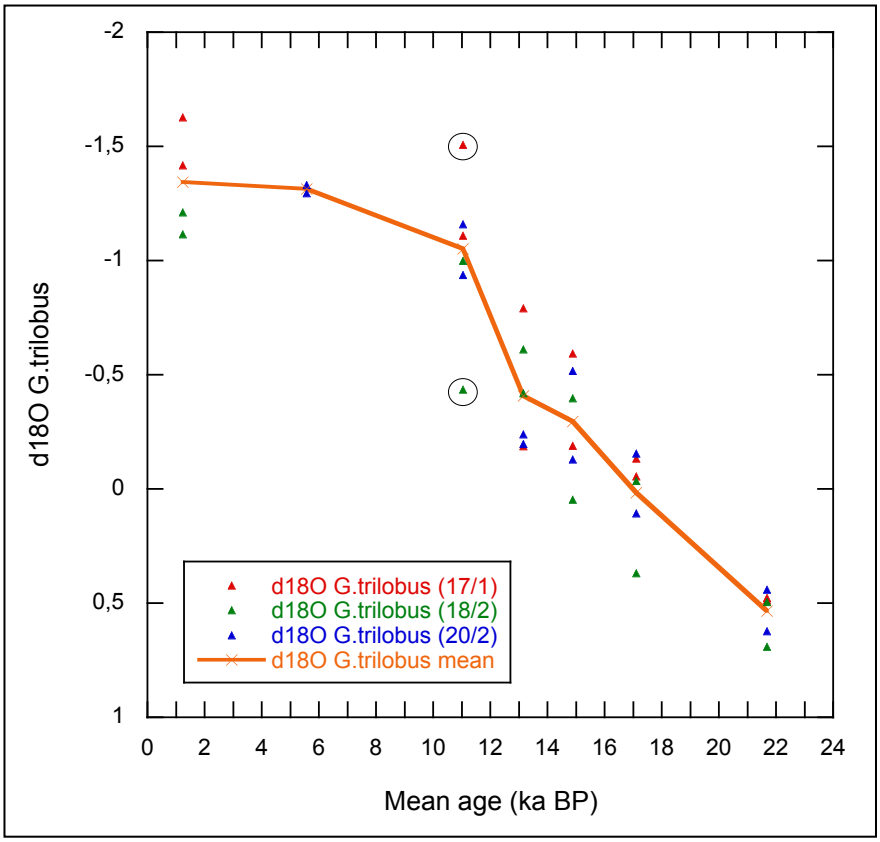

Figure 26: Measured $\delta^{18}O$ for G. trilobus in the six timeslices. Each timeslice is given a mean age for all the three cores. Values from cores 20/2, 18/2 and 17/1 are marked in blue, green and red, respectively. The yellow line marks the average $\delta^{18}O$ for each timeslice. Circles are drawn around outliers, identified based on the criterion described in Section 5.2.3.

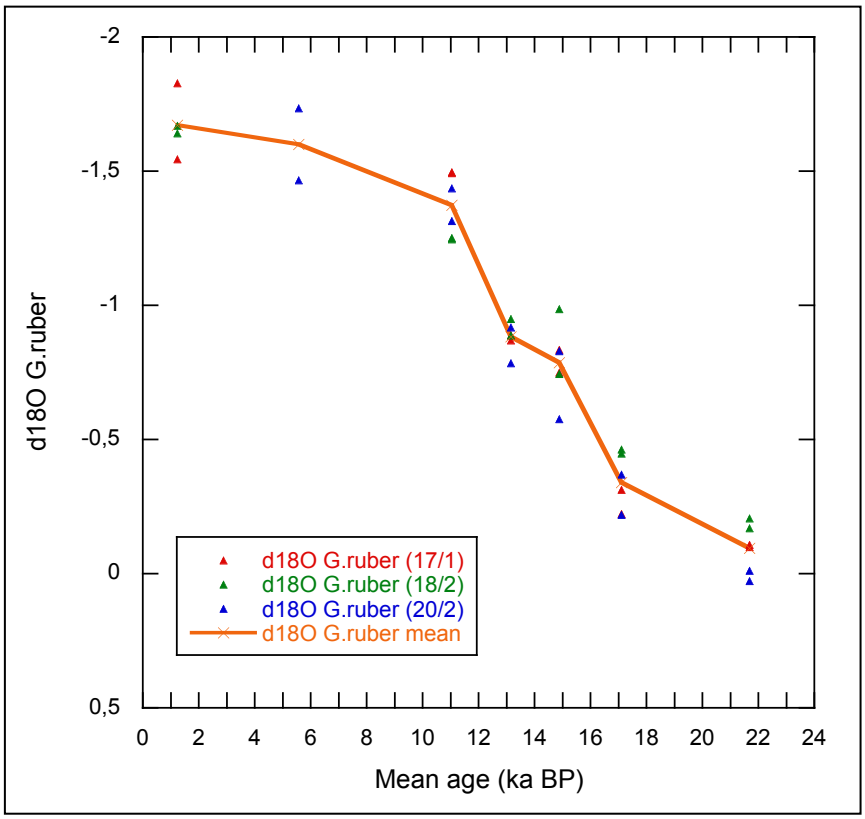

Figure 27: Measured $\delta^{18}O$ for G. ruber (w) in the six timeslices. Each timeslice is given a mean age for all the three cores. Values from cores 20/2, 18/2 and 17/1 are marked in blue, green and red, respectively. The yellow line marks the average $\delta^{18}O$ for each timeslice.

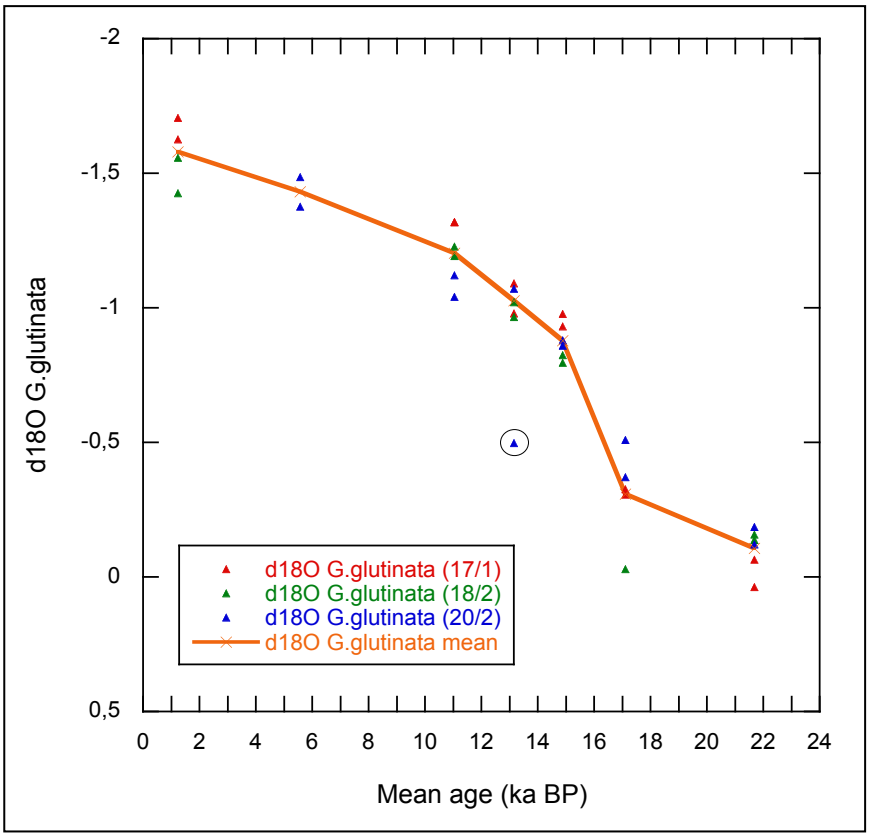

Figure 28: Measured $\delta^{18}O$ for G. glutinata in the six timeslices. Each timeslice is given a mean age for all the three cores. Values from cores 20/2, 18/2 and 17/1 are marked in blue, green and red, respectively. The yellow line marks the average $\delta^{18}O$ for each timeslice. One outlier is marked with a circle. The outlier was identified based on the criterion described in Section 5.2.3.

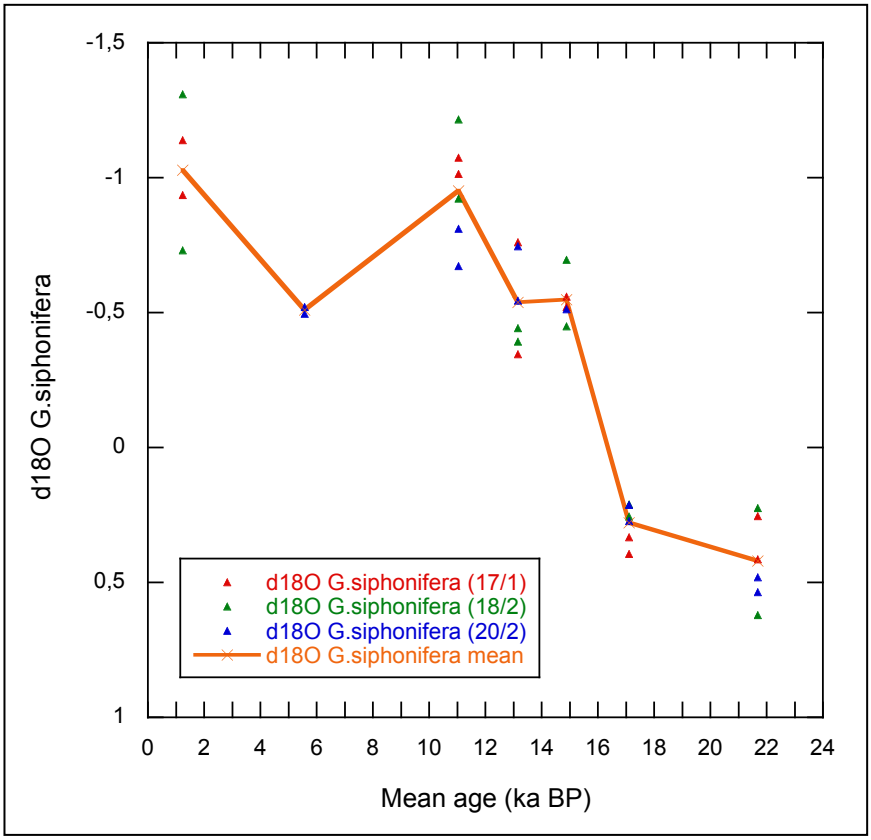

Figure 29: Measured $\delta^{18}O$ for G. siphonifera in the six timeslices. Each timeslice is given a mean age for all the three cores. Values from cores 20/2, 18/2 and 17/1 are marked in blue, green and red, respectively. The yellow line marks the average $\delta^{18}O$ for each timeslice.

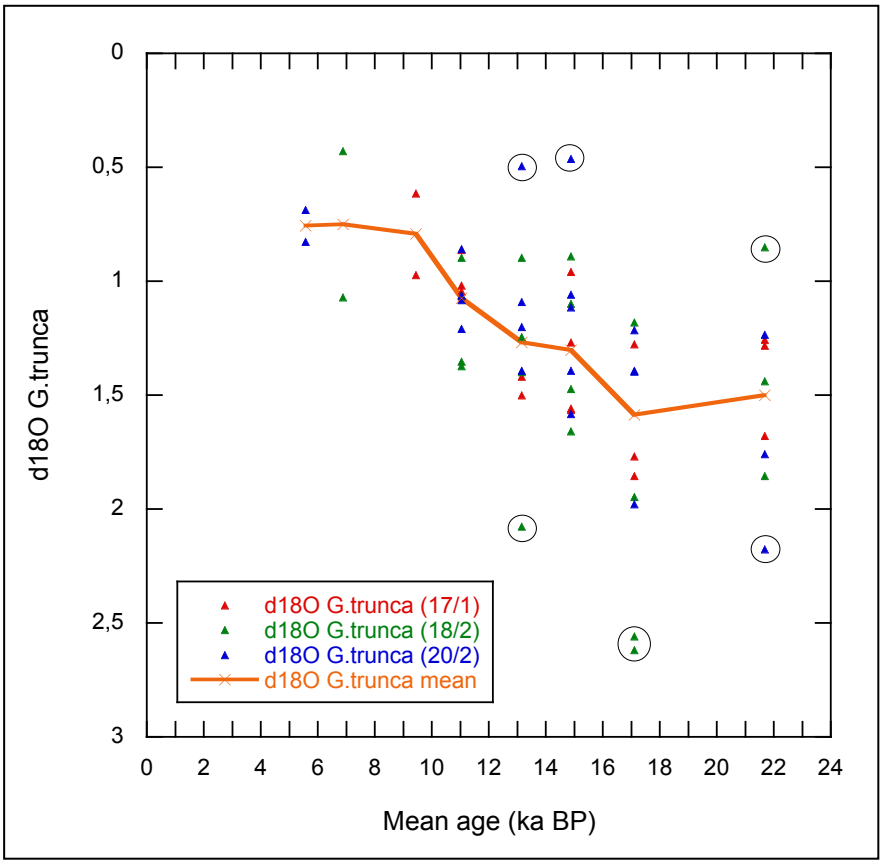

Figure 30: Measured $\delta^{18}O$ for G. truncatulinoides (dex) in the six timeslices. Each timeslice is given a mean age for all the three cores. Values from cores 20/2, 18/2 and 17/1 are marked in blue, green and red, respectively. The yellow line marks the average $\delta^{18}O$ for each timeslice. Circles are drawn around

5.2.3 Intraspecific variability in the oxygen isotope measurements

Duplicate measurements were acquired for the shallow and intermediate species in each sample, and four replicate measurements were obtained for most samples of the deep-dwelling *G. truncatulinoides*. While the replicate measurements for some of the species are well in agreement with each other, the replicates of other species show significant deviations. In order to reduce the intraspecific spread in the measurements, a composite data set is made with the $\delta^{18}O$ values from all three cores. It is assumed that the correlations between the cores are good, and that the core-sites have experienced the same environmental conditions through time. Still, although the composite plot reduces the spread in the data, the intraspecific variability is high for some species. This affects the precision of the paleotemperature reconstruction.

A few measurements deviate a lot from the rest of the data. Using Chauvenet's criterion, ten measured values are identified as outliers and removed from the dataset (marked in Figures 26, 28 and 30). Chauvenet's criterion states that if there is less than 0.05 probability that the suspect value occurs among the measurements recorded, it should be rejected. Removing outliers without external evidence that the measurement is incorrect is controversial, and repeated measurements of the suspect values would be preferrable to rejecting data without further investigation. However, as time does not allow for more measurements, Chauvenet's criterion provides an objective and quantitative method for dealing with strongly deviating data.

The $\delta^{18}O$ values of deep dwelling *G. truncatulinoides* show an especially high scatter. This could be a result of the ontogenic effect or the large depth range over which the species califies (Section 3.4.2). However, the variability might also reflect seasonal changes in the ambient water temperatures, which are best expressed in the subsurface waters below the mixed layer. The changes are caused by vertical migration of the thermocline in response to seasonal changes in the ITCZ and the trade wind strength. *G. truncatulinoides* lives and calcifies in this depth range of high seasonal temperature variability, and incorporates the seasonal signal in their shells. Berben (2010) also observed large variability in $\delta^{18}O$ values for this species in samples from cores close to the study area in the present study.

Post depositional processes can also influence the intraspecific variability in the oxygen isotope measurements. This can affect the preservation of the original signal by changing the over-all geochemical composition of the tests after deposition or otherwise contaminate the samples. The major parameters in this respect are post-depositional dissolution, post-depositional calcification and contamination by clays and other materials. Measured [CO_3^{2-}] from GEOSECS station 46 shows that the seawater in the region is saturated with respect to carbonate ions (Bainbridge, 2004). Moreover, the samples used in this study are from cores collected well above the lysocline. Together this indicates that little post-depositional dissolution occurs at the core-sites, so no attempts to correct for dissolution are made. Post-depositional calcification is not a problem either, as indicated by the Mn/Ca ratios measured in the element analysis (Section 5.2.2). Contamination by clays and other materials could, however, be a bias in the measurements as some of the samples were visually dirty and no cleaning steps were performed before the measurements were done. *G. siphonifera* and *G. truncatulinoides* were quite rare in some samples. Therefore, dirty specimens were used for some of the measurements, and this could have affected the results.

To decrease the intraspecific variability in the measurements, more replicate measurements would be of interest. Alternatively, the number of specimens used in each measurement could be increased. As demonstrated by the results, the amount of scatter in the data for a given species, seem to be related to the number of specimens measured for each $\delta^{18}O$ value. The lowest intraspecific variability is shown for the smallest species, *G. glutinata,* for which up to 23 specimens were picked for each sample. Higher variability is displayed by the larger species, for which only a few specimens were used per measurement. Despite the large scatter in data displayed by some species, there is a certain consistency between the cores in the repsective $\delta^{18}O$ developement of the different species. For each measurement, various sources of error might be influencial. However, if focus is put on the glacial-interglacial trends in the data, which are recognized in all cores, the spread in the oxygen isotope measurements is considered acceptable.

5.2.4 Corrected oxygen isotope data

In Figure 31 the mean ice volume corrected $\delta^{18}O$ ($\delta^{18}O_{IVC}$) is plotted against age for all species. In each plot, standard deviations are indicated with black bars, and a red dotted line

shows the glacial-interglacial trend in the $\delta^{18}O_{IVC}$ values. The uppermost panel displays the $^{231}Pa/^{230}Th$ data of McManus (2004) and N-GRIP data over the last 24, 000 years. $^{231}Pa/^{230}Th$ is a kinematic proxy for the MOC, where decreasing ratios are interpreted as an increase in overturning. The N-GRIP data represent a $\delta^{18}O$ record from an ice core from Greenland. The different climate periods are marked through all the plots, and temperature change represetenting approximately 1°C (Shackleton, 1974) is indicated for all the species.

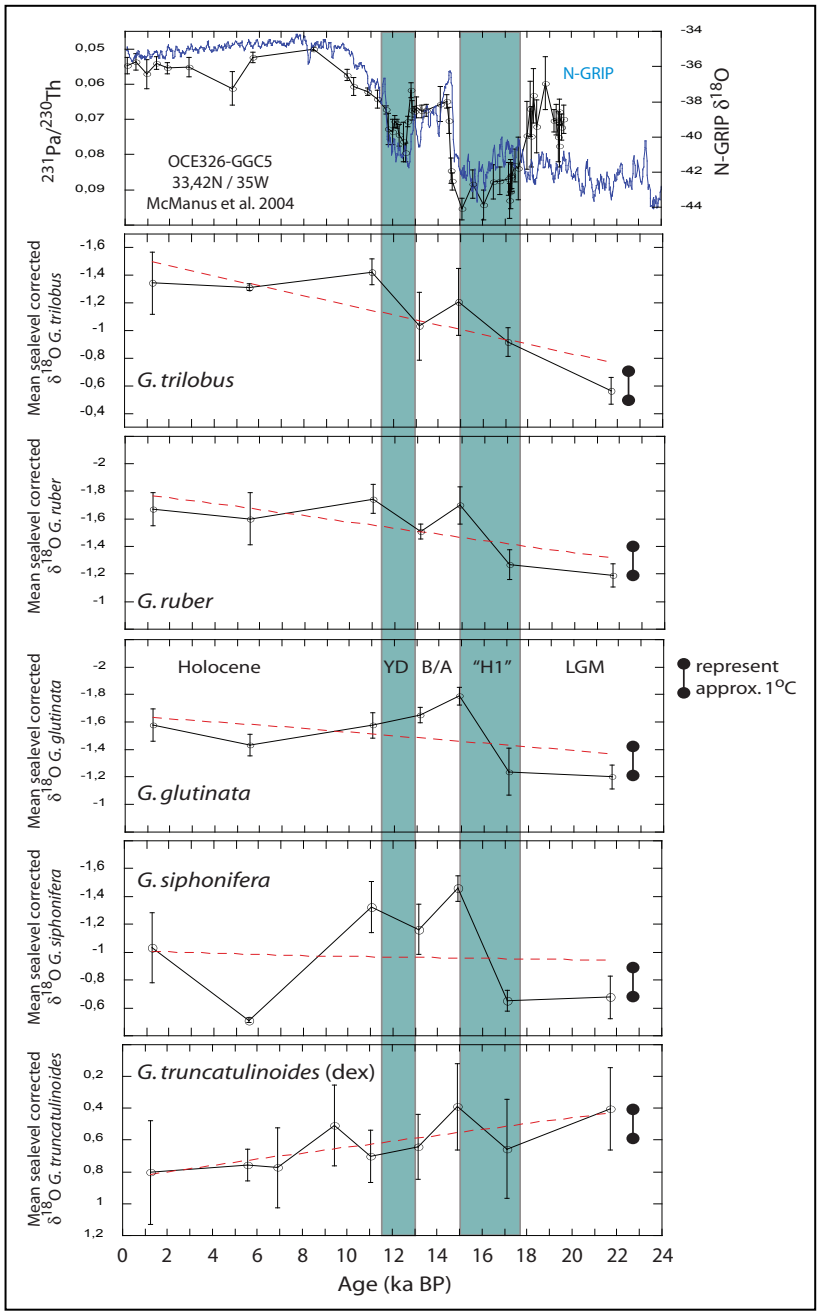

Figure 31: Average corrected $\delta^{18}O$ values for all species. Standard deviations are indicated by blue bars, and the over-all trends are depicted by red dotted lines. The upper panel is showing the results of Pa/Th indicating the strength of overturning rate as indicated from the $^{231}Pa/^{230}Th$ data of McManus (2004) and the N-GRIP $\delta^{18}O$ ice-core record from Greenland. The different climate periods are marked through all the plots, and temperature change represetenting approximately 1°C (Shackleton, 1 974) is indicated for all the species.

The ice-volume effect on $\delta^{18}O_w$ for a particular time is estimated based on studies of fossil coral reefs in the Barbados and Tahiti which give a detailed record of the global sea-level during the last deglaciation (Fairbanks, 1989) As global sea-level is related to the amount of ice stored on the world's continents, such a record has been used to construct a curve reflecting the global ice effect on the $\delta^{18}O$ of ocean water since the last glacial maximum (Peltier and Fairbanks, 2006). Correction of the foraminferal $\delta^{18}O$ measurements can, thus, easily be made. Naturally, larger corrections have to be made to the measurements from time periods with large build-up of ice than to those from times of less continental ice. As a result, the $\delta^{18}O$ values representing the timeslices from the last glacial are lowered by up to 1.1 ‰, while the late Holocene values remain unchanged. The glacial-deglacial trends in the data are thus altered. Less steeply decreasing $\delta^{18}O$ gradients from the LGM to the Holocene are revealed for the shallow-dwelling and intermediate-dwelling species, while the $\delta^{18}O$ of *G. truncatulinoides* show an increasing trend in the same time period.

After the corrections for the ice-volume effect have been made, the residual $\delta^{18}O_{IVC}$ reflect variations in temperature, the $\delta^{18}O$ of the ambient water and potential vital effects. Vital-effects are responsible for out-of-equilibrium fractionation of the oxygen isotopes during calcification. As mentioned in Section 3.4.2, correcting the $\delta^{18}O_{IVC}$ for vital-effects is not considered crucial for the interpretation of the results. Since the study ultimately concerns changes in $\delta^{18}O$ gradients between different species, vital effects can be ignored if assumed to be constant through time. However, it can be noted that the difference in $\delta^{18}O_{IVC}$ betweem shallow and deep dwellers is probably exaggerated due to the symbiont effect on the shallow dwellers.

Variations in water mass properties can be a major bias for the temperature proxy. Such variations can result from changes in salinity and/or a change in the influence of different water masses at the depth at which a given foraminiferal species lives. As mentioned, the combination of Mg/Ca and oxygen isotope measurements can potentially be used to estimate salinity changes through time, but due to the large scatter in the Mg/Ca measurements such calculations are not made. The area of investigation is characterized by excess evaporation and, consequently, high sea surface salinity (SSS). In a study from the western tropical Atlantic, Arz et al (1999b) supposed near-constant SSS since the LGM, and Wolff et al. (1998) assigned only 0.2 ‰ change in $\delta^{18}O$ to local SSS changes in the area. Furthermore, Arz et al. (1999b) claim that the variations in SSS due to direct riverine input are negligible,

because only small rivers discharge from the adjacent continent. Hence, it is more likely that variations in the $\delta^{18}O_{IVC}$ values were caused by changes in temperature than changes in salinity.

5.3 Mg/Ca measurements

5.3.1 Mg/Ca raw data

The Mg/Ca ratio results from the element analysis of the timeslices in cores GS07-150 20/2, 18/2 and 17/1 are presented below. Figure 32 shows the Mg/Ca ratios of *G. ruber* (w) plotted versus age after the intensity calibration. The measurements from core 17/1, 18/2 and 20/2 are indicated by red, green and blue triangles, respectively. Three outliers are marked with circles, and Mg/Ca *G. ruber* (mean) with and without the outliers are indicated by orange and blue line. The late Holocene measurement from core 20/2 is also not included by the blue line. The dotted lines (orange and blue) indicate the glacial-interglacial trends in the data (with and without outliers). The equivalent results for *G. truncatulinoides* (dex) are displayed in Figure 33. No outliers were identified in these data, and Mg/Ca *G. truncatulinoides* (mean) is illustrated by the orange line. An evaluation of the raw data is presented in the following section.

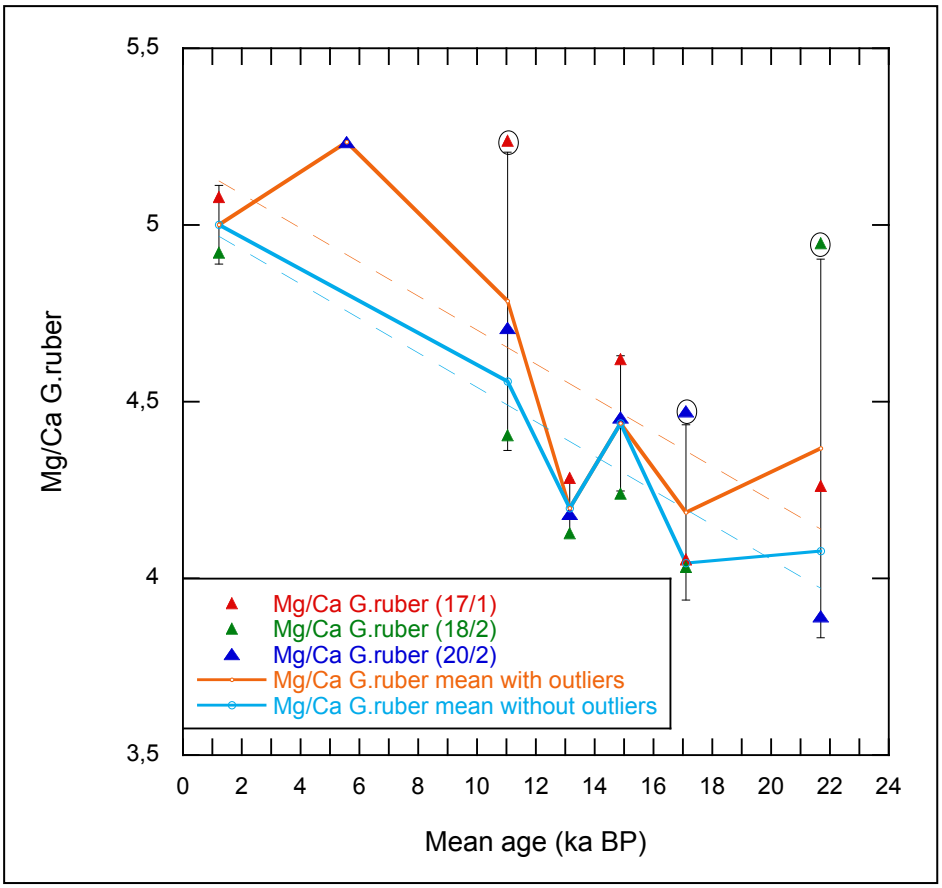

Figure 32: Mg/Ca ratios of G. ruber (w) plotted versus age. The Mg/Ca ratios are given as intensity concentrations (mmol/mol). The red, green and blue triangles show the results for cores GS07-150 17/1, 18/2 and 20/2, respectively. The orange line indicates the mean results from all the cores. The blue line indicates the mean result, not including the results from three measurements indicated by circles and also excluding the late Holocene measurement of core 20/2. The dotted lines (orange and blue) indicate the linear regression (trend) lines.

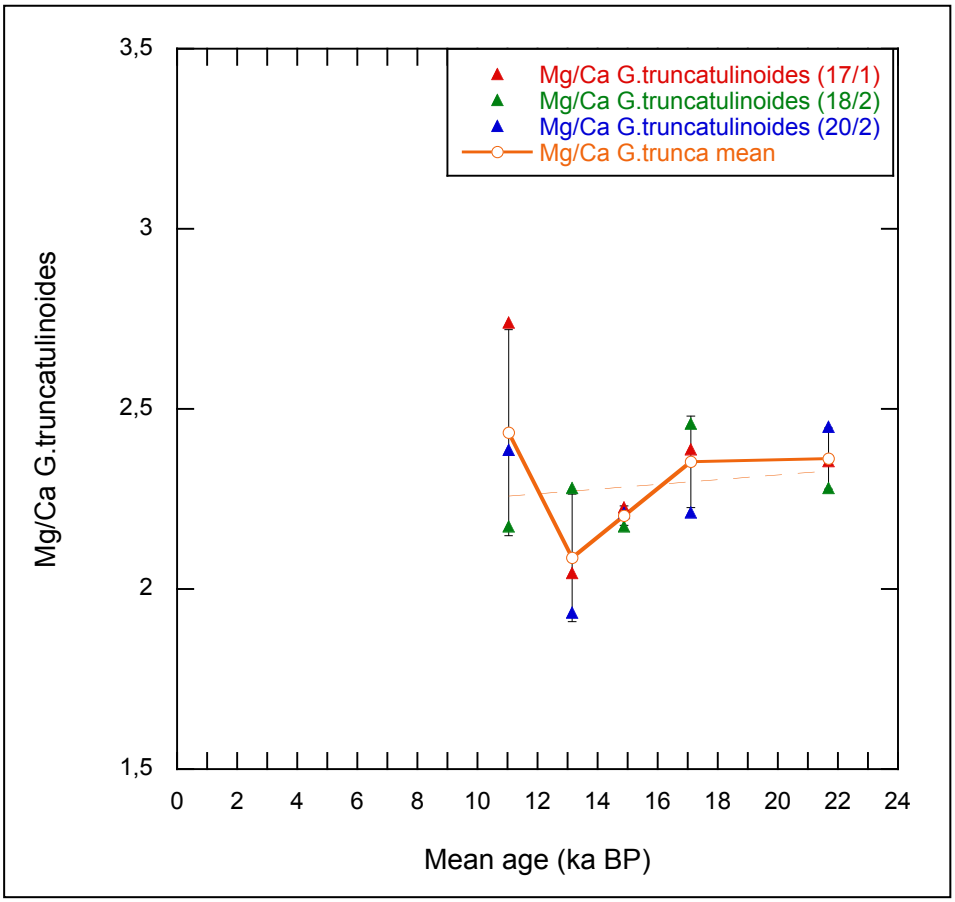

Figure 33: Mg/Ca ratios of G. truncatulinoides (dex) plotted versus age. The Mg/Ca ratios are given as intensity concentrations (mmol/mol). The red, green and blue triangles show the results for individual cores GS07-150 17/1, 18/2 and 20/2, respectively. The orange line indicate the mean result from all the cores. The dotted orange line indicates the linear regression (trend) line.

5.3.2 Evaluation of the Mg/Ca measurements

The possible sample contamination by clays and other materials is evaluated by the measured Fe/Ca ratios in the samples. During element analysis, the iron (Fe) content of the samples is measured on line 259. If the Fe/Ca ratio is higher than a critical value, it is possible that contaminants in the samples have affected the measured Mg/Ca concentrations. Barker et al. (2003) reject measured sample Fe/Ca ratios of >0.1 mmol/mol as potentially significantly contaminated by silicate clays. Figure B.1 and B.2 in Appendix B show the Fe/Ca ratios for *G. ruber* (w) and *G. truncatulinoides* (dex), respectively. They reveal that many of the measurements have a Fe/Ca ratio higher than 0.1 mmol/mol. However, silicate contamination of the samples can also be highlighted by a covariance between Mg/Ca and Fe/Ca (Barker et al., 2003). As indicated in Figure B.3 (Appendix B), there is no evident correlation between Mg/Ca and Fe/Ca in this study. Therefore, despite high Fe/Ca concentrations, none of the measurements are discarded, and possible contaminants are assumed to have been successfully removed.

Post-depositional calcification can occur when carbonate react with the sediment pore water. Secondary calcite is precipitated as Mn-oxide rich «coatings» on the foraminiferal shells. The high content of Mn oxide is caused by anoxic breakdown of organic matter deeper in the sediments. Hence, secondary calcification is indicated by increasing manganese (Mn) content with sediment depth. The secondary calcite can affect the Mg content in the samples. To avoid such influence in the dataset, Barker et al. (2003) reject samples with Mn/Ca ratios of >0.1 mol/mol as potentially significantly influenced by secondary calcification. None of the samples in this study showed Mn/Ca exceeding this limit (Figure B.4 and B.5, Appendix B), so post-depositional calcification is not considered a problem.

As previously mentioned, many planktonic foraminfera migrate vertically in the water column during their life-cycle. As they mature, they commonly descend to deeper waters often forming calcite over a large depth- and temperature range (Barker et al., 2005). Moreover, many species add a secondary crust of calcite in deep waters right before reproduction (gametogenesis). Due to biophysiological controls, this gametogenic calcite may have a Mg/Ca ratio which is distinct from the primary calcite even when formed under similar temperature conditions (Nürnberg et al., 1996). The Mg/Ca ratio of the test of an individual thus reflect the average ratio incorporated througout the life-cycle of the organism

at different times, depths and temperatures (Barker et al., 2005). While this is not considered a problem for *G. ruber*, the Mg/Ca values of *G. truncatulinoides* are most likely affected by vertical migration over great depths. Hence, part of the interspecific variability in the Mg/Ca data for this species, can be attributed to this.

With only one measurement per sample, it is very difficult to assess the reliability of the Mg/Ca measurements. However, the mean Mg/Ca values of the measurments from all three cores, enable some evaluation of the measurements in each timeslice. As seen in Figure 32 and Figure 33, both species display large spread in Mg/Ca values, and three outliers are removed for *G. ruber*. Due to the large scatter in the data, a detailed study of the Mg/Ca development through time is far-fetched. The focus will thus be on the main trends.

5.3.3 Temperature estimates

A temperature equation by Dekens et al. (2002) (without any dissolution corrections) was chosen for the estimation of temperatures based on the Mg/Ca results of *G. ruber*. This equation provides estimates for the youngest timeslice that are well within the range of Holocene temperatures, and gives the over-all closest estimates to the modern temperature at 25 m. Their calibration is based on core-tops from the sub-tropical South-Atlantic. The advantage of core-top calibrations over sediment-trap and culture-based calibrations is that they are based on foraminifers that are part of the sediment record and have gone through a complete life-cycle including gametogenesis and any secondary calcification. A disadvantage is that post-depositional alteration of the material can introduce errors to the calibration (Lea et al., 2003). Moreover, in contrast to culture studies, core-top calibrations are based on temperatures that must be estimated. Hence, temperature becomes a dependent variable, which can cause large errors (Anand et al., 2003). Post-depositional dissolution and calcification are not likely to have affected the samples, as shown in Section 5.3.2. A culture-based study would provide a calibration with an independent temperature variable, but this method also has disadvantages. All taken into consideration, the calibration equation of Dekens et al. is preferred. This equation is able to reconstruct modern sea surface temperature well, and is based on material from a subtropical South-Atlantic core from a location fairly close to the study area. The calibration shows the following relationship between Mg/Ca and temperature:

$$Mg/Ca = 0.38 \exp(0.09T) \qquad R^2 = 0.70 \qquad \text{(Equation 11)}$$

The derived temperature equation is as follows:

$$T = 1/0.09 * \ln(MgCa/0.38) \qquad \text{(Equation 12)}$$

Since the depth habitat of *G. truncatulinoides* is not precisely known, it is difficult to evaluate different temperature equations based on the comparison of core-top Mg/Ca:temperature estimates and modern temperature profiles. Moreover, no Mg/Ca measurements were done on recent samples of *G. truncatulinoides* because of the scarcity of this species in the Holocene samples. Hence, estimating modern ocean temperatures is not possible, and the selection of a temperature equation for *G. truncatulinoides* is more random. An equation by Cléroux et al. (2008) is chosen. Cléroux et al. provide a recent study concerning the Mg/Ca-temperature calibration for *G. truncatulinoides* (dex), and the temperature equation used is based on core-top sediments from the Atlantic ocean. The equation provides temperature estimates that are well within the range of Holocene temperatures. It shows the following relationship between Mg/Ca and temperature:

$$Mg/Ca = 0.62 \pm 0.16 \exp(0.074 \pm 0.017\ Tiso), \qquad R^2 = 0.65 \qquad \text{(Equation 13)}$$

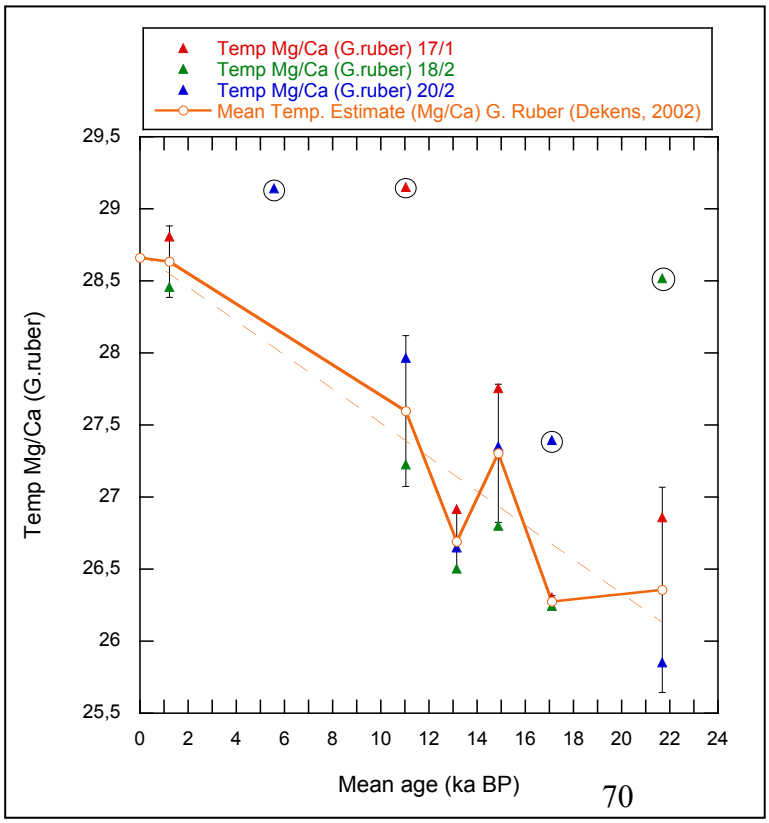

Figure 34: G. ruber Mg/Ca-derived temperature estimates based on the calibration of Dekens et al., 2002. The red, green and blue triangles show the estimates for individual cores GS07-150 17/1, 18/2 and 20/2, respectively. The orange line indicate the mean result from all the cores, excluding the outliers. The dotted orange line indicates the linear regression (trend) line, excluding the outliers. Modern observed temperature at 25 m is also included in the plot.

The derived temperature equation is as follows:

$$T = 1/0.074 * \ln(MgCa/0.62) \qquad \text{(Equation 14)}$$

The Mg/Ca-derived temperature estimates based on the equations of Dekens et al. (2002) and are presented in Figure 34 and Figure 35. Figure 34 shows the Mg/Ca-derived temperature estimates of *G. ruber* (w) based on the calibration of Dekens et al. (2002) for each core plotted versus age. The equivalent results for *G. truncatulinoides* (dex) are shown in Figure 35. Cléroux et al. (2008)

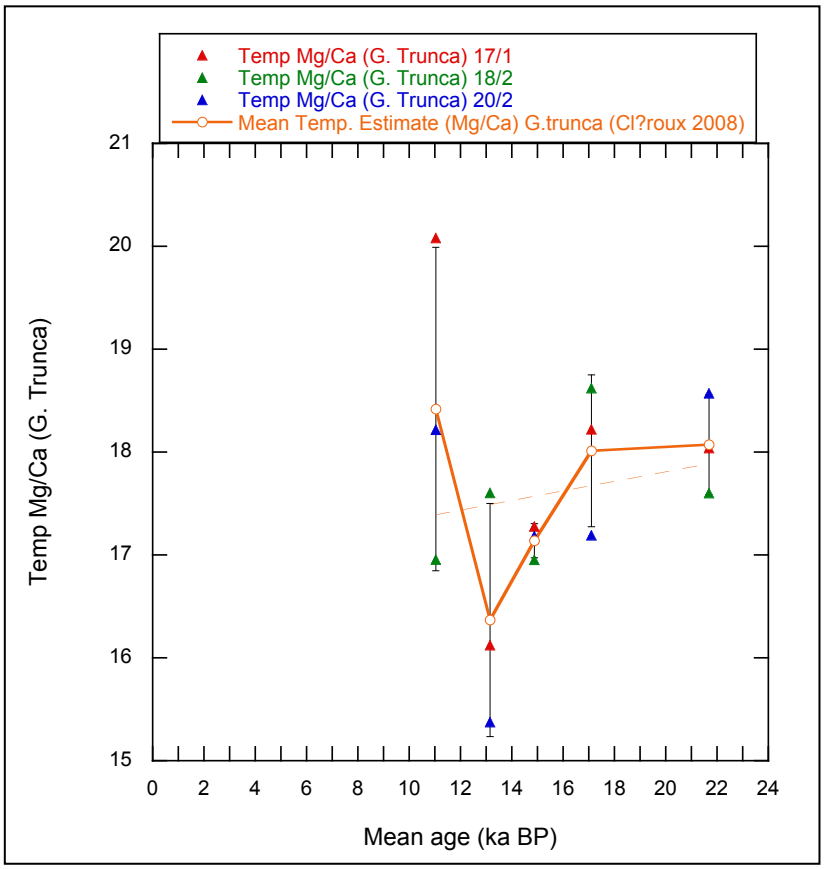

Figure 35: G. truncatulinoides (dex) Mg/Ca-derived temperature estimates based on the calibration of Cléroux et al., 2008. The red, green and blue triangles show the estimates for individual cores GS07-150 17/1, 18/2 and 20/2, respectively. The orange line indicate the mean result from all the cores, excluding the outliers. The dotted orange line indicates the linear regression (trend) line, excluding the outliers.

5.3.4 Glacial-interglacial trends

Figure 34 and Figure 35 show the estimated temperature development of *G. truncatulinoides* and *G. ruber* for core GS07-150 17/1, 18/2 and 20/2, respectively. The observed modern temperatures at the assumed mean calcification depths of *G. ruber* is included in Figure 34.

This temperature was measured at 37.33°W, 3.87°S (WOCE, 2002), where the observed November temperature at 25 m is 28.67°C. In agreement with the trends of the of the shallow and intermediate dwelling species in the oxygen isotope analyses, the shallow-dwelling *G. ruber* show a rising trend in SST from the LGM to the Holocene. The deep-dwelling *G. truncatulinoides* show the opposite trend in the same time period, just as in the oxygen isotope analyses. These temperature trends are evident in all three cores.

5.4 Stratification index

Downcore variations of interspecific planktonic foraminiferal $\Delta\delta^{18}O$ are thought to reflect vertical migration of the thermocline through time. The $\delta^{18}O$ difference between deep and shallow dwellers is a proxy for the stratification of surface waters, and has been used to estimate both temporal and spatial variations in thermocline depth (Mulitza et al., 1997). A deepening of the thermocline would produce higher $\Delta\delta^{18}O$ values, while a shallower thermocline would be reflected by lower $\Delta\delta^{18}O$ values. In Figure 36, this approach is applied using *G. ruber*, *G. trilobus* and *G. glutinata* as shallow-dwellers and *G. truncatulinoides* as a deep-dweller. The plots reveal a glacial-interglacial trend of increasing $\Delta\delta^{18}O$.

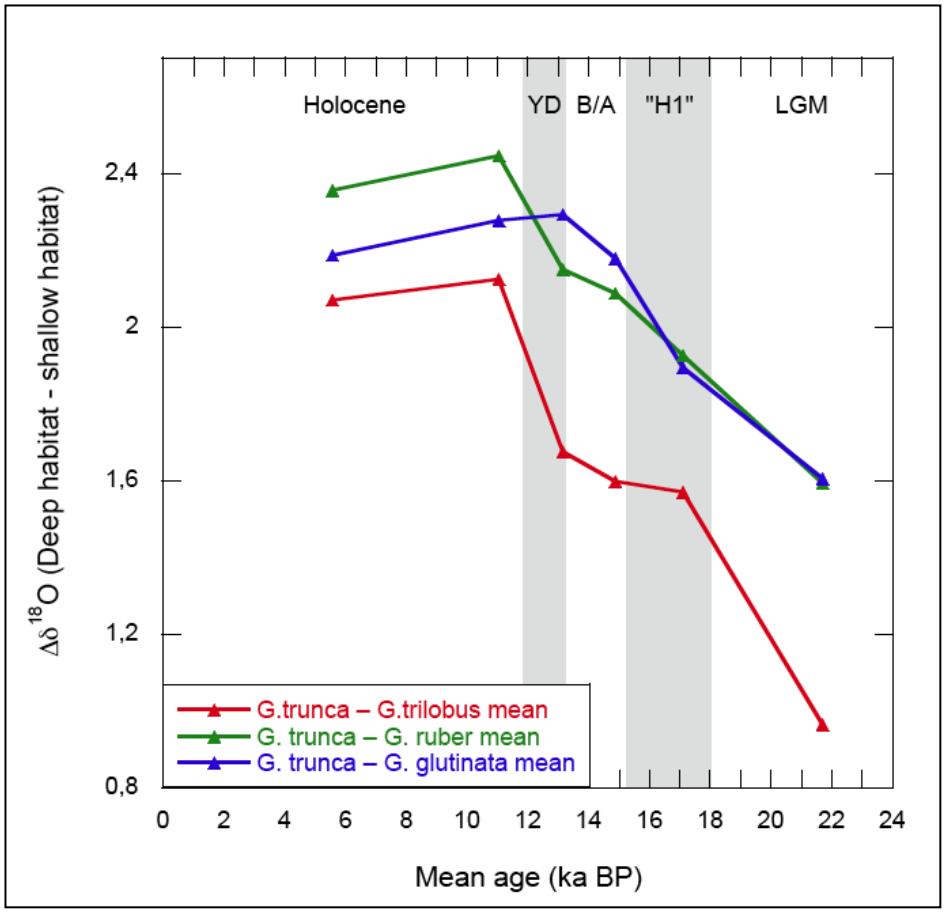

Figure 36: Stratification proxy: Δδ18O between shallow and deep species.

6 Discussion

In this chapter the results presented in Chapter 5 are analysed and put into a paleoclimatic perspective. Assuming that $\delta^{18}O_{IVC}$ is predominantly a function of temperature, variations in the oxygen isotope measurements of the different foraminiferal species are used to indicate changes in the upper-ocean thermal stratification. The $\delta^{18}O$ values are not translated into temperature estimates, but are used as a tool to indicate relative changes in temperature, taking the Mg/Ca results and various other parameters into consideration. As mentioned, large spread in the oxygen isotope measurements complicates the interpretation of the temperature signal for the different timeslices. In order to reduce the scatter in the data, it would be of interest to get more measurements per species for each timeslice. Still, several inferences can be made from the measurements that have been obtained. Focus is put on the large glacial-interglacial trends in $\delta^{18}O$ developement which are evident in all three cores, but variations centred on the different timeslices are also discussed. In the first section, the expectations, given by the hypothesis formulated in Chapter 1, are described. In the next sections the results are compared to the expected temperature developement, and the hypothesis is assessed.

6.1 Expectations

As explained in Chapter 1, it is believed that different modes of circulation prevailed in the Atlantic Ocean during the transition from the last glacial to the present interglacial (Figure 5). Shifts between the different modes have been linked to abrupt changes in climate at a variety of locations on Earth, and several studies have related variations in tropical climate and oceanography to changes in ocean circulation. Manabe and Stouffer (1997) suggest an accumulation of heat in tropical waters during times of weak AMOC. This is believed to be a response to the reduced transport of warm surface and intermediate waters through the tropics to the Northern Hemisphere. The positive temperature anomalies shown by their model, are highest at intermediate depths, while changes in sea surface temperatures are less pronounced (Figure 1).

If Manabe and Stouffer (1997) presents a realistic picture of the relationship between ocean

circulation and the thermal stratification in the tropical Atlantic, it should be possible to detect similar temperature variations in the $\delta^{18}O$ records obtained, as well as in the Mg/Ca derived temperature estimates. Figure 37 shows a simplified illustration of the temperature developement expected from surface and intermediate waters of the western tropical Atlantic from the LGM to the present. The black lines show the expected over-all glacial-interglacial temperature trends at the surface and at subsurface to intermediate depth. Superimposed on these trends, the temperature development reflecting deglacial temperature shifts in response to changes in overturning, is drawn in dark grey. The different climatic extremes investigated, are separated with lighter grey lines, and the strength of the MOC is noted for each period.

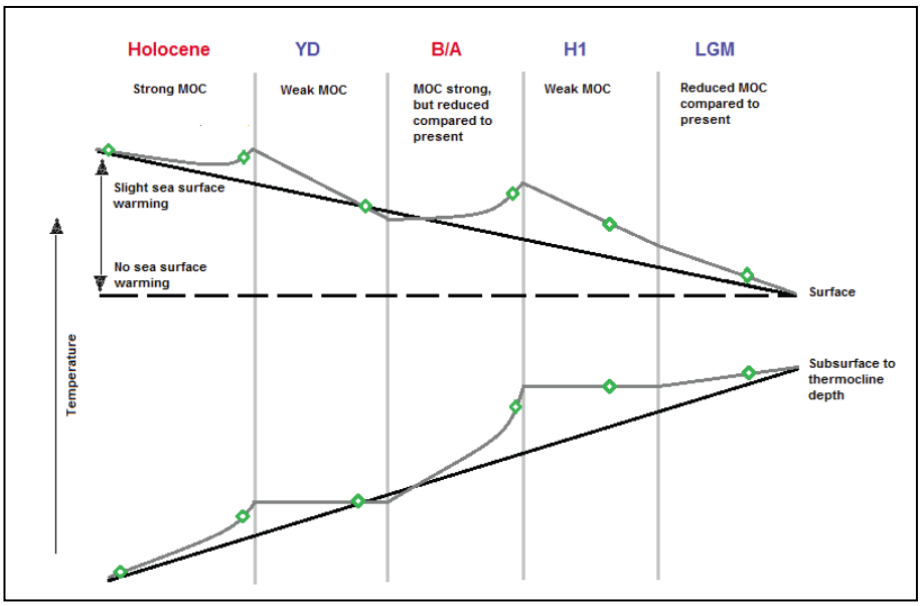

Figure 37: Simplified illustration of the temperature development expected from surface and intermediate waters of the western tropical Atlantic from the LGM to the present. The black lines show the expected temperature trends at the surface and subsurface to intermediate depth. Deglacial temperature shifts are depicted by dark grey lines. Green diamonds indicate the age of the timeslice samples.

As indicated in Figure 37 and Figure 1, the shallow-dwelling foraminiferal species are expected to reveal a slight increase in SST from the last glacial to the present interglacial. This development was described by Mix et al. (1986) in a study concerning the spatial variability in SST inferred for the tropical Atlantic during the last 20,000 years. Their findings suggest that the tropical surface waters were characterized by cold glacial conditions and warm interglacial conditions. Hence, on a glacial-interglacial scale, tropical SST variations are believed to be in agreement with SST changes in the North-Atlantic.

At intermediate depths, however, the glacial-interglacial temperature trend is thought to be different. Lynch-Stieglitz et al. (1999) suggest that the AMOC was reduced to about 2/3 of the present circulation during the LGM. As a consequence, the northward cross-equatorial heat transport was reduced, and heat is believed to have accumulated in the southern hemisphere and the upper-ocean of the tropical Atlantic. This response is related to the interhemispheric see saw effect (Stocker, 1998). As shown by Manabe and Stouffer (1997), accumulation of heat is thought to be best expressed at subsurface to thermocline depths. Hence, the deep dweller, *G. truncatulinoides*, and perhaps also the deepest intermediate dweller, *G. siphonifera*, are considered as potential recorders of this heat storage. Through the transition to interglacial conditions, when the AMOC is strong, a general increase in the northward transport of heat is expected. Accumulated heat is believed to have been released, and as a consequence, a temperature developement opposite to that of the surface-dwellers is expected at intermediate depths from the LGM to the Holocene (Figure 37).

Superimposed on the long-term trends, shifts in temperature are expected for the different timeslices. The temperature extremes centred on the deglaciation are believed to have been hemispherically asymmetrical (Mix et al., 1986). The modelling results of Manabe and Stouffer (1997) show the same pattern for both sea surface and sub surface temperatures, only with higher anomalies at depth. The deglacial variations are assumed to reflect changes in MOC strength believed to result in variations in heat storage in the upper ocean of the tropical Atlantic. For the LGM, H1 and the YD when the overturning slowed down (McManus et al., 2004), a relatively deep thermocline is expected as heat accumulated. During the B/A and the Holocene, more vigorous deepwater formation and deeper overturning prevailed (McManus et al., 2004). This is expected to have caused a shoaling of the thermocline as heat was released northwards. Hence, the temperature variability on this timescale is expected to be opposite to that of the North Atlantic. This anti-phase relationship between the high-latitude North Atlantic and the western tropical Atlantic has been documented in several studies (Arz et al., 1999b; Mix et al., 1986; Rühlemann et al., 1999).

In Figure 37, the green diamonds mark the approximate age of each set of timeslice samples. This gives a better indication of what temperature developement can be expected between the timeslices, as large changes in climate characterize several of the climatic extremes that are investigated. For instance, the B/A, YD and early Holocene timeslices represent early stages

in these three periods. Hence, the paleotemperature data from these timeslices reflect conditions that are more similar to the end of the previous periods: H1, B/A and YD, respectively. Taking this into account, the temperature developement expected to be reflected in the data, can be formulated more precicely:

The shallow-dwellers are expected to reveal small variations in temperature close to the sea surface, as indicated by Manabe and Stouffer's model (Figure 1). An increase in SST is expected from the LGM timeslice to the B/A timeslice, reflecting heat accumulation through the LGM and especially H1. This development has been observed in alkenone data from the Caribbean (Rühlemann et al., 1999). A decrease in temperature is then expected between the B/A- and YD timeslice, reflecting the release of heat through the B/A period. Accumulation of heat is exptected during the YD, indicated by an increase in temperature from the YD timeslice to the early Holocene timeslices. Such a development was also show by the SST proxy of Rühlemann (1999). The Holocene developement is assumed to reveal a decrease in SST as the MOC became strong and heat was released northwards across the Equator. *G. truncatulinoides* and *G. siphonifera* are expected to display the same developement as the other species. However, since the shifts in temperature are believed to have been stronger at intermediate depths, larger amplitudes in the records of one or both of these two species can be predicted.

6.2 Preliminary indications

The general $\delta^{18}O$ records of the three cores give a preliminary indication that western tropical Atlantic SST variations through the last deglacial period can be linked to changes in North Atlantic climate. Figure 25 reveals a glacial-interglacial decrease in the $\delta^{18}O$ of the surface-dweller *G. sacculifer*, which is consistent with the expected SST development. Furthermore, pronounced shifts in the $\delta^{18}O$ values seem to concur with deglacial climatic extremes that have been documented in the North Atlantic. Assuming that changes in $\delta^{18}O$ primarily reflect temperature variations, the records are largely in agreement with the studies of Arz et al. (1999b) and Ruhlemann et al. (1999) which indicate that the deglacial temperature variations in the western tropical Atlantic were opposite of the temperature variations in the North Atlantic. If good age control is assumed, the $\delta^{18}O$ records in Figure 25 show an increase in

SST during H1, followed by cooling in the Bølling-Allerød period. A subsequent warming is implied for the Younger Dryas before another cooling occurred in the beginning of the Holocene.

6.3 Preferential habitat depths of the different species

No attempt is made to estimate the calcification depths of the different species in this study. Still, to some extent, the measured $\delta^{18}O_{IVC}$ can be used as an indication of the depth range and water mass in which each species lives (Figure 31). If the $\delta^{18}O_{IVC}$ is primarily a function of temperature, the shallow dwellers are expected to give lower $\delta^{18}O_{IVC}$ values than the intermediate dwellers, and the deep dweller is expected to record the highest values. It is obvious that the deep-dwelling *G. truncatulinoides* records a very different $\delta^{18}O_{IVC}$ signal than the other species, and *G. siphonifera* seems to live in subsurface water. This intermediate dweller is expected to primarily record temperature conditions of the TSW, but has been known to migrate deeper to the SACW (Field, 2004). As mentioned, the $\delta^{18}O_{IVC}$ values of intermediate dweller *G. glutinata* does not express the expected $\delta^{18}O_{IVC}$ relative to the shallow dwellers. The isotopic values of this species are more similar to those of shallow dweller, *G. ruber*. Hence, in this study *G. glutinata*, *G. ruber* and *G. trilobus* are all considered to be confined to the upper part of the Tropical Surface Water.

G. truncatulinoides is known to calcify in deeper waters. As seen in Figure 31, *G. truncatulinoides* deviates a lot in $\delta^{18}O_{IVC}$ and glacial-interglacial trend when compared to the results of the other species. The relative positive offset from the values of the other species is taken as a confirmation that *G. truncatulinoides* indeed is a recorder of deeper waters. Since the offset is so large and the over-all trend opposite to those of the other species, it is believed that the species record conditions below the mixed-layer as suggested by Ravelo and Fairbanks (1992) and Mulitza et al. (1997) . *G. truncatulinoides* is thus expected to primarily record the temperature conditions of the SACW, the water mass underlying the mixed layer. In the tropical Atlantic the SACW today extends to about 500 m. A shallowing of the underlying AAIW might potentially have affected G. truncatulinoides over time.

6.4 Stratification proxy

The use of interspecific $\delta^{18}O$ gradients as a proxy for the vertical temperature gradient in the upper water column, has been proposed by several authors for well-stratified regions of the tropical ocean (e.g. Mulitza et al., 1997; Ravelo and Fairbanks, 1992; Steph et al., 2009). The difference in $\delta^{18}O$ between species with different preferential habitat depths, provides a useful tool for monitoring variations in thermocline depth (TCD). Since the proxy is based on differences in $\delta^{18}O$ between species, it is independent of the global ice volume. From the recontructed variations in TCD, changes in heat storage in the tropical upper ocean water, can be inferred. The method assumes little vertical migration of the foraminfera in response to changes in TCD, and salinity gradients are also presumed to be relatively constant.

As mentioned in Chapter 3, increased $\Delta\delta^{18}O$ between shallow- and deep-living species is taken as an indication of increased stratification of the upper ocean with shallower mixing and shoaling of the thermocline. Decreasing $\Delta\delta^{18}O$ suggests low-stratified surface waters with deeper mixing and a smaller vertical temperature gradient. In other words, the thermocline deepens as $\Delta\delta^{18}O$ drops. If the climate model of Manabe and Stouffer (1997) shows a realistic image of the response of the tropical Atlantic ocean to changes in the THC, lower $\Delta\delta^{18}O$ values would be expected for periods associated with a reduced AMOC. In times of more vigorous ocean circulation, a shallower thermocline would be reflected by higher $\Delta\delta^{18}O$ values.

The over-all glacial-interglacial trends displayed in Figure 36 show an increase in $\delta^{18}O$ difference between the shallow-dwelling species and the deep-living *G. truncatulinoides* (dex). The positive glacial-interglacial trends are interpreted as a shoaling of the thermocline through the deglacial period. In other words, the amount of heat stored in the upper-ocean of the western tropical Atlantic decreased from the LGM to the Holocene period. This development concurs with the general strengthening of the AMOC through the transition from glacial to interglacial conditions (McManus et al., 2004) (Figure 31), as the northward transport of heat through the tropical Atlantic increased. Hence, the observed development in the stratification proxy supports the hypothesis on the glacial-interglacial scale.

On the timeslice level, the results of the stratification proxy do not agree with the anticipated development (Figure 36). This might be linked to the abruptness and short duration of the

climatic shifts. While the long glacial-interglacial $\delta^{18}O_{IVC}$ trends show large differences between the inferred surface and subsurface temperatures, the abrupt temperature changes centred on the deglaciation, are expressed equally in the upper water column. Both surface and subsurface seem to experience an instant repsonse to AMOC changes, and all species display temperature variations opposite to those documented in the northern hemisphere (Figure 31). Since the difference in the temperature response to short-lasting interruptions of the AMOC is small between the surface and subsurface, the heat accumulation in the tropical upper ocean is not reflected by the stratification proxy. The difference between surface and subsurface temperatures seems build up over longer periods, such as the glacial-interglacial period for which the stratification proxy expresses the expected signal.

6.5 Glacial-interglacial trends

To aquire a more detailed assessment of the long-term temperature developement, the $\delta^{18}O_{IVC}$ values of the different species are examined. As seen in Figure 31 a clear glacial-interglacial decrease in $\delta^{18}O_{IVC}$ is evident for *G. trilobus*, *G. ruber* and *G. glutinata*. The change is considered to mostly reflect an increase in temperature. *G. ruber* is regarded as the best foraminiferal recorder of SST (Ravelo and Fairbanks, 1992) , and since the two other species also display similar temperature evolutions, changes in preferential habitat depth of the shallow dwelling species are considered less important for the interpretation of the long-term $\delta^{18}O$ developement than temperature variations. The average difference between the LGM and Late Holocene $\delta^{18}O_{IVC}$ values for the three species is 0.4‰. Assuming that the $\delta^{18}O_{IVC}$ can be attributed to temperature alone, a glacial-interglacial shift in surface water temperature of almost 2°C can be inferred using the $\delta^{18}O$-temperature relationship estimated by Shackleton (1974) . The trend in $\delta^{18}O_{IVC}$ for the surface living species is consistent with the study of Mix et al. (1986) which suggest an interhemispheric symmetry in the SST development on this time scale- It also agrees with the $\delta^{18}O$ data from N-GRIP shown in Figure 26.

The trend of intermediate-dwelling *G. siphonifera* only shows a slight decrease in $\delta^{18}O_{IVC}$ from the LGM to the Holocene, although (as discussed below) large variations are associated with this species between the timeslices. Hence, only a small over-all change in temperature in the depth range of this species is inferred from the LGM to present. *G. truncatulinoides*,

however, displays a clear glacial-interglacial increase in $\delta^{18}O_{IVC}$ from the LGM to the Holocene. Assuming that temperature constitutes the only control on the oxygen isotopic signal, a temperature decrease of about 1.5°C can be inferred in the depth range of *G. truncatulinoides* (Shackleton, 1974). Changes in preferential habitat depths over time have been proposed for this species in the western Atlantic (Cléroux and Lynch-Stieglitz, 2010). As discussed in Section 6.3 and Section 6.7, such changes would severely complicate the interpretation of the isotopic measurements.

The Mg/Ca-derived temperatures for *G. ruber* show a glacial-interglacial trend that is in very well agreement with the mean $\delta^{18}O_{IVC}$ of the same species (Figure 38). Figure C.1 in Appendix C also reveals the good correlation between the two variables. This implies that *G. ruber* is a suitable species for Mg/Ca paleotemperature reconstructions, and that the changes in $\delta^{18}O_{IVC}$ are mainly dependent on temperature. The difference in Mg/Ca-temperatures for *G. ruber* between the LGM and the Late Holocene is about 1.6°C. Although this estimate is uncertain, the good agreement with the temperature difference inferred from the $\delta^{18}O_{IVC}$ values, can be noted.

The Mg/Ca-derived temperatures for *G. truncatulinoides* does not display the same degree of covariance with the species' mean $\delta^{18}O_{IVC}$ values Figure 39. However, the Mg/Ca temperature estimates do indicate a decreasing glacial-interglacial trend. For *G. truncatulinoides* the calculation of the glacial-interglacial temperature shift is a lot more uncertain than for *G. ruber*. Since no late Holocene Mg/Ca measurements were obtained, a comparison can only be made between the Mg/Ca-temperature from the LGM and the observed modern temperature at an assumed fixed habitat depth (Bainbridge, 2004). This gives a glacial-interglacial temperature difference at intermediate depths of almost 4°C. The estimate is probably not realistic, but at least the expected negative trend in temperature at intermediate depth is confirmed in the Mg/Ca as well.

The fact that both the oxygen isotope results and the Mg/Ca data reveal the same glacial-interglacial trends, strengthens the hypothesis that more heat was stored in the upper ocean in of the western tropical Atlantic during the LGM than today. When comparing the obtained data with the $^{231}Pa/\ ^{230}Th$ data of McManus (2004) in Figure 31, further support for the hypothesis is gained. $^{231}Pa/\ ^{230}Th$ is a kinematic proxy for the AMOC, where decreasing ratios are interpreted as an increase in overturning. Both McManus et al. (2004) (Figure 31)

and Lynch-Stieglitz et al. (1999) indicate that the strength of the AMOC increased from the LGM to the present. The increase in AMOC strength occurs alongside the decrease in inferred heat accumulation in the western tropical Atlantic, supporting the idea that variations in tropical Atlantic heat storage is related to AMOC strength.

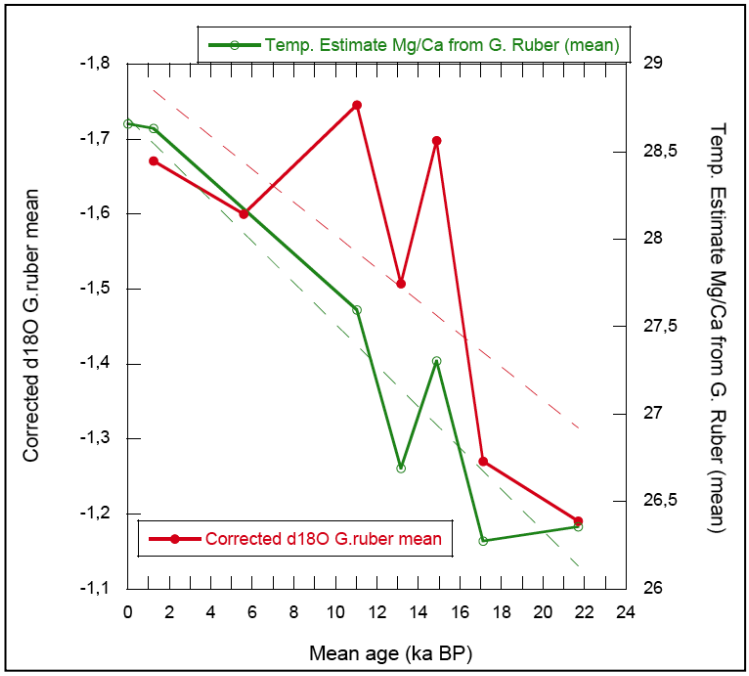

Fig. 38: Comparing Mg/Ca temperature estimate of G. Ruber with $\delta^{18}O$

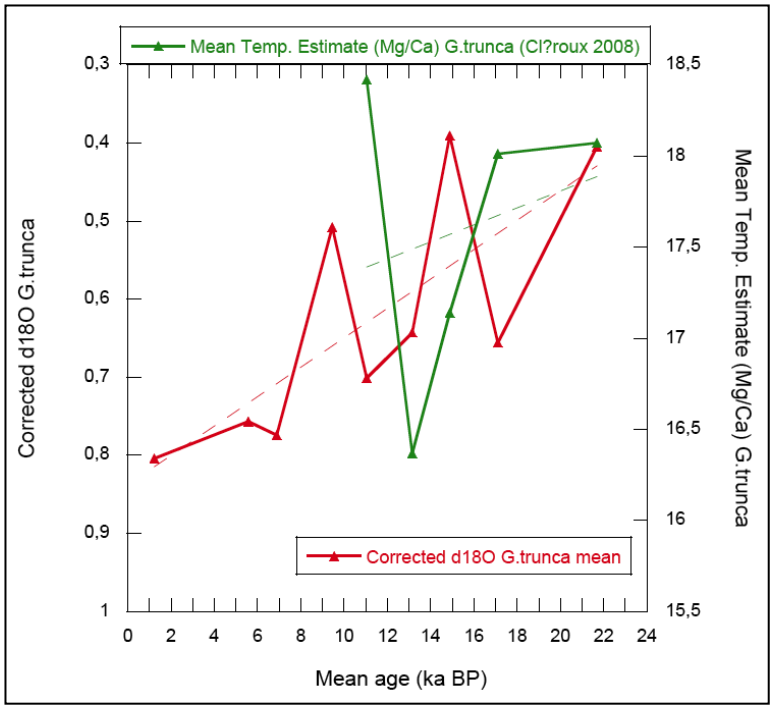

Fig. 39: Comparing Mg/Ca temperature estimate of G. Truncatulinoides with $\delta^{18}O$

6.6 Timeslice reconstructions

As seen in Figure 31, an over-all temperature increase from the LGM to the B/A is indicated by a decrase in $\delta^{18}O_{IVC}$. The drop in oxygen isotope composition is evident for all species between the H1 and the B/A timeslices, while the $\delta^{18}O_{IVC}$ developement from the LGM to the beginning of H1 is more variable. During the LGM, *G. truncatulinoides* (and *G. siphonifera*) show an increase in $\delta^{18}O_{IVC}$. This might reflect the onset of the deglaciation as the AMOC increased in strength and heat was released northwards across the equator before the AMOC was interupted in H1. In H1 the AMOC is believed to have been strongly reduced, causing heat to accumulate in the upper tropical Atlantic. From the B/A timeslice to the timeslice representing early YD, an increase in $\delta^{18}O_{IVC}$ is shown for all species. Therefore, a drop in temperature can be inferred through the B/A. This is in agreement with the expected developement for B/A, where a stronger AMOC causes the accumulated heat to be released as it is transported north across the Equator.

During the YD, accumulation of heat is again believed to have happened. The records of *G. ruber*, *G. glutinata and G. siphonifera* supports this expectation. These species show a decrease in $\delta^{18}O_{IVC}$ through the YD. However, *G. glutinata* and *G. truncatulinoides* display an increase in $\delta^{18}O_{IVC}$ during the same period. This could partly be a result of the selection of timeslices. The timeslices are not optimal for the temperature reconstructions as they do not capture the minimum or maximum temperatures of all of the different climatic extremes (Figure 31 and Figure 37). This is particularly problematic for the B/A-YD transition. Through the Holocene a general increase in $\delta^{18}O_{IVC}$ is shown for all species. This is interpreted to reflect a decrease in temperature as accumulated heat is transported northwards with the surface and intermediate currents of the strong interglacial AMOC.

Although the timeslice developements in $\delta^{18}O_{IVC}$ for the different species are not completely in agreement with each other, the records are consistent with the hypothesis to a large extent. For the most part, all the species indicate similar temperature developements for each timeslice, regardless of their habitat depths. Hence, the previously described anti-phase relationship with North-Atlantic SST is demonstrated. *G. siphonifera* shows shifts in $\delta^{18}O_{IVC}$ with very large amplitudes in some of the timeslices. This might imply that the large changes

in temperature, occurred at the depth where *G. siphonifera* calcifies. This agrees with the idea that the temperature anomalies associated with changes in the AMOC are best expressed in subsurface waters.

As mentioned, the Mg/Ca-derived temperatures of *G. ruber* agree very well with the inferred temperatures from the $\delta^{18}O_{IVC}$ results. The species reflect a SST developement that largely confirms the expectations given in Section 6.1. Figure 38 displays the mean $\delta^{18}O_{IVC}$ and the Mg/Ca temperature estimates of *G. ruber* versus age in one plot, where both y-axes span 3°C. Hence, the difference in the amplitudes of the fluctuations of Mg/Ca temperatures and $\delta^{18}O_{IVC}$ can easily be observed. While the over-all LGM – Holocene development is very similar, the fluctuations of $\delta^{18}O_{IVC}$ display larger amplitudes than the Mg/Ca temperature in the timeslices. This might indicate that the $\delta^{18}O_{IVC}$ values are influenced by $\delta^{18}O$ varations in the water mass which are not related to temperature. The difference in the signal is largest for H1 and the YD. Decreased salinity during these periods could explain the difference in amplitudes. Such changes in salinity could be related to increased freshwater input caused by a southward migration of the ITCZ during H1 and the YD. As described in Chapter 1, such migrations of the ITCZ have been suggested by several authors (e.g. Peterson et al., 2000; e.g. Wang et al., 2004) . The migrations have been linked to variations in rainfall, reflected in the Ti and Fe content of marine sediments off the northern South American coast. Arz (1999a) linked increased runoff from north-eastern Brazil to periods of northern coolings (Arz et al., 1999a). This is consistent with the salinity variations that could possibly be inferred from Figure 38, and also with the XRF intensity records obtained for the correlation of the cores in this study (Figure 24).

As mentioned, in contrast to *G. ruber*, the Mg/Ca results of *G. truncatulinoides* show a very poor correlation with the $\delta^{18}O_{IVC}$ values. Through H1 the temperatures develop in the opposite direction of what is expected. For B/A and the YD, however, the results support the temperature developement inferred from the $\delta^{18}O_{IVC}$ values. The large scatter in the data, makes the interpretation very uncertain, so no conclusions based on the Mg/Ca measurements, are drawn about the subsurface temperature variations between the timeslices.

6.7 Paleoceanographic implications

As discussed in Section 6.5 the $\delta^{18}O_{IVC}$ values are in well agreement with the expected glacial-interglacial temperature trends. Hence, the hypothesis that changes in heat accumulation in the tropics is related to AMOC strength, seems viable. However, the changes in $\delta^{18}O_{IVC}$ could be a result of other influences. As mentioned, changes in the preferential habitat depth of G. truncatulinoides have been suggested by (Cléroux and Lynch-Stieglitz, 2010). Moreover, changes in water mass properties by increasing influence of AAIW could also alter the oxygen isotopic composition of the deep-dweller. Since *G. truncatulinoides* is the species recording the glacial-interglacial temperature shift at intermediate depth, the change in $\delta^{18}O_{IVC}$ of species is investigated more closely below.

6.7.1 Changes in preferential habitat depth

The reconstruction of upper ocean temperature stratification is based on the observation that different species of planktonic foraminifera live vertically dispersed in the water column. The previous interpretations of the foraminiferal $\delta^{18}O_{IVC}$ values are made, assuming that the variations in the data reflect temperature changes within a relatively fixed depth range. The preferential habitat depths of the various species are assumed to be constant through time, so that each species record temperature variations within a particular range of water depths. However, as preferential habitat depth depends on various properties of the water column, such as salinity, temperature, density and nutrients, the preferential habitat of a given species most likely varies through time. Changes in the depth habitats of several species in the tropical Atlantic have been indicated by Steph et al. (2009). Their results suggest that most species do not maintain a fixed habitat depth under different hydrographic conditions. Hence, variations in the preferential habitat depths of the various species potentially constitute a major bias in the paleotemperature reconstructions in this study, as hydrographic conditions are likely to have varied on glacial-interglacial timescales.

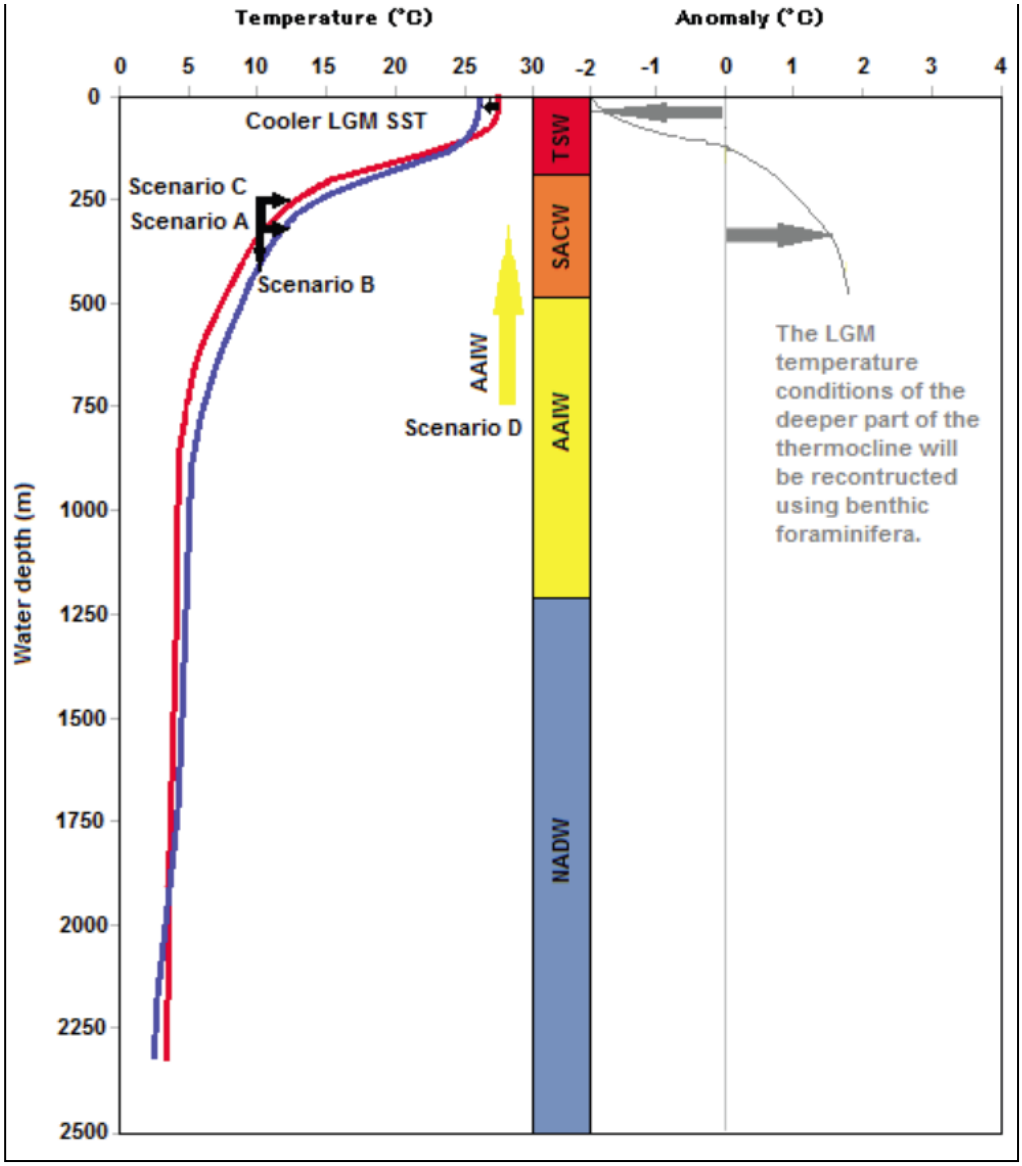

Figure 40: Plot to the left: vertical temperature profiles for the western tropical Atlantic. The red curve represents modern conditions, while the blue curve depicts LGM temperatures inferred from the oxygen isotope results. Four scenarios that might have caused changes in the $\delta^{18}O_{IVC}$ *of G. truncatulinoides, are illustrated. Plot to the right: the temperature shifts from the LGM to the present, inferred from the* $\delta^{18}O_{IVC}$ *of the different species, are illustrated by the grey line. The approximate glacial-interglacial change in the* $\delta^{18}O_{IVC}$ of the shallow-dwellers and G. *truncatulinoides* are given by the grey arrows. For *G. siphonifera* the shift in $\delta^{18}O_{IVC}$ is about zero. The modern vertical stratification of water masses is given by the colour bar.

6.7.2 The glacial-interglacial shift in $\delta^{18}O_{IVC}$ of G. truncatulinoides

Figure 40 displays two vertical temperature profiles given for the western tropical Atlantic. The red curve represents modern conditions, while the blue curve depicts LGM temperatures inferred from the oxygen isotope results. Compared to the modern profile, the LGM curve show cooler SST and a deeper thermocline. The LGM temperatures at depth are not necessarily realistic, as they are merely based on the temperature anomalies found by Manabe and Stouffer in their model experiment. As indicated by the glacial-interglacial difference in the oxygen isotope results of the shallow dwellers, the LGM SST temperature is almost 2°C lower than the present SST. At subsurface depths, where *G. siphonifera* lives, the temperature difference is about zero. Around the habitat depth of *G. truncatulinoides* the LGM temperature is about 1.5°C higher than at present. The anomalies are depicted in the plot at the right. The $\delta^{18}O_{IVC}$ of the shallow and intermediate dwellers are considered to primarily reflect temperature change at a relatively constant depth range. However, four different scenarios that could result in the observed glacial-interglacial shifts in the $\delta^{18}O_{IVC}$ of *G. truncatulinoides*, are illustrated in the plot. The various scenarios are explored below to see which of them could produce the glacial-interglacial difference in $\delta^{18}O_{IVC}$ that agrees with the results.

Scenario A

Scenario A is illustrated by the horisontal arrow in Figure 40. In this scenario, the preferential habitat depth of *G. truncatulinoides* is assumed to be relatively constant through time and any variations in $\delta^{18}O_{IVC}$ are governed by temperature only. SST increases from the LGM to the present, and the temperature at intermediate depths decrease in the same time interval. The glacial warming of subsurface waters supports the hypothesis that heat is accumulated at intermediate water depths in the tropical Atlantic during periods of weaker AMOC. This is the scenario described in Section 6.5 which agrees well with the expectations for the results.

Scenario B

Scenario B is illustrated by the downward arrow. In this scenario *G. truncatulinoides* migrates to greater depths, while temperature conditions in the water column stays the same. The change in habitat depth does not, however, result in the positive temperature anomaly

expected from the hypothesis and reflected by the measured $\delta^{18}O_{IVC}$ of *G. truncatulinoides*. In order to account for the higher LGM temperature indicated by the $\delta^{18}O_{IVC}$, the thermocline would have to be even deeper. Hence, this scenario does not support the hypothesis.

Scenario C

Scenario C is illustrated by the upward arrow. Any changes in $\delta^{18}O_{IVC}$ are attributed to upward vertical migration of *G. truncatulinoides* to warmer waters. Cléroux and Lynch-Stieglitz (2010) suggested large changes in the preferential depth habitat of *G. truncatulinoides* based on oxygen isotope analyses on samples from the Gulf of Mexico and the western Atlanic. Their study proposed a much shallower habiatat for *G. truncatulinoides* between 8 and 10 ka BP compared to the deglaciation and the late Holocene. An shallower preferred habitat depth of *G. truncatulinoides*, would result in a temperature increase. Therefore, Scenario C could give the expected change in $\delta^{18}O_{IVC}$ without implying any temperature changes.

Scenario D

Scenario D is illustrated by the light blue arrow. Here, the preferential habitat depth of *G. truncatulinoides* is assumed to be relatively constant through time, and the changes in $\delta^{18}O_{IVC}$ are considered to be a response to changes in watermass properties due to an increased influence of Antarctic Intermediate Water. AAIW taking up more of the upper water column, could explain the relatively higher LGM $\delta^{18}O_{IVC}$ values of *G. truncatulinoides* as this water mass has a lower $\delta^{18}O$ signature than the TSW and SACW. In todays water column AAIW $\delta^{18}O$ at the site is about 0-0.2 ‰, while the $\delta^{18}O$ of the surface waters is about 0.8-1 ‰ (Schmidt et al., 1999) . Hence, as a rough estimate, the influence of AAIW could account for a decrease of up to 1 ‰ in $\delta^{18}O_{IVC}$ between the LGM and the Holocene, which is a lot more than the glacial-interglacial difference given by the measurements. However, one would expect AAIW to be colder than the TSW and SACW. Therefore, the thermocline would be pushed upwards and the cold water would cause a relative lowering of the $\delta^{18}O_{IVC}$ in *G. truncatulinoides.* Hence, the measured $\delta^{18}O_{IVC}$ values could be explained by the joint influence of change in the temperature and the isotopic signature of the water.

As a near-independent temperature proxy, the measured Mg/Ca ratios of *G. truncatulinoides* can be used to assess the chance that AAIW acutally caused the trends seen in the oxygen isotope data. As mentioned, the Mg/Ca results cannot be regarded as very robust for each

timeslice due to few measurements and large scatter in the data. Still, the decreasing deglacial temperature trend seen in all the three records, implies that the LGM temperature was in fact warmer at intermediate depths. Since the Mg/Ca trends are considered trustable, Scenario D can most probably be discarded. To check further, the effect of AAIW could be evaluated by Mg/Ca measurements of benthic foraminfera, and changes in $\delta^{13}C$ can indicate if any change in water mass influence took place at the preferential habitat depth range of *G. truncatulinoides.*

6.8 Paleoceanographic implications inferred from the timeslice reconstructions

Manabe and Stouffer's modelling study tries to simulate a Younger Dryas-like event. Hence, the hypothesis that they present a realistic picture of the tropical response to AMOC variability, is best evaluated by comparing the model results with the timeslice reconstructions since they represent changes on the same timescale as the modelling study. Because of the large scatter in the data, the timeslice reconstructions are not conclusive. However, some indications about the temperature developement are found. Figure 41 show the temperature anomalies with depth as given by Manabe and Stouffer (1997). The model show an increase of 0.5°C in SST and an increase of about 3°C in the depth range where *G. truncatulinoides* is assumed to calcify. In the figure, the approximate temperature change inferred through the YD are indicated by grey arrows for surface and subsurface waters by the $\delta^{18}O_{IVC}$ *G. ruber* and *G. siphonifera.* Although the magnitudes of the temperature changes are uncertain, the oxygen isotope results reveal a similar temperature response in the YD as shown by the model results. Both SST and subsurface temperature respond in the same direction, and the largest variations are shown in the habitat depth range of intermediate-dwelling *G. siphonifera*. For H1 (not illustrated), a similar pattern is seen. Hence, in addition to supporting the hypothesis on the glacial-interglacial scale, the results also indicate a possible heat accumulation in the western tropical upper ocean during shorter interruptions of the AMOC.

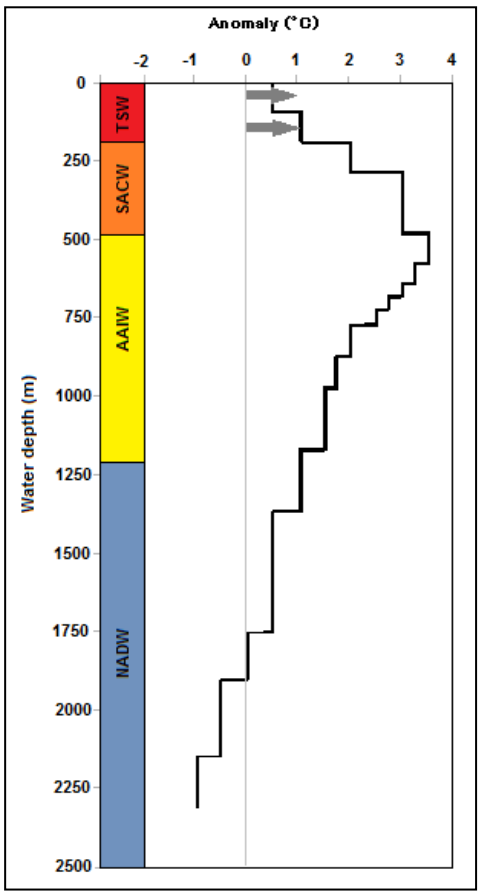

Figure 41: Temperature anomalies with depth as given by Manabe and Stouffer (1997). The approximate temperature change inferred by $\delta^{18}O_{IVC}$ through the YD are indicated by grey arrows for surface and subsurface waters by the G. ruber and G. siphonifera. The modern vertical stratification of water masses is given by the colour bar.

7 Conclusion

This study sets out to test the hypothesis that variations in the strength of the AMOC are related to changes in the thermal stratification of the upper tropical Atlantic Ocean, as suggested in Manabe and Stouffer's (1997) modelling study. During periods of weak AMOC, reduced cross-equatorial heat transport by tropical ocean currents is believed to result in heat accumulation in the southern hemisphere, expressed by a warmer upper tropical water column. An attempt to reconstruct past thermal stratification of the tropical upper ocean is made for six time slices, believed to be associated with different modes of AMOC. The six time slices represent the Last Glacial Maximum, Heinrich event 1, Bølling-Allerød, the Younger Dryas and the early and late Holocene. Using the oxygen isotope composition and Mg/Ca ratios of the tests of five species of planktonic foraminfera, changes in temperatures at various depths in the upper water column are inferred.

On a glacial-interglacial timescale, the results of the oxygen isotope analysis support the hypothesis that AMOC strength is linked to thermal stratification in the western tropical Atlantic. Variations in the species' preferential habitat depths could contribute to the observed variations in $\delta^{18}O$. However, whether the species' habitat depths are constant through the climate transitions, remains an unsolved question, and the conclusion drawn here is based on the assumption that the species maintained a relatively constant habitat depth during the deglaciation. For the LGM, which has been associated with weak AMOC, a relatively deep thermocline can be inferred by the oxygen isotope stratification proxy. In contrast, the stratification proxy implies stronger thermal stratification during the Holocene when strong AMOC prevailed. The glacial-interglacial trends in the $\delta^{18}O_{IVC}$ values of the different species indicate that SST was lower during the LGM than at present, while subsurface temperatures were higher. *G. truncatulinoides* appear to be a good recorder of temperature variability at intermediate depths on this timescale. The Mg/Ca measurements support the oxygen isotope results, as the same trends are shown in these data. Together both the stratification proxy and the trends in the data given by the two paleotemperature proxies, suggest that more heat was stored in the western tropical Atlantic during the LGM than during the present interglacial.

On the timeslice level the stratification proxy is not useful since the difference in surface and subsurface temperatures seem to build up over longer time periods. The oxygen isotope

results for the LGM and YD are not conclusive as the temperature developments shown by the different species, are not in agreement with each other. However, the temperature induced changes in $\delta^{18}O_{IVC}$ agree with the expected developement for the other time periods. All species reveal an increase in temperature during H1, and a drop in temperature during B/A and through the Holocene. *G. siphonifera* displays the largest amplitudes, indicating that the largest variations in temperature happened in the habitat depth range of this species. Hence, *G. siphonifera* might be the best recorder of thermocline variations on this timescale. The Mg/Ca results for *G. ruber* strongly support the SST developement suggested by the $\delta^{18}O_{IVC}$. However, higher amplitudes in the $\delta^{18}O_{IVC}$ values compared to the Mg/Ca-inferred temperatures suggest that the $\delta^{18}O_{IVC}$ values are influenced by an other component than temperature. If this component is salinity, the results indicate lower salinity during H1 and YD, and increased freshwater runoff related to a southward migration of the ITCZ during these periods is suggested. The Mg/Ca results of *G. truncatulinoides* support the $\delta^{18}O_{IVC}$ results for some timeslices, but the interpretation of the temperature developement is uncertain.

All taken into account, the hypothesis of the study can not be rejected. The results suggest that more heat was stored in the western tropical Atlantic upper ocean during the LGM when the AMOC was reduced, than during the Holocene, when vigorous overturning prevailed. Stronger uncertainty is tied to the link between tropical heat storage and the deglacial interuptions of the AMOC. However, the results of the study give incentive for further investigation of the topic. The optimal approach would be a full oxygen isotope stratigraphy with replicate measurements of all species from each cm down-core. However, a less time consuming alternative would involve the introduction of a few more time slices in order to capture the minimum and maximum temperatures for each climate period. Better tuning of the cores would be helpful in the selection of the new time slices.

The oxygen isotopes of *G. ruber* proves to be a good indicator of temperature change, and *G. truncatulinoides* and *G. siphonifera* appear to record subsurface temperature variations. Therefore, further studies could focus on obtaining a more robust signal these three species. Additional Mg/Ca measurements are also needed in order to reduce the scatter in these data and acquire a more robust temperature signal. Finally, it would be useful to estimate the apparent calcification depths of each species, and hence, better constrain the temperature estimates to certain depth ranges.

Appendices

Appendix A Stable oxygen isotope measurements

Table A.1 Stable oxygen isotope measurements of *G. sacculifer* from cores GS07-150 20/2, GS07-150 18/2 and GS07-150 17/1.

Core GS07-150 20/2	
Depth (cm)	δ18O
10	-0.83
20	-1.14
30	-1.06
40	-0.39
50	-0.49
60	-0.39
70	-0.21
80	-0.78
90	-0.83
100	-0.71
110	0.05
120	0.12
130	-0.57
140	-0.11
150	0.17
160	0.44
170	0.63
180	0.28
190	0.37
200	0.53
210	0.24
220	0.13
230	0.02
240	-0.16
250	0.44

Core GS07-150 18/2	
Depth (cm)	δ18O
0	-0.87
10	-1.19
20	-0.98
30	-1.10
40	-0.89
50	-0.56
60	-0.48
70	-0.44
90	-0.24
100	0.06
110	0.16
120	-0.75
130	0.88
140	0.18
150	0.46
160	0.37
170	0.47
190	0.38
200	0.23
210	0.39
220	0.46
230	0.22
240	0.18
250	-0.11
260	0.02

Core GS07-150 17/1	
Depth (cm)	δ18O
0	-0.78
0	-1.30
10	-1.25
10	-1.15
20	-1.32
20	-0.95
30	-1.07
40	-1.07
50	-0.63
60	-1.03
70	-1.26
80	-0.56
90	-0.67
100	-0.01
110	-0.26
120	-0.29
130	-0.04
140	0.45
150	0.58
160	0.46
170	0.59
180	0.41
190	0.37
200	0.85
210	-0.11
220	0.67
230	-0.06
240	0.33
250	0.21
260	0.19
270	-0.16
280	-0.21

Table A.2 Stable oxygen isotope measurements of *G. trilobus* from cores GS07-150 20/2, GS07-150 18/2 and GS07-150 17/1.

Core GS07-150 20/2	
Depth (cm)	δ18O
2	-1.30
2	-1.33
42	-0.94
42	-1.16
90	-0.24
90	-0.20
116	-0.52
116	-0.13
150	-0.16
150	0.11
185	0.62
185	0.44

Core GS07-150 18/2	
Depth (cm)	δ18O
2	-1.12
2	-1.21
55	-0.44
55	-1.00
75	-0.61
75	-0.42
98	0.05
98	-0.40
120	-0.04
120	0.37
150	0.69
150	0.49

Core GS07-150 17/1	
Depth (cm)	δ18O
2	-1.63
2	-1.42
70	-1.51
70	-1.11
96	-0.79
96	-0.19
116	-0.59
116	-0.19
140	-0.06
140	-0.13
165	0.49
165	0.48

Table A.3 Stable oxygen isotope measurements of *G. ruber* (w) from cores GS07-150 20/2, GS07-150 18/2 and GS07-150 17/1.

Core GS07-150 20/2	
Depth (cm)	δ18O
2	-1.73
2	-1.47
42	-1.32
42	-1.44
90	-0.92
90	-0.79
116	-0.83
116	-0.58
150	-0.22
150	-0.37
185	-0.01
185	0.03

Core GS07-150 18/2	
Depth (cm)	δ18O
2	-1.67
2	-1.64
55	-1.25
55	-1.25
75	-0.95
75	-0.89
98	-0.75
98	-0.99
120	-0.46
120	-0.45
150	-0.21
150	-0.17

Core GS07-150 17/1	
Depth (cm)	δ18O
2	-1.83
2	-1.55
70	-1.50
70	-1.49
96	-0.89
96	-0.87
116	-0.75
116	-0.83
140	-0.22
140	-0.31
165	-0.10
165	-0.11

Table A.4 Stable oxygen isotope measurements of *G. glutinata* from cores GS07-150 20/2, GS07-150 18/2 and GS07-150 17/1.

Core GS07-150 20/2	
Depth (cm)	δ18O
2	-1.38
2	-1.49
42	-1.04
42	-1.12
90	-0.50
90	-1.07
116	-0.86
116	-0.88
150	-0.51
150	-0.37
185	-0.19
185	-0.12

Core GS07-150 18/2	
Depth (cm)	δ18O
2	-1.56
2	-1.43
55	-1.23
55	-1.19
75	-0.97
75	-1.02
98	-0.80
98	-0.82
120	-0.03
120	
150	-0.16
150	-0.14

Core GS07-150 17/1	
Depth (cm)	δ18O
2	-1.71
2	-1.63
70	-1.32
70	-1.32
96	-0.98
96	-1.09
116	-0.93
116	-0.98
140	-0.33
140	-0.31
165	-0.07
165	0.04

Table A.5 Stable oxygen isotope measurements of *G. siphonifera* from cores GS07-150 20/2, GS07-150 18/2 and GS07-150 17/1.

Core GS07-150 20/2	
Depth (cm)	δ18O
2	-0.50
2	-0.52
42	-0.81
42	-0.67
90	-0.75
90	-0.55
116	-0.51
116	1.24
150	0.21
150	0.27
185	0.54
185	0.48

Core GS07-150 18/2	
Depth (cm)	δ18O
2	-0.73
2	-1.31
55	-1.22
55	-0.92
75	-0.39
75	-0.44
98	-0.70
98	-0.45
120	0.21
120	0.25
150	0.62
150	0.22

Core GS07-150 17/1	
Depth (cm)	δ18O
2	-1.14
2	-0.94
70	-1.01
70	-1.07
96	-0.76
96	-0.35
116	-0.52
116	-0.56
140	0.39
140	0.33
165	0.41
165	0.25

Table A.6 Stable oxygen isotope measurements of *G. truncatulinoides* (dex) from cores GS07-150 20/2, GS07-150 18/2 and GS07-150 17/1.

Core GS07-150 20/2	
Depth (cm)	δ18O
2	0.69
2	0.83
42	0.86
42	1.06
42	1.08
42	1.21
90	1.09
90	1.39
90	1.20
90	0.49
116	1.06
116	1.39
116	0.46
116	1.12
116	1.58
150	1.39
150	1.98
150	1.40
150	1.22
185	2.18
185	1.76
185	1.23

Core GS07-150 18/2	
Depth (cm)	δ18O
30	1.07
30	0.43
55	1.06
55	0.90
55	1.37
55	1.35
75	1.40
75	2.08
75	0.90
75	1.24
98	0.89
98	1.10
98	1.47
98	1.66
120	1.18
120	1.95
120	2.56
120	2.62
150	0.85
150	1.44
150	1.85

Core GS07-150 17/1	
Depth (cm)	δ18O
53	0.61
53	0.97
70	1.05
70	1.02
70	0.86
70	1.07
96	1.50
96	1.42
116	1.56
116	1.56
116	1.27
116	0.96
140	1.28
140	1.85
140	1.86
140	1.77
165	1.26
165	1.68
165	1.28

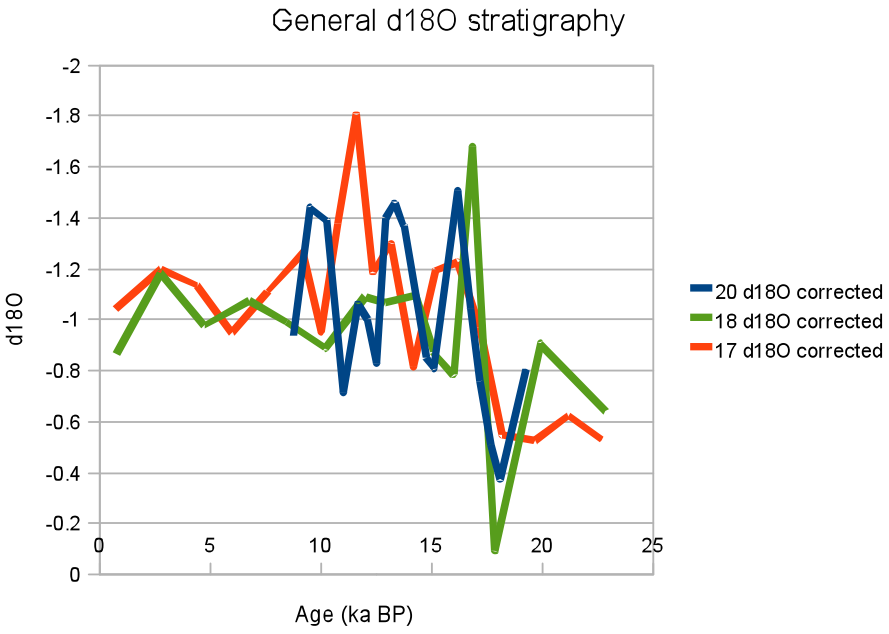

Figure A.1 Ice-volume corrected $\delta^{18}O$ stratigraphies of cores GS07-150 20/2, 18/2 and 17/1 plotted against age.

Appendix B Mg/Ca, Fe/Ca and Mn/Ca results

Table B.1 Mg/Ca, Fe/Ca and Mn/Ca ratios of *G. ruber* (w) from cores GS07-150 20/2, GS07-150 18/2 and GS07-150 17/1.

Core GS07-150 20/2			
Depth (cm)	Mg/Ca	Fe/Ca	Mn/Ca
2	5.234	0.086	0.012
42	4.709	0.183	0.039
90	4.183	0.104	0.052
116	4.456	0.070	0.027
150	4.473	0.170	0.050
185	3.893	0.119	0.023

Core GS07-150 18/2			
Depth (cm)	Mg/Ca	Fe/Ca	Mn/Ca
2	4.922	0.023	0.010
55	4.405	0.104	0.032
75	4.128	0.101	0.040
98	4.240	0.121	0.029
120	4.033	0.191	0.038
150	4.949	0.133	0.010

Core GS07-150 17/1			
Depth (cm)	Mg/Ca	Fe/Ca	Mn/Ca
2	5.080	0.049	0.001
70	5.239	0.189	0.044
96	4.285	0.117	0.057
116	4.621	0.197	0.042
140	4.054	0.145	0.050
165	4.262	0.126	0.039

Table B.1 Mg/Ca, Fe/Ca and Mn/Ca ratios of *G. truncatulinoides* (dex) from cores GS07-150 20/2, GS07-150 18/2 and GS07-150 17/1.

Core GS07-150 20/2			
Depth (cm)	Mg/Ca	Fe/Ca	Mn/Ca
2			
42	2.387	0.090	0.036
90	1.934	0.115	0.039
116	2.211	0.051	0.041
150	2.213	0.083	0.025
185	2.451	0.091	0.018

Core GS07-150 18/2			
Depth (cm)	Mg/Ca	Fe/Ca	Mn/Ca
2			
55	2.175	0.071	0.039
75	2.281	0.102	0.034
98	2.174	0.129	0.039
120	2.460	0.189	0.059
150	2.281	0.054	0.033

Core GS07-150 17/1			
Depth (cm)	Mg/Ca	Fe/Ca	Mn/Ca
2			
70	2.740	0.091	0.055
96	2.045	0.115	0.045
116	2.227	0.107	0.039
140	2.388	0.164	0.082
165	2.356	0.189	0.063

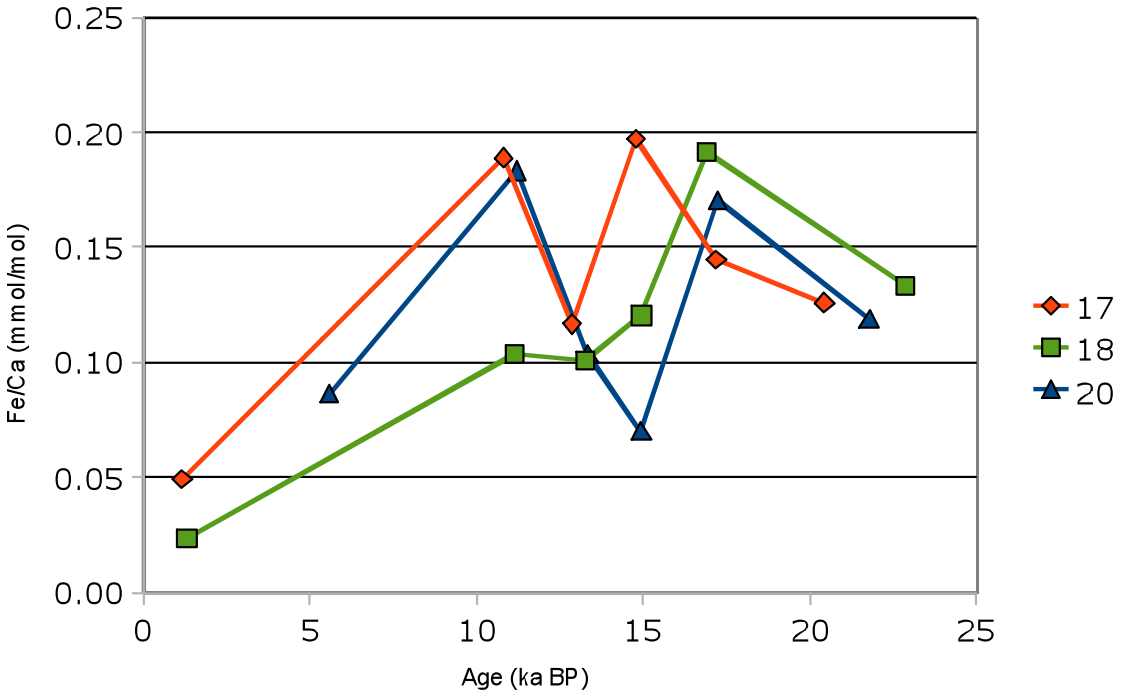

Figure B.1 Fe/Ca ratios of *G. ruber* (w) plotted versus age. The Fe/Ca ratios are given as intensity concentrations (mmol/mol). The red, green and blue lines show the results for cores GS07-150 17/1, 18/2 and 20/2, respectively.

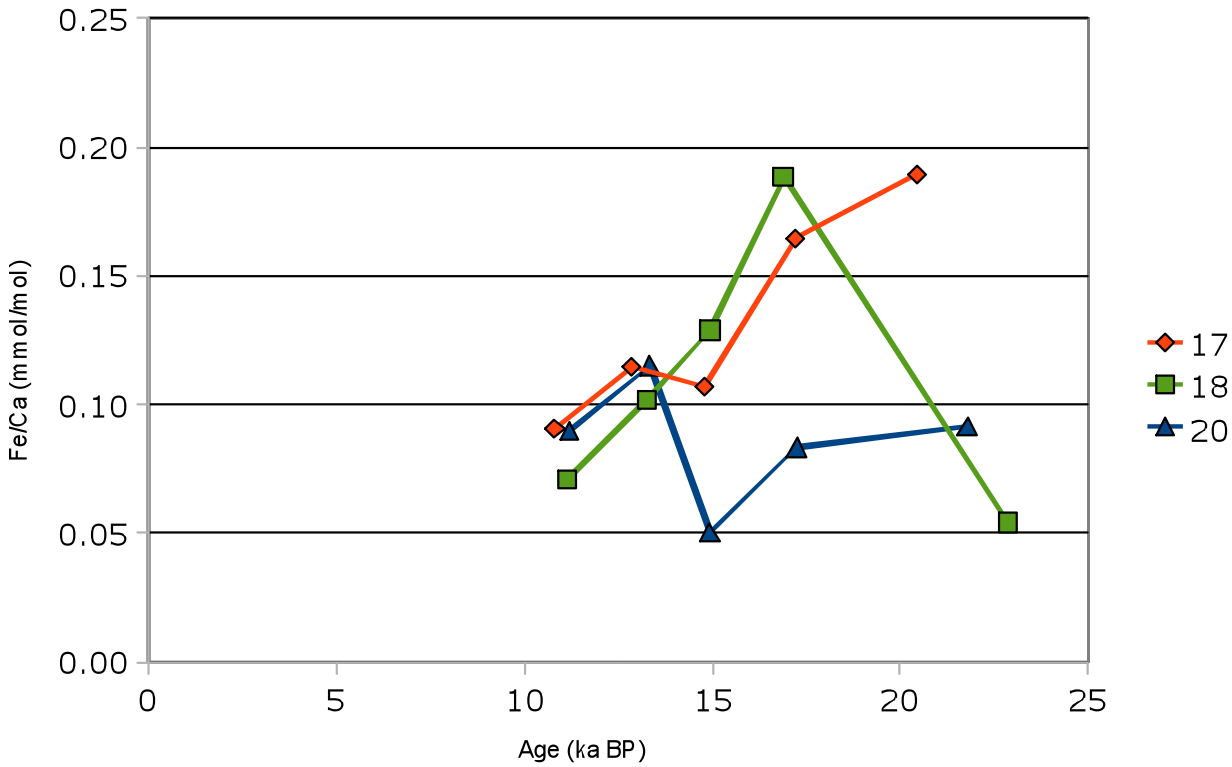

Figure B.2 Fe/Ca ratios of *G. truncatulinoides* (dex) plotted versus age. The Fe/Ca ratios are given as intensity concentrations (mmol/mol). The red, green and blue lines show the results for cores GS07-150 17/1, 18/2 and 20/2, respectively.

Figure B.3 Fe/Ca versus Mg/Ca of *G. ruber* (w) and *G. truncatulinoides* (dex) for cores GS07-150 17/1, 18/2 and 20/2.

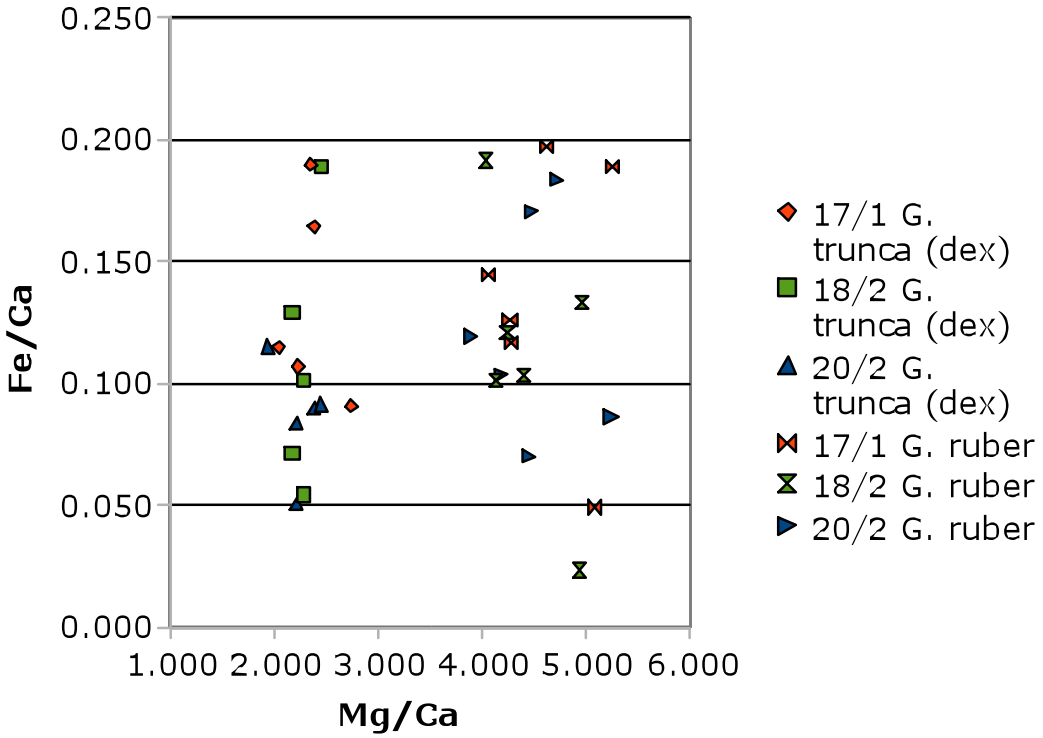

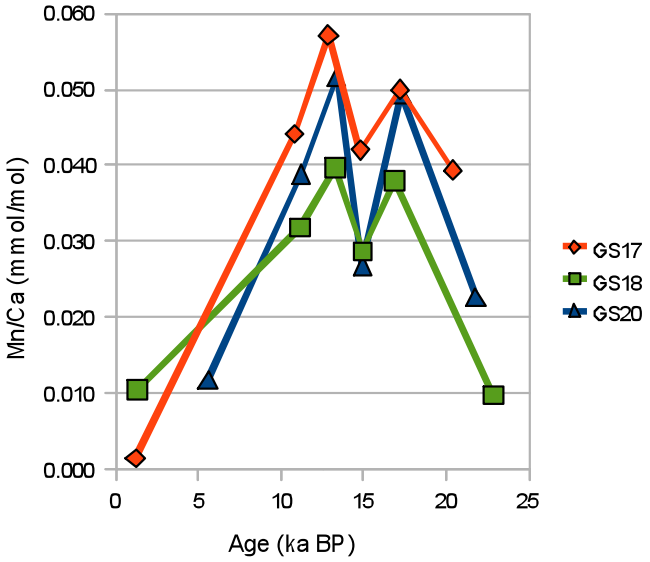

Figure B.4 Mn/Ca ratios of *G. ruber* (w) plotted versus age. The Mn/Ca ratios are given as intensity concentrations (mmol/mol). The red, green and blue lines show the results for cores GS07-150 17/1, 18/2 and 20/2, respectively.

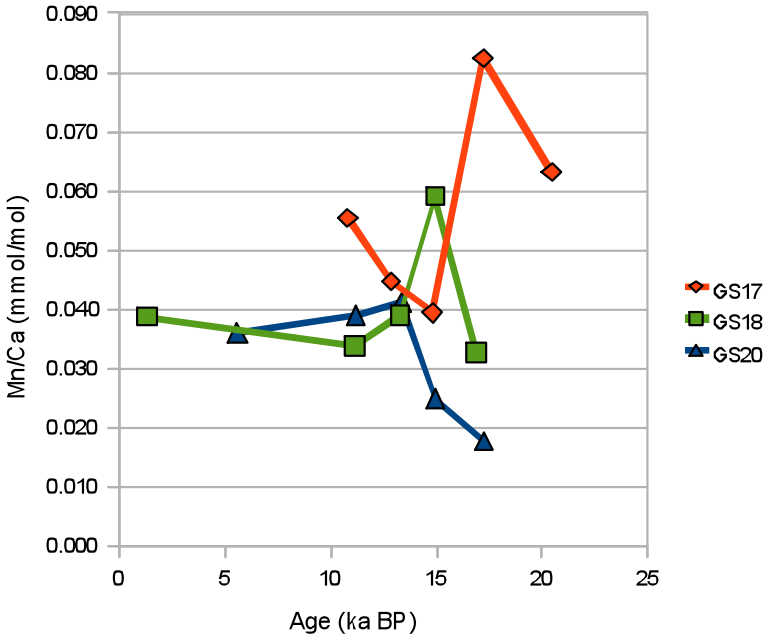

Figure B.5 Mn/Ca ratios of *G. truncatulinoides* (dex) plotted versus age. The Mn/Ca ratios are given as intensity concentrations (mmol/mol). The red, green and blue lines show the results for cores GS07-150 17/1, 18/2 and 20/2, respectively.

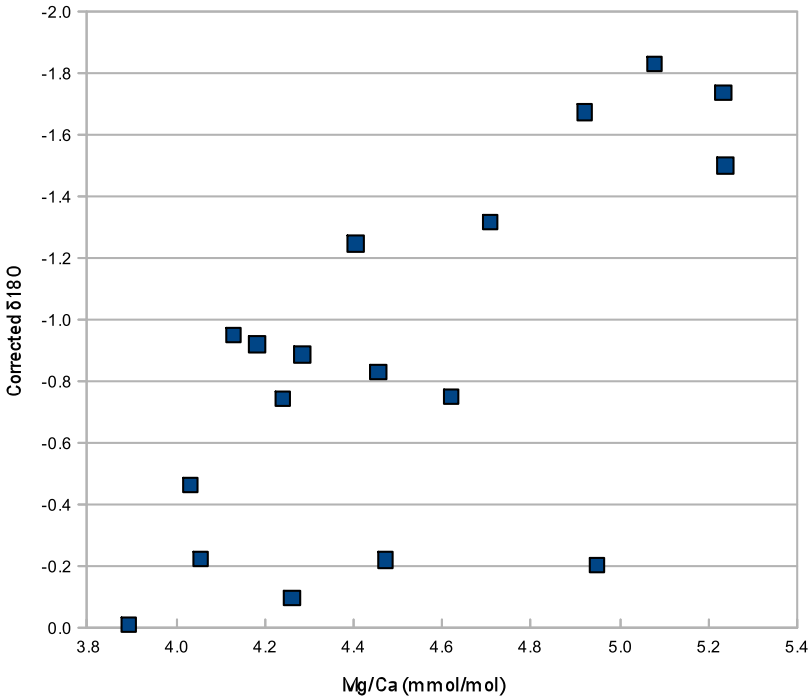

Figure C.1 *G. ruber* $\delta^{18}O_{IVC}$ versus Mg/Ca. Pearson's correlation coefficient, r =-0.69.

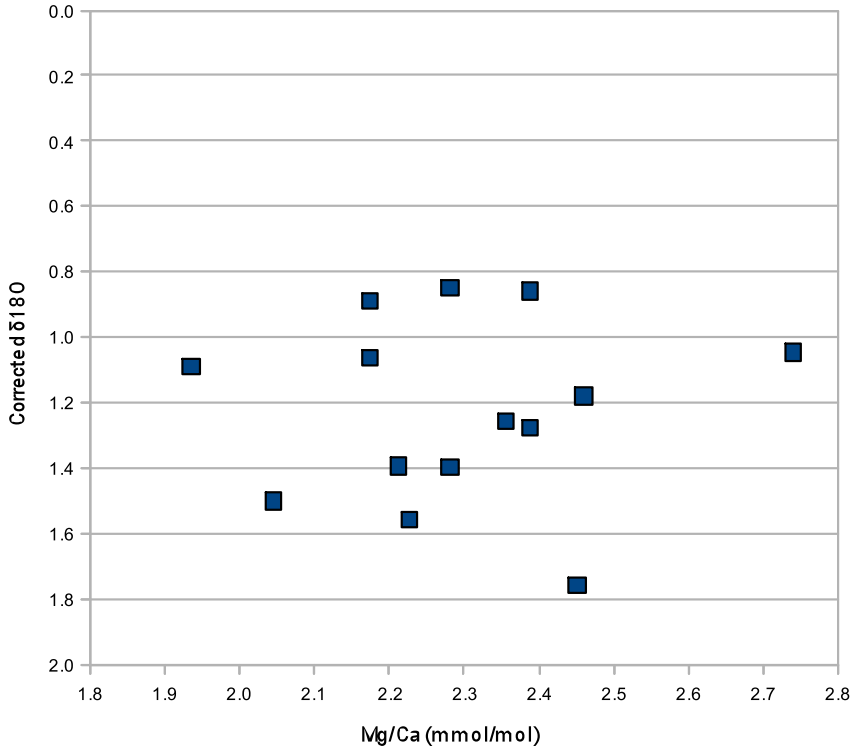

Figure C.2 *G. truncatulinoides (dex)* $\delta^{18}O_{IVC}$ versus Mg/Ca. Pearson's correlation coefficient, r =-0.04.

Reference list

Allègre, C.J., 2008, Isotope Geology: Cambridge, Cambridge University Press.

Alley, R.B., Brook, E.J., and Anandakrishnan, S., 2002, A northern lead in the orbital band: north-south phasing of ice-age events.: Quaternary Science Reviews, v. 21, p. 431-441.

Alley, R.B., and Clark, P.U., 1999, The deglaciation of the northern hemisphere: A Global Perspective.: Annual Reviews Earth Planet Science, v. 27, p. 149-182.

Anand, P., Elderfield, H., and Conte, M.H., 2003, Calibration of Mg/Ca thermometry in planktonic foraminifera from a sediment trap time series: Paleoceanography, v. 18, p. 28-31.

Arz, H.W., Pätzold, J., and Wefer, G., 1998, Correlated millennial-scale changes in surface hydrography and terrigenous sediment yield inferred from last-glacial marine deposits off northeastern Brazil: Quaternary Research, v. 50, p. 157-166.

—, 1999a, Climatic changes during the last deglaciation recorded in sediment cores from the northeastern Brazilian Continental Margin: Geo-Marine Letters, v. 19, p. 209-218.

—, 1999b, The deglacial history of the western Tropical Atlantic as inferred from high resolution stable isotope records off northeastern Brazil: Earth and Planetary Science Letters, v. 167, p. 105-117.

Bainbridge, A.E., 2004, Water chemistry at station GEOSECS46.

Bard, E., 1988, Correction of accelerator mass spectrometry ^{14}C ages measured in planktonic foraminifera: Paleoceanographic implications: Paleoceanography, v. 3, p. 635-645.

Barker, S., Cacho, I., Benway, H., and Tachikawa, K., 2005, Planktonic foraminiferal Mg/Ca as a proxy for past oceanic temperatures: a methodological overview and data compilation for the Last Glacial Maximum: Quaternary Science Reviews, v. 24, p. 821-834.

Barker, S., Greaves, M., and Elderfield, H., 2003, A study cleaning of procedures used for foraminiferal Mg/Ca paleothermometry: Geochemistry, Geophysics, Geosystems.

Bé, A.W.H., 1960, Ecology of recent planktonic foraminifera: Part 2: Bathymetric and seasonal distributions in the Sargasso Sea off Bermuda: Micropaleontology, v. 6, p. 373-392.

—, 1967, FORAMINIFERA Families: Globigerinidae and Globorotaliidae, *in* University, L.G.O.o.C., ed.: New York.

Bé, A.W.H., and Hamlin, W.H., 1967, Ecology of recent planktonic foraminifera: Part 3: Distribution in the North Atlantic During the Summer of 1962: Micropaleontology

Vol. 13, No. 1 (Jan., 1967), pp. 87-106 v. 13, p. 87-106.

Bé, A.W.H., and Tolderlund, D.S., 1971a, Distribution and ecology of living planktonic foraminifera in surface waters of the Atlantic and Indian oceans: London, Cambridge University Press.

—, 1971b, Seasonal Distribution of Planktonic Foraminifera in the Western North Atlantic: Micropaleontology, v. 17, p. 297-329.

Bemis, B.E., Bijma, J., and Lea, D.W., 1998, Reevaluation of the oxygen isotopic composition of planktic foraminifera: Experimental results and revised paleotemperature equations.: Paleoceanography, v. 13, p. 150-160.

Berben, S., 2010, Paleothermocline reconstructions of the western tropical Atlantic ocean: A multiplanktonic foraminifera stable oxygen isotope approach.: The Netherlands, Vrije Universiteit Amsterdam.

Boltovskoy, E., 1981, Foraminifera, *in* Boltovskoy, D., ed., Atlas del Zooplancton del

Atlántico Suroccidental y métodos de trabajo con el zooplancton marino: Argentina, Publicación Especial del INIDEP Mar del Plata, p. 317-352.
Boltovskoy, E., and Wright, R., 1976, Recent foraminifera: The Hague, 515 p.
Boyle, E.A., and Keigwin, L., 1987, North Atlantic thermohaline circulation during the past 20,000 years linked to high-latitude surface temperatures.: Nature, v. 330, p. 35-40.
Broecker, W.S., Andree, M., Bonani, G., Wolfli, W., Oeschger, H., and Klas, M., 1988, Can the Greenland climatic jumps be identified in records from ocean and land?: Quaternary Research, v. 30, p. 1-6.
Broecker, W.S., Peteet, D.M., and Rind, D., 1985, Does the ocean–atmosphere system have more then one stable mode of operation?: Nature, v. 315, p. 21-26.
Brouwer, P., 2003, Theory of XRF. Getting acquainted with the principles: Almelo, The Netherlands, PANalytical B.V.
Brown, E., Colling, A., Park, D., Phillips, J., Rothery, D., and Wright, J., 2001, Ocean Circulation: Oxford, Butterworth, Heinemann.
Chave, K.E., 1954, Aspects of the biochemistry of magnesium 2. Calcareous sediments and rocks: Journal of Geology, v. 62, p. 587–599.
Chiang, J.C.H., Biasutti, M., and Battisti, D., 2003, Sensitivity of the Atlantic Intertropical Convergence Zone to LAst Glacial Maximum boundary conditions: Paleoceanography, v. 18, p. 1-18.
Clarke, F.W., and Wheeler, W.C., 1922, The inorganic constituents of marine invertebrates: USGS Prof. Pap., v. 124.
Cléroux, C., Cortijo, E., Anand, P., Labeyrie, L., Bassinot, F., Caillon, N., and Duplessy, J.C., 2008, Mg/Ca and Sr/Ca ratios in planktonic foraminifera: Proxies for upper water column temperature reconstruction: PALEOCEANOGRAPHY, v. 23.
Cléroux, C., and Lynch-Stieglitz, J., 2010, What caused G. truncatulinoides to calcify in shallower water during the early Holocene in the western Atlantic / Gulf of Mexico?: Earth and Environmental Science, v. 9, p. 1-7.
Cooke, S., and Rohling, E.J., 1999, Stable Isotopes in Foraminiferal Carbonate, *in* Barun, K.S.G., ed., Modern foraminifera: Great Britain, Kluwer Academic Publishers.
Coplen, T.B., Kendall, C., and Hopple, J., 1983, Comparison of stable isotope reference samples: Nature, v. 302, p. 236-238.
Cronblad, H.G., and Malmgren, B.A., 1981, Climatically controlled variation of Sr and Mg in Quaternary planktic foraminifera: Nature, v. 291, p. 61-64.
Croudace, I.W., Rindby, A., and Rothwell, G., 2006, ITRAX: description and evaluation of a new multi-function X-ray core scanner., *in* Rothwell, R.G., ed., New Techniques in Sediment Core Analysis, Volume 267: Geological Society, London, Special Publications: London, Geological Society of London, p. 51-63.
Crowley, T.J., 1992, North Atlantic Deep Water cools the southern hemisphere.: Paleoceanography, v. 7, p. 489-497.
Culver, S.J., 1993, Chapter 12: Foraminifera, *in* Lipps, J.H., ed., Foraminifera from Fossil Prokaryotes and
Protists., Blackwell Scientific Publications, p. 203-247.
Dahl, K.A., Broccoli, A.J., and Stouffer, R., 2005, Assessing the role of North Atlantic freshwater forcing in millennial scale climate variability: A tropical Atlantic perspective.: Climate Dynamics, v. 24, p. 325-346.
de Vargas, C., Renaud, S., Hilbrecht, H., and Pawlowski, J., 2001, Pleistocene adaptive radiation in Globorotalia truncatulinoides: genetic, morphologic, and environmental evidence: Paleobiology, v. 27, p. 104–125.
Dekens, P.S., Lea, D.W., Pak, D.K., and Spero, H.J., 2002, Core top calibration of Mg/Ca in tropical foraminfera: Refining paleotemperature estimation: Geochemistry,

Geophysics, Geosystems, v. 3.
Delworth, T.L., Clark, P.U., Holland, M., Johns, W.E., Kuhlbrodt, T., Lynch-Stieglitz, J., Morrill, C., R., S., Weaver, A.J., and Zhang, R., 2008, The potential for abrupt change in the Atlantic Meridional Overturning Circulation., Abrupt Climate Change. A report by the U. S. Climate Change Science Program and the Subcommittee on Global Change Research: Reston, VA, U. S. Geological Survey, p. 258-359.
deVilliers, S., Greaves, M., and Elderfield, H., 2002, An intensity ratio calibration method for the accurate determination of Mg/Ca and Sr/Ca of marine carbonates by ICP-AES: Geochemistry Geophysics Geosystems, v. 3.
Elderfield, H., and Ganssen, G., 2000, Past temperature and δ18O of surface ocean waters inferred from foraminiferal Mg/Ca ratios: Nature, v. 405, p. 442-445.
Emiliani, C., 1955, Pleistocene temperatures.: The journal of geology, v. 63, p. 538-576.
Epstein, S., R., B., H., L., and C., U.H., 1953, Revised carbonate-water isotopic temperature scale.: Bulletin of the Geological Society of America, v. 64, p. 1315-1326.
Erez, J., 2003, The source of ions for biomineralization in foraminifera and their implications for paleoceanographic proxies: Reviews in Mineralogy and Geochemistry, v. 54, p. 115-149.
Fairbanks, R.G., 1989, A 17,000-year glacio-eustatic sea level record: influence of glacial melting rates on the Younger Dryas event and deep-ocean circulation: Nature, v. 342, p. 637-642.
Field, D.B., 2004, Variability in vertical distributions of planktonic foraminifera in the Californian Current: Relationships to vertical ocean structure: Paleoceanography, v. 19.
Garzoli, S.L., Field, A., Johns, W.E., and Yao, Q., 2004, North Brazil Current retroflection and transports: Journal of Geophysical Research, v. 109, p. C01013.
Hastenrath, S., and Merle, J., 1987, Annual cycle of subsurface thermal structure in the tropical Atlantic Ocean: Journal of Physical Oceanography, v. 17.
Haug, G.H., Hughen, K.A., Sigman, D.M., Peterson, L.C., and Röhl, U., 2001, Southward Migration of the Intertropical Convergence Zone Through the Holocene: Science, v. 293, p. 1304-1307.
Heinrich, H., 1988, Origin and consequences of cyclic ice rafting in the northeast Atlantic Ocean during the past 130,000 years.: Quaternary Research, v. 29, p. 143-152.
Hilbrecht, H., 1996, Extant planktic foraminifera and the physical environment in the Atlantic and Indian Oceans: Zürich, Technischen Hochschule und der Universität Zürich, Neue Folge.
Hoefs, J., 2004, Stable Isotope Geochemistry: Berlin, Springer Verlag.
Hughen, K.A., Overpeck, J.T., Lehman, S.J., Kashgarian, M., Southon, J., Peterson, L.C., Alley, R., and Sigman, D.M., 1998, Deglacial changes in ocean circulation from an extended radiocarbon calibration: Nature, v. 391, p. 65-68.
Hughen, K.A., Overpeck, J.T., Peterson, L.C., and Trumbore, S., 1996, Rapid climate changes in the tropical Atlantic region during the last deglaciation.: Nature, v. 380, p. 51-54.
Johns, W.E., Lee, T.N., Beardsley, R.C., Candela, J., Limeburner, R., and Castro, B., 1998, Annual cycle and variability of the North Brazil Current.: Journal of Physical Oceanography, v. 28, p. 103-128.
Keigwin, L.D., and Lehman, S.J., Paleoceanography 9 (1994) 185–194., 1994, Deep circulation change linked to HEINRICH event 1 and Younger Dryas in a middepth North Atlantic core.: Paleoceanography, v. 9, p. 185-194.
Kleiven, H.F., Kissel, C., Laj, C., Ninnemann, U.S., Richter, T.O., and Cortijo, E., 2008, Reduced North Atlantic Deep Water Coeval with the Glacial Lake Agassiz

Freshwater Outburst.: Nature, v. 319, p. 60-64.
Knoppers, B., Ekau, W., and Figueiredo, A.G., 1999, The coast and shelf of east and northeast Brazil and material transport
: Geo-Marine Letters, v. 19, p. 171-178.
Kuhlbrodt, T., Griesel, A., Montoya, M., Levermann, A., Hofmann, M., and Rahmstorf, S., 2007, On the driving processes of the Atlantic meridional overturning circulation.: Reviews of Geophysics, v. 45.
Lea, D.W., 2003, Elemental and Isotopic Proxies of Past Ocean Temperatures, *in* Turkien, K., ed., Treaties On Geochemistry, Elsevier.
Lea, D.W., Mashiotta, T.A., and Spero, H.J., 1999, Controls on magnesium and strontium uptake in planktonic foraminifera determined by live culturing: Geochimica et Cosmochimica Acta, v. 63, p. 2369–2379.
—, 2000, Controls on magnesium and strontium uptake in planktonic foraminifera determined by live culturing: Geochemica et Cosmochimica Acta, v. 63, p. 2369-2379.
Lea, D.W., Pak, D.K., Peterson, L.C., and Hughen, K.A., 2003, Synchroneity of Tropical and High-Latitude Atlantic Temperatures over the Last Glacial Termination: Science, v. 301, p. 1361-1364.
Lin, H.L., Peterson, L.C., Overpeck, J., Trumbore, S.E., and Murray, D.W., 1997, Late Quaternary climate change from δ18O records of multiple species of planktonic foraminifera: High-resolution records from the anoxic Cariaco Basin, Venezuela: Paleoceanography, v. 12, p. 415-427.
Liu, G., and Curry, J.A., 1999, Tropical ice water amount and its relations to other atmospheric hydrological parameters as inferred from satellite data: Journal of Applied Meterology, v. 38, p. 1182-1194.
Lowe, J.J., and Walker, M.J.C., 1997, Reconstructing Quaternary Environments: Edinburgh, Addison Weasly Longman, 446 p.
Lynch-Stieglitz, J., Curry, W.B., and Slowely, N., 1999, Weaker Gulf Stream in the Florida Straits during the Last GlacialMaximum: Nature, v. 402.
Manabe, S., and Stouffer, R.J., 1997, Coupled ocean-atmosphere model response to freshwater input: Comparison to Younger Dryas event.: Paleoceanography, v. 12, p. 312-336.
Manning, T., and Grow, W.R., 1997, Inductively Coupled Plasma - Atomic Emission Spectrometry: The Chemical Educator, v. 2, p. 1-19.
Martin, P.A., and Lea, D.W., 2002, A simple evaluation of cleaning procedures on fossil benthic foraminferal Mg/Ca: Geochemistry, Geophysics, Geosystems, v. 3.
Mashiotta, T.A., Lea, D.W., and Spero, H.J., 1999, Glacial-interglacial changes in Subantarctic sea surface temperature and δ18O-water using foraminferal Mg: Earth and Planetary Science Letters, v. 170, p. 417-432.
McConnell, M.C., and Thunell, R.C., 2005, Calibration of the planktonic foraminiferal Mg/Ca paleothermometer: Sediment trap results from the Guaymas Basin, Gulf of California: Paleoceanography, v. 20.
McCrea, J.M., 1950, On the isotopic chemistry of carbonates and a paleotemperature scale.: J. Chem. Phys., v. 18, p. 849-857.
McIntyre, A., and Molfino, B., 1996, Forcing of Atlantic Equatorial and Subpolar Millennial Cycles by Precession: Science, v. 274, p. 1867-1870.
McIntyre, A., Ruddiman, W.F., Karlin, K., and Mix, A.C., 1989, Surface water response of the equatorial Atlantic Ocean to orbital forcing: Paleoceanography, v. 4, p. 19-55.
McManus, J.F., Francois, R., Gherardi, J.-M., Keigwin, L.D., and Brown-Leger, S., 2004, Collapse and rapid resumption of Atlantic meridional circulation linked to deglacial

climate changes: Nature, v. 428, p. 834-837.
Mix, A.C., Ruddiman, W.F., and McIntyre, A., 1986, Late Quaternary paleoceanography of the tropical Atlantic, 2: The seasonal cycle of sea surface temperatures, 0-20,000 years BP: Paleoceanography, v. 1, p. 339-353.
Mulitza, S., Donner, B., Fischer, G., Paul, A., Pätzold, J., Rühlemann, C., and Segl, M., 2003, The South Atlantic Oxygen Isotope Record of Planktic Foraminifera: Berlin Heidelberg New York Tokyo, Springer-Verlag.
Mulitza, S., Dürkoop, A., Hale, W., Wefer, G., and H.S., N., 1997, Planktonic foraminifera as recorders of past surface-water stratification: Geology, v. 25, p. 335-338.
NGRIPMembers, 2004, Nature, Volume 431.
Nürnberg, D., 1995, Magnesium in tests of Neogloboquadrina pachyderma sinistral from high northern and southern latitudes: Journal of Foraminiferal Research, v. 25, p. 350-368.
Nürnberg, D., Bijma, J., and Hemleben, S., 1996, Assessing the reliability of magnesium in foraminiferal calcite as a proxy for water mass temperatures: Geochemica et Cosmochimica Acta, v. 60, p. 803-814.
Paillard, D., Labeyrie, L., and Yiou, P., 1996, Macintosh program performs time-series analysis: Eos Trans., v. 77.
Parker, F.L., 1962, Planktonic foraminiferal species in Pacific sediments: Micropaleontology, v. 8, p. 219-254.
Peltier, W.R., and Fairbanks, R.G., 2006, Global glacial ice volume and Last Glacial Maximum duration from an extended Barbados sea level record: Quaternary Science Reviews, v. 25, p. 3322-3337.
Peterson, L.C., Haug, G.H., Hughen, K.A., and Röhl, U., 2000, Rapid Changes in the Hydrologic Cycle of the Tropical Atlantic During the Last Glacial
: Science, v. 290, p. 1947-1950.
Peterson, R.G., 1990, On the volume transport in the southwestern South Atlantic Ocean.: Eos, v. 71.
Peterson, R.G., and Stramma, L., 1991, Upper-level circulation in the South Atlantic Ocean: Progress in Oceanography, v. 26, p. 1-73.
Rahmstorf, S., 2002, Ocean circulation and climate during the past 120,000 years: Nature, v. 419, p. 207-214.
—, 2006, Thermohaline Ocean Circulation., *in* Elias, S.A., ed., Encyclopedia of Quaternary Sciences.: Amsterdam, Elsevier.
Ravelo, A.C., and Fairbanks, R.G., 1992, Oxygen isotopic composition of multiple species of planktonic foraminifera: recorders of the modern photic zone temperature gradient.: Paleoceanography, v. 7, p. 815-831.
—, 1995, Carbon isotope fractionation in multiple species of planktonic foraminifera from core-tops in the tropical Atlantic.: Journal of Foraminiferal Research, v. 25.
Regenberg, M., Steph, S., Nürnberg, D., Tiedemann, R., and Garbe-Schönberg, D., 2009, Calibrating Mg/Ca ratios of mulitple planktonic foraminiferal species with δ18O-calcification temperatures: Paleothermometry for the upper water-column: Earth and Planetary Science Letters, v. 278, p. 324-336.
Reimer, P.J., Baillie, M.G.L., Bard, E., Bayliss, A., Beck, J.W., Blackwell, P.G., Bronk Ramsey, C., Buck, C.E., Burr, G.S., Edwards, R.L., Friedrich, M., Grootes, P.M., Guilderson, T.P., Hajdas, I., Heaton, T.J., Hogg, A.G., Hughen, K.A., Kaiser, K.F., Kromer, B., McCormac, F.G., Manning, S.W., Reimer, R.W., Richards, D.A., Southon, J.R., Talamo, S., Turney, C.S.M., van der Plicht, J., and Weyhenmeyer, C.E., 2009, IntCal09 and Marine09 radiocarbon age calibration curves, 0–50,000 years cal BP.: Radiocarbon, v. 51, p. 1111-1150.
Richardson, P.L., 2008, On the history of meridional overturning circulation schematic

diagrams.: Progress in Oceanography, v. 76, p. 466-486.
Rosenthal, Y., Lohmann, G.P., Lohmann, K.C., and Sherell, R.M., 2000, Incorporation and preservation of Mg in Globigerinoides sacculifer: Implications for reconstructing the temperature and 18O/16O of seawater: Paleoceanography, v. 15, p. 135-145.
Ruddiman, W.F., 2001, Earth's Climate Past and Future: New York, W.H. Freeman and Company.
Rühlemann, C., Mulitza, S., Lohmann, G., Paul, A., Prange, M., and Wefer, G., 2004, Intermediate depth warming in the tropical Atlantic related to weakened thermohaline circulation: Combining paleoclimate data and modeling results for the last deglaciation: Paleoceanography, v. 19, p. 1025-1034.
Rühlemann, C., Mulitza, S., Müller, P.J., Wefer, G., and Zahn, R., 1999, Warming of the tropical Atlantic Ocean and slowdown of thermohaline circulation during the last deglaciation: Nature, v. 402, p. 511-514.
Sarnthein, M., Winn, K., Jung, S.J.A., Duplessy, J.C., Labeyrie, L., Erlenkeuser, H., and Ganssen, G., 1994, Changes in east Atlantic deepwater circulation over the last 30 000 years: eight time slice reconstructions.: Paleoceanography v. 9, p. 209-267.
Schmidt, G.A., Bigg, G.R., and Rohling, E.J., 1999, Global Seawater Oxygen-18 Database Volume 2010.
Schott, F., Fischer, J., Reppin, J., and Send, U., 1993, On mean and seasonal currents and transports at the western boundary of the equatorial Atlantic.: Journal of Geophysical Research, v. 98, p. 14353-14368.
Schott, F.A., Dengler, M., Brandt, P., Affler, K., Fischer, J., Bourlés, B., Gouriou, Y., Molinari, R.L., and Reihn, M., 2003, The zonal currents and transports at 35°W in the tropical Atlantic: Geophysical Research Letters, v. 30, p. 1349-1352.
Seager, R., and Battisti, D.S., 2006, Challenges to Our Understanding of the General Circulation: Abrupt Climate Change, *in* Schneider, T., Sobel, A.S., ed., The Global Circulation of the Atmosphere, Princeton University Press.
Shackleton, N.J., 1974, Attainment of isotopic equilibrium between ocean water and benthonic foraminifera genus Uvigerina: Isotopic changes in the ocean during the last glacial, *in* Labeyrie, L., ed., Les méthodes quantitatives d'étude des variations du climat au cours du Pléistocène, Volume 219, p. 203-209.
Shackleton, N.J., and Opdyke, N.D., 1973, Oxygen isotope and palaeomagnetic stratigraphy of equatorial pacific core V28-238: Oxygen isotope temperature and ice volumes on a 10^5 year and 10^6 year scale: Quaternary Research, v. 3, p. 39-55.
Sharp, Z., 2007, Principles of Stable Isotope Geochemistry: Upper Saddle River, New Jersey, Pearson Prentice Hall.
Skinner, L.C., and Elderfield, H., 2005, Constraining ecological and biological bias in planktonic Mg/Ca and δ18Occ: A multispecies approach to procy calibration testing: Paleoceanography, v. 20.
Spero, H.J., and Lea, D.W., 1993, Intraspecific stable isotope variability in the planktic foraminifera *Globogerinoides sacculifer*: results from laboratory experiments: Marine Micropaleontology, v. 28.
Spero, H.J., Lea, D.W., and Bemis, B.E., 1997, Effect of seawater carbonate concentration on foraminiferal carbon and oxygen isotopes.: Nature, v. 390, p. 497-500.
Sprintall, J., and Tomczak, M., 1993, On the formation of central water in the southern hemisphere.: Deep-Sea Research, v. 40, p. 827-848.
Steph, S., Regenberg, M., Tiedemann, R., Mulitza, S., and Nürnberg, D., 2009, Stable isotopes of planktonic foraminifera from tropical Atlantic/Caribbean core-tops: Implications for reconstructing upper ocean stratification: Marine Micropaleontology, v. 71, p. 1-19.

Stocker, T.F., 1998, The Seesaw Effect: Science, v. 282, p. 61-62.
Stramma, L., Fischer, J., and Reppin, J., 1995, The North Brazil Undercurrent: Deep Sea Research, Part I, v. 42, p. 773-795.
Stramma, L., and Schott, F., 1999, The mean flow field of the tropical Atlantic Ocean
: Deep-Sea Research II, v. 46, p. 279-303.
Stuiver, M., Reimer, P.J., Bard, E., Beck, J.W., Burr, G.S., Hughen, K.A., Kromer, B., McCormac, F.G., van der Plicht, J., and Spurk, M., 1998, INTCAL 98 radiocarbon age calibration, 24,000-0 cal BP: Radiocarbon, v. 40, p. 1041-1083.
Swart, P.K., 1983, Carbon and oxygen isotope fractionation in scleratinian corals: a review.: Earth-Science Reviews, v. 19, p. 51-80.
Takahashi, T., Broecker, W.S., Bainbridge, A.E., and Weiss, R.F., 1980, Carbonate chemistry of the Atlantic, Pacific and Indian oceans: the results of the GEOSECS expeditions, 1972-1978: Technical Report, v. 1.
Tedesco, K.A., and Thunell, R.C., 2003, Seasonal and interannual variations in the planktonic foraminiferal flux and assemblage flux composition in the Cariaco Basin, Venezuela: Journal of Foraminiferal Research, v. 33, p. 192-210.
Teller, J.T., 1990, Meltwater and precipitation runoff to the North Atlantic, Arctic, and Gulf of Mexico from Laurentide Ice Sheet and adjacent regions during the Younger Dryas.: Paleoceanography, v. 5, p. 897-905.
Tietjen, G.L., and Beckman, R.J., 1974, On duplicate measurements in the laboratory: Technometrics, v. 16, p. 53-56.
Tisserand, A., 2009, Chart of the western tropical Atlantic Ocean showing the locations of the surface sediment samples and the temperature profiles in modern conditions and based on model by *Manabe and Stouffer* (1997).
Tomczak, M., and Godfrey, J.S., 1994, Regional Oceanography: An Introduction.: Oxford.
Urey, H.C., 1947, The thermodynamic properties of isotopic substances.: Journal of Chemical Society, p. 562-581.
—, 1948, Oxygen Isotopes in Nature and in the Laboratory.: Science, v. 108, p. 489-496.
Vellinga, M., and Wood, R.A., 2002, Global climate impacts of a collapse of the Atlantic thermohaline circulation.: Climate Change, v. 54, p. 251-267.
Walker, M.J.C., 2005, Quaternary Dating Methods: West Sussex, John Wiley & Sons Ltd, 286 p.
Wang, X.F., Auler, A.S., Edwards, R.L., Cheng, H., Cristalll, P.S., Smart, P.L., Richards, D.A., and Shen, C.C., 2004, Wet periods in northeastern Brazil over the past 210 kyr linked to distant climate anomalies.: Nature, v. 432, p. 740-743.
Wefer, G., Berger, W.H., Bijma, J., and Fischer, G., 1999, Clues to Ocean History: a Brief Overview of Proxies: Berlin Heidelberg, Springer-Verlag.
WOCE, 2002, World Ocean Circulation Experiment, Global Data, Version 3.0. WOCE International Project Office, *in* Office, W.I.P., ed., WOCE Report, Volume 180/02: Silver Spring, U.S. national Oceanographic Data Center.
Wolff, T., Mulitza, S., Arz, H.W., Pätzold, J., and Wefer, G., 1998, Oxygen isotopes versus CLIMAP (18 ka) temperatures: A comparison from the tropical Atlantic: Geology, v. 26, p. 675-678.
Wolff, T., Mulitza, S., Rühlemann, C., and Wefer, G., 1999, Response of the tropical Atlantic thermocline to late Quaternary trade wind changes: Paleoceanography, v. 14, p. 374-383.
Yarincik, K.M., Murray, R.W., and Peterson, L.C., 2000, Climatically sensitive eolian and hemipelagic deposition in the Cariaco Basin, Venezuela, over the past 578,000 years: Results from AI/Ti and K/AI: Paleoceanography, v. 15.